MONDRAGON UNIBERTSITATEA

GOI ESKOLA POLITEKNIKOA

FACULTY OF ENGINEERING

Brake–clutch squeal prediction and suppression

PhD Thesis

Author
Ondiz Zarraga

Supervisors
Ibai Ulacia
José Manuel Abete

20th December 2016

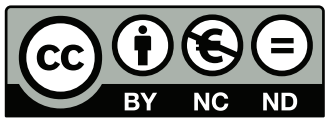

As the world is round, road is long

— The Pogues

Statement of originality

I hereby declare that this submission is my own work and to the best of my knowledge it contains no materials previously published or written by another person, or substantial proportions of material which have been accepted for the award of any other degree or diploma at Mondragon Unibertsitatea or any other educational institution, except where due acknowledgement is made in the thesis. Any contribution made to the research by others, with whom I have worked at Mondragon Unibertsitatea or elsewhere, is explicitly acknowledged in the thesis. I also declare that the intellectual content of this thesis is the product of my own work, except to the extent that assistance from others in the project's design and conception or in style, presentation and linguistic expression is acknowledged.

Acknowledgements

I would like to thank every person that has helped bring this work to life. It's impossible to thank individually everyone that has contributed, so please don't feel offended if you are in the generic section.

First, thanks to my colleagues for planning the overthrow of the system in every lunch and specially to my coffee group because coffee time has been (too) many times the only reason for coming to work.

Thanks also to my brother for his 24/7 tech support and IT consultancy service at zero flat rate. We'll conquer the world someday — but no today.

To finish the custom–thanks, I would like to thank the other warrior in the fight against noise and vibration for so many reasons but above all for all the conversations challenging the ideology of this far leftist punk that is writing. You are the reason why I haven't quit and started a bakery — time will tell if you are to thank or to blame. Seriously now, the best part of starting a PhD has been meeting you.

To the rest that are not explicitly mentioned here: I haven't forgot you, thank you all and see you at the other side!

It wouldn't be fair to finish the acknowledged section without thanking the free software community for making available to everybody such amazing tools. The developers of `Emacs`, `Git`, `Pandoc` and `Cygwin` — and LaTeX, don't forget LaTeX— deserve a special mention, without them this PhD thesis wouldn't have been possible. Literally.

Funding

This work was supported by Goizper S. Coop. and IK4-Tekniker and funded by the Basque Government under the Manunet project BRAKESQ.

Abstract

This work studies the high frequency noise in brake–clutch systems known as squeal. The work is divided into two parts, the first is focused on the development of both a theoretical and experimental simplified model of a brake–clutch and the second is centred on squeal modelling in the real system.

For the simple model, on the theoretical side, a FE model was developed including anisotropic material properties, pressure and speed dependent friction coefficient and friction damping. The pertinent characterisation tests were performed as needed. On the experimental side, squeal tests were performed in the test bench in order to check the ability of the system for squeal prediction.

Once the model was thought as accurate enough, a methodology to decide over point structural modifications for squeal suppression based on the receptance function was designed. Using this process squeal was successfully eliminated from the simplified model both theoretically and experimentally.

In the second part the modelling of squeal in a real brake–clutch system was tackled. With this objective a FE model of the whole system was developed and its validity was checked first by EMA and after, comparing the experimental squeal frequencies with the ones predicted by simulation. To finish, the methodology for structural modifications previously designed was applied to the system and several theoretical modifications were proposed and studied.

Resumen

El presente trabajo estudia el ruido de alta frecuencia que se da en los freno–embragues conocido como *squeal*. El trabajo se divide en dos partes, la primera enfocada en el desarrollo de un modelo simple tanto teórico como experimental del freno–embrague y la segunda centrada en la modelización del *squeal* en el sistema real.

En lo referente al modelo simple, en la parte teórica se desarrolló un modelo de elementos finitos que incluía propiedades anisótropas para el material de fricción, un coeficiente de fricción dependiente de la presión y la velocidad y amortiguamiento por fricción. Estas propiedades se caraterizaron en los correspondientes ensayos independientes cuando fue necesario. En la parte experimental, se llevaron a cabo ensayos de *squeal* en banco con la idea de verificar la capacidad del modelo para predecir el *squeal*.

Una vez que el modelo se consideró lo suficientemente exacto, se desarrolló una metodología para proponer y valorar modificaciones estructurales para la supresión de *squeal*. El método propuesto está basado en la función de receptancia. Gracias a este proceso fue posible eliminar el *squeal* del modelo primero en la teoría y a continuación en el banco de ensayos.

En la segunda parte se aborda la modelización de *squeal* en un freno–embrague real. Con esto en mente se desarrolló un modelo de elementos finitos del sistema completo y se validó en primer lugar mediante AME y a continuación comparando las frecuencias experimentales de *squeal* con las predichas por la simulación. Por último, la metodología desarrollada para modificaciones estructurales se aplicó al sistema real y se propusieron y analizaron varias modificaciones teóricas.

Laburpena

Lan honetan balazta–enbrage unitate konbinatuetan agertzen den *squeal* izeneko frekuentzia altuko zarata aztertzen da. Lana bi zatitan banatuta dago: alde batetik, balazta–enbragearen eredu sinplifikatu bat garatu da, bai teorikoa zein esperimentala; bestetik, *squeal*a sistema errealean modelizatu da.

Eredu sinplean, alde teorikoari dagokionez, elementu finitutako eredu bat garatu da. Eredu honek marruskadura materialaren propietate anisotropoak, presio eta abiaduraren menpeko marruskadura koefizientea eta marruskadurak eragindako moteltzea kontutan hartzen ditu. Propietate hauek saiakuntza independentetan neurtu dira. Alde esperimentalean, *squeal* saiakuntzak burutu dira ereduak *squeal*a aurreikusteko duen gaitasuna balioztatzeko asmoz.

Behin eredua nahiko zehatza izanik, zarata kentzeko aldaketa estrukturalak proposatu eta baloratzeko metodologia bat diseinatu da. Proposatutako metodoa errezeptantzia funtzioan oinarrituta dago. Metodo honi esker *squeal*a eredu teorikoan lehenengo eta ondoren saiakuntza bankuan kentzea posible izan da.

Bigarren atalean, balazta–enbragearen modelizazioari ekin zaio *squeal*ari dagokionez. Helburu honekin, sistema osoaren eredu bat garatu da eta lehengo AME bidez eta gero *squeal* frekuentzia esperimentalak ereduak aurreikusitakoekin konparatuz balioztatu da. Azkenik, aldaketa estrukturalak proposatzeko metodologia sistema errealari aplikatu zaio eta aldaketa teoriko batzuk planteatu eta aztertu dira.

Contents

List of Tables

List of Figures

Glossary

Symbols

$\mathbf{C}$	Damping matrix
$\mathbf{e}_i$	Unit vector in i
E	Energy, general
f	Frequency, Hz
F_N	Normal force
F_R	Friction force
k	Stiffness
$\mathbf{K}$	Stiffness matrix
$\mathbf{K_F}$	Stiffness matrix due to friction
m	Mass
$\mathbf{M}$	Mass matrix
P	Pressure
h_{ij}	Receptance function between points i and j
$\mathbf{H}$	Receptance matrix
T	Period
U	Strain energy
v	Speed
$\mathbf{X}$	Displacement vector

Greek symbols

λ	Eigenvalue
ν	Poisson's coefficient
μ	Friction coefficient
$\boldsymbol{\varphi}$	Eigenvector or mode shape

Acronyms

CEA	Complex Eigenvalue Analysis
DOF	Degrees of freedom
EMA	Experimental Modal Analysis
FE	Finite Element
FRF	Frequency Response Function
MAC	Modal Assurance Criterion
SI	Squeal Index

Chapter 1

Motivation

1.1 Introduction

Industrial brake–clutches show in some operating conditions high frequency noise similar to automotive brake squeal[1]. This is a major concern in industrial applications because compliance issues with current occupational health legislation [2]. Despite the fact that the techniques used for squeal prediction in automotive brakes can be potentially extended to analyse brake–clutch squeal, there is a need for a specific model that captures the distinctive features of this application, such as the ring shaped contact area and the asymmetric boundary conditions. Besides, as for automotive brake squeal, there is no standard methodology to suppress squeal from a brake–clutch that already presents it.

1.2 Definition of squeal noise

Squeal is a high frequency noise produced by self excited vibrations due to friction. In general, it is considered squeal noise ranging from 1 kHz to 20 kHz. It is divided into two categories depending on its frequency: *low frequency squeal* from 1 kHz to 3 kHz and *high frequency squeal* from 3 kHz to 20 kHz[2]. Squeal is characterised by being a pure tone, even if its amplitude can change through time [5], it has constant frequency content and a sound pressure higher than 70 dB [6]. Generally it is a non repetitive noise that can nearly be considered random and that appears at low speeds [7].

[1] In automotive clutches this high frequency noise is also known as *eek* [1]

[2] There is no uniform criteria for the separation of low frequency and high frequency squeal. Some authors divide the two types of noise regarding the number of nodal diameters of the disk [3]; other relate high frequency squeal to in–plane modes of the disk [4]

As squeal is the result of a dynamic instability in the system [8], it will always appear when any mechanism is able to store enough energy in a short period of time [9]. This can happen with a low excitation level at the less stable frequencies of the system or in any other if the excitation is sufficiently high, though it is usually necessary to get over a friction coefficient threshold around 0.3 for squeal to appear in a braking system [10].

1.3 Description of a brake–clutch

Typically, the role of a brake–clutch is to control the power transmission in a punch–press (Figure 1.1 (a)) by a series of alternating braking and clutch engagement manoeuvres. When the clutch is engaged, it forces the flywheel and the shaft to spin together; in turn, when the brake is engaged, it couples the lining holder on brake side with the rotor to stop the system (Figure 1.1 (b)). For safety reasons, at rest position the brake is engaged thanks to the force exerted by some springs and it is necessary to apply either pneumatic or hydraulic pressure to start the clutch–engagement manoeuvre.

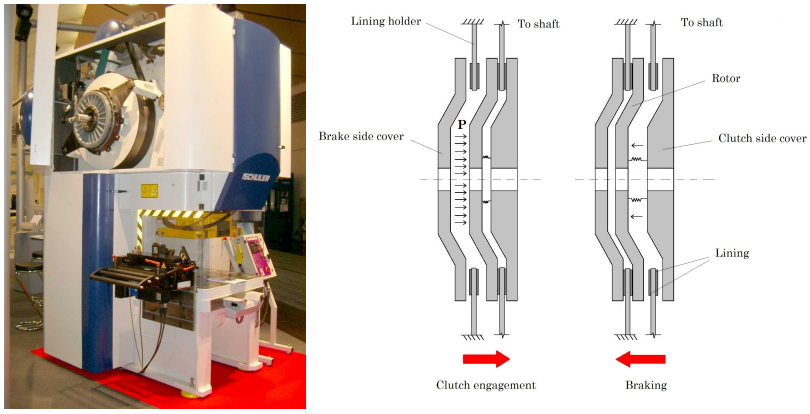

(a) (b)

Figure 1.1: (a) A brake–clutch in a punch–press, its typical application in industry; (b) schematic of the brake–clutch showing its main parts and functioning

Unlike in automotive brakes, the contact in brake–clutches occurs in a ring shaped area. Besides, as it is possible for the brake–clutch rotor to move axially, contact only takes place on one of the sides of the rotor depending on the manoeuvre. Accordingly, contact stiffness is different on each side due to the two different pressure application methods, the springs or the pneumatic pressure.

Another difference is that the application time of the normal force is much shorter in a brake–clutch than in an automotive brake, lasting only few milliseconds. It is for this reason that brake–clutch squeal is short lived even if it reaches high sound pressure values.

1.4 Objectives

After analysing the available literature, the development of a predictive model for brake–clutch squeal than can be used to propose structural modifications for squeal suppression is selected as research topic.

The following hypothesis is proposed:

> *Brake–clutch squeal appears due to mode coupling and therefore it is possible to predict its apparition only taking into account the dynamic features of the system, i.e. its mass, stiffness and damping and the friction coefficient. This implies that it is possible to suppress squeal by structural modifications.*

The following objectives are set to verify the hypothesis:

Objetive 1: Check the validity of the stability criteria in the frequency as a tool for brake–clutch squeal prediction.

Objetive 2: Confirm that the mechanism responsible for brake–clutch squeal generation is mode coupling, both theoretically and experimentally.

Objetive 3: Study the effect of structural modification in the frequency and amplitude of squeal.

Objetive 4: Analise the relative effect in stability of the dynamic features and the operating conditions, both theoretically and experimentally.

Objetive 5: Design a brake–clutch specific methodology for squeal prediction and suppression.

Objetive 6: Propose structural modifications for squeal suppression in brake–clutches.

1.5 Outline of the thesis

The thesis is structured as follows:

Chapter 1: Motivation: the problem of brake–clutch squeal is presented and the hypothesis and the objectives of the work are set.

Chapter 2: Literature review: a revision of the available literature is presented. Taking into account the reduced number of publications about brake–clutch squeal, the literature review is focused in brake squeal in other applications, mostly automotive. A critical review of the literature can be found at the end of the chapter.

Chapter 3: Description of the simple model of the brake–clutch: the tribometer based experimental and simulation model developed in this work is described in this chapter.

Chapter 4: Squeal simulation in the simple model: complex modes are computed and compared with experimental occurrences of squeal. Material properties, pressure and velocity dependent friction coefficient and friction damping are taken into account. The tests for obtaining the properties are also described.

Chapter 5: Structural modifications in the simple model: point modifications for squeal suppression based on the receptance method are proposed and tested in the experimental setup.

Chapter 6: Real brake–clutch model: the process for the development of a real brake–clutch model is described. The model is validated by correlating squeal simulation and experimental measurements in a brake–clutch test bench.

Chapter 7: Structural modifications in the brake–clutch: the procedure described in Chapter 5 is extended in order to propose theoretical point structural modifications for the real system.

Chapter 8: Conclusions: the main conclusions of the work are drawn.

Chapter 2

Literature review

2.1 Introduction

As literature regarding brake–clutch squeal is scarce, this literature review will mostly focus on automotive squeal, a comparable phenomenon that has been much widely studied. Literature referring to clutch squeal will be also reviewed when it is available.

The chapter starts with a description of different squeal generation mechanism proposed during the decades of brake squeal study. The most common approaches for addressing the problem will be presented afterwards, including the vibratory, tribological, acoustic and thermomechanical points of view. As this thesis focuses on squeal modelling and suppression, the typical methods for modelling found in literature will be revised, both theoretical and experimental. Finally, the most commonly used squeal suppression methods will be described.

2.2 Squeal generation mechanisms

There are five major theories to explain the origin of squeal noise, divided into three groups:

- The ones related to the tribological properties, such as **stick–slip** and **negative damping**
- The ones that have geometrical origin, **sprag–slip** and **modal coupling**, for instance.
- The one that states that the imperfections in the surfaces cause a **hammering** action that excites the natural frequencies and thus produces squeal

Some other theories can also be found, but they are not as widely accepted in the scientific community. A description of the evolution of these theories over time can be found in [11].

2.2.1 Stick–slip

The theory of stick–slip was the first one developed in order to explain the occurrence of squeal noise. The stick–slip phenomenon appears in multiple applications and its main feature is the saw tooth pattern in the speed – friction force curve (Figure 2.1) due to the differences between static and dynamic friction coefficients, being this the latter lower than the first.

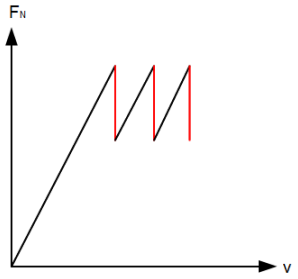

Figure 2.1: Typical speed – friction force curve under stick–slip conditions

Stick–slip is generally associated with vibrations in a wide frequency range, from 10^{-9} Hz to several thousands of Hertz, depending on the friction properties and elasticity of the system [4].

The most common model for describing stick–slip is shown in Figure 2.2, in which a little perturbation in a mass–spring–damper system can be amplified by the energy fed to the system from an external source, even with high damping. The amplitude of the perturbation grows until the speed of the mass and the conveyor belt are identical. This limit is known as the adhesion or stick state.

The process can be seen in Figure 2.3(a) in which is usually known as the *brush theory* and the stick–slip cycle is shown in Figure 2.3(b)[13].

Nowadays this theory has been abandoned except for explaining low frequency friction induced noise [3]. Still, the separation waves created during a stick–slip cycle are considered a possible excitation mechanism because of the hammering action they produce (see Section 2.2.5).

2.2.2 Negative damping

This theory, also known as *negative slope of the friction coefficient – relative speed curve*, relates squeal noise to an increase in friction coefficient as speed

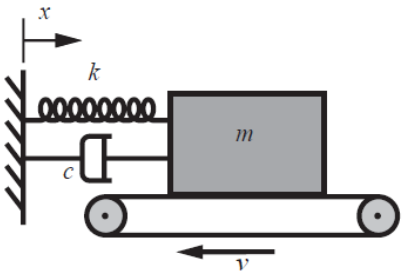

Figure 2.2: Model for explaining stick–slip and negative damping [12]

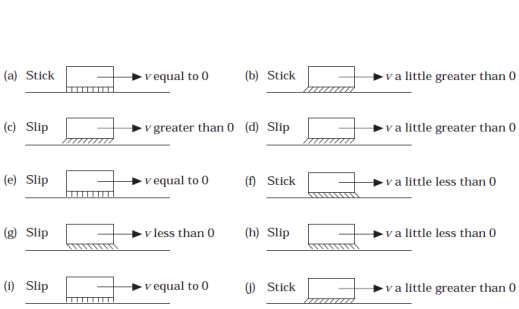

(a) Stick–slip process. Phenomenological model

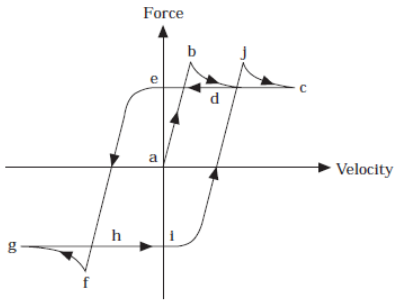

(b) Stick–slip cycle

Figure 2.3: Stick–slip

decreases. To consider this, one can use the system in Figure 2.2 in which friction coefficient has the form shown in Equation 2.1 [7]:

$$\mu = \mu_s \left(1 - \lambda \left(v - \dot{x}\right)\right) \tag{2.1}$$

Where μ_s stands for the static friction coefficient and λ for the slope of the friction coefficient – relative speed curve, which will be a positive number.

Therefore, the movement equation becomes, leaving out damping:

$$m\,\ddot{x} + k\,x = \mu_s\,F_N\left[1 - \lambda\left(v - \dot{x}\right)\right] \tag{2.2}$$

And after rearraging:

$$m\,\ddot{x} - \mu_s\,F_N\,\lambda\,\dot{x} + k\,x = \mu_s\,F_N\left(1 - \lambda\,v\right) \tag{2.3}$$

As λ is a positive number, the system presents negative damping, so it will destabilise. However, experimental observations contradict this hypothesis, since squeal can appear under constant friction coefficient. Thus, the hypothesis of negative damping is not enough to explain the origin of squeal noise.

2.2.3 Sprag–slip

Developed by Spurr in 1961, the sprag–slip theory was the first one to step aside from the main stick–slip hypothesis at the time. Unlike the previous theories, according to the sprag–slip theory, squeal can be originated even with constant friction coefficient. The instablity is due to reaching a limit value in friction force, which causes the system to get stuck in a concrete position. Thanks to the elasticity of the different elements the system can get out of this position provoking the repetition of the cycle. The instability depends on the value of the friction coefficient, normal force and friction force.

The model used to explain this phenomenon consist in a bar pinned in its upper end and with its lower end leaning and sliding onto a moving plane. The bar is under the effect of a external force L in its lower end (Figure 2.4).

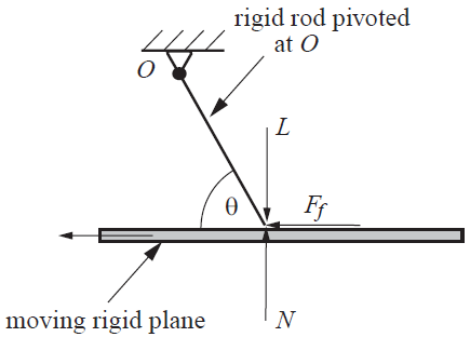

Figure 2.4: Model to explain the sprag–slip mechanism [12]

In this case, the value of the friction force will be:

$$F_R = \frac{\mu N}{1 - \mu \tan\theta} \tag{2.4}$$

It is easy to see that, when the friction coefficients reaches que critical value of $\mu_{lim} = \frac{1}{\tan\theta}$, the bar stops moving.

As this model is very far from a real brake, several researchers added new features to it in order to make it resemble the real system. The first ones were Jarvis and Mills, by means of their pin–on–disk model [14], which actually was the first

model for the theoretical treatment of sprag–slip [12]. They were followed by Earles, who connected instability with the attack angle of the pin on the disk [7].

This theory has been combined with others to better explain the phenomenon, for instance, Murakami developed a model that included both negative damping and sprag–slip in 1984. After a theoretical and experimental analysis, he concluded that for squeal to occur a particular combination of friction force, material properties and geometry should take place [15].

Even though it is possible to find sprag–slip in real systems and that it can explain how the out–of–plane modes are excited by the in–plane modes [7], the difficulty of modelling limits it applicability. It is useful, though, to explain the physical phenomenon behind certain vibrations where the other mechanims fail to give a satisfactory explanation [4].

2.2.4 Mode coupling

The first one to propose this new mechanism for squeal generation was North first in his 1972 article [16] with a 8 DOF system and later in 1976 using a 2 DOF model (Figure 2.5). He suggested that the instability existent in brakes could be assimilated to *flutter*, the coupling between translational and rotational degrees of freedom that occurs in plane wings. In the specific case of a brake, this instability would come from the coupling of two vibration modes of the system.

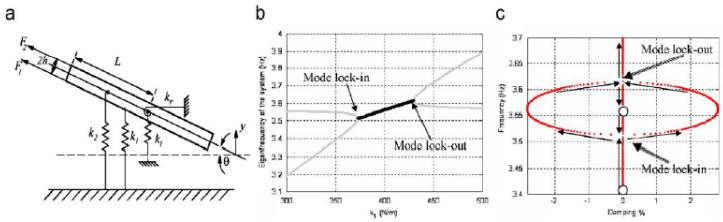

Figure 2.5: 2 DOF model proposed by North (a) Description of the system. (b) Mode coupling depending on k_1. (c) Mode coupling depending on damping [17]

In order to understand the mechanism, the system shown in Figure 2.6 is proposed in [18]. This model represents a two degree of freedom system in which a point mass slides over a conveyor belt moving at constant v_B speed. Springs k_1 and k_2 hold the block in its position and k_3 stands for the contact stiffness. The friction coefficient μ between the mass and the conveyor belt is constant. This model is basically a the model used for explaining stick–slip in Section 2.2.1.

In this case, the movement equations of the system are:

$$\begin{bmatrix} m & 0 \\ 0 & m \end{bmatrix} \begin{Bmatrix} \ddot{x} \\ \ddot{y} \end{Bmatrix} + \begin{bmatrix} k_{11} & k_{12} \\ k_{21} & k_{22} \end{bmatrix} \begin{Bmatrix} x \\ y \end{Bmatrix} = \begin{Bmatrix} F_R \\ F_N \end{Bmatrix} \tag{2.5}$$

where:

$$
\begin{aligned}
k_{11} &= k_1 \cos^2 \alpha_1 + k_2 \cos^2 \alpha_2 \\
k_{12} &= k_{21} = k_1 \sin \alpha_1 \cos \alpha_1 + k_2 \sin \alpha_2 \cos \alpha_2 \\
k_{22} &= k_1 \sin^2 \alpha_1 + k_2 \sin^2 \alpha_2 + k_3
\end{aligned}
\tag{2.6}
$$

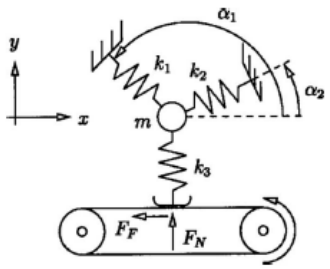

Figure 2.6: Simplified model for explaining mode coupling

If the mass of the block is much lower than the mass of the conveyor belt, normal force can be estimated as $F_N = k_3\, y$ and, therefore, friction force will be $F_R = \mu\, k_3\, y$. Thus, the equation of motion becomes:

$$
\begin{bmatrix} m & 0 \\ 0 & m \end{bmatrix} \begin{Bmatrix} \ddot{x} \\ \ddot{y} \end{Bmatrix} + \begin{bmatrix} k_{11} & k_{12} - \mu\, k_3 \\ k_{21} & stiff_{22} \end{bmatrix} \begin{Bmatrix} x \\ y \end{Bmatrix} = \begin{Bmatrix} 0 \\ 0 \end{Bmatrix} \tag{2.7}
$$

This system of equations represent an eigenvalue problem with the paricularity that the stiffness matrix is asymmetric. Due to this asymmetry eigenvalues are complex and, depending on the value of the friction coefficient, modes can couple.

This effect can be seen in Figure 2.7 where the evolution of the real and the imaginary part of the eigenvalues with increasing friction coefficient is shown. Initially, there are two different modes at two different frequencies and the real part of both of them is zero. Once a critical μ value has been reached, the modes couple, i.e they occur at the same frequency. In addition, one of them is stable as the real part of its eigenvalue is negative and the other is unstable, owing to the positive real part of the eigenvalue.

For a real brake system the mode coupling process has been described in [19]. It goes as follows:

1. The rotor and the pads experiment normal and tangential forces in the interface. These forces present a uniform distribution during static contact, but develop a non-uniform distribution when there is relative movement.

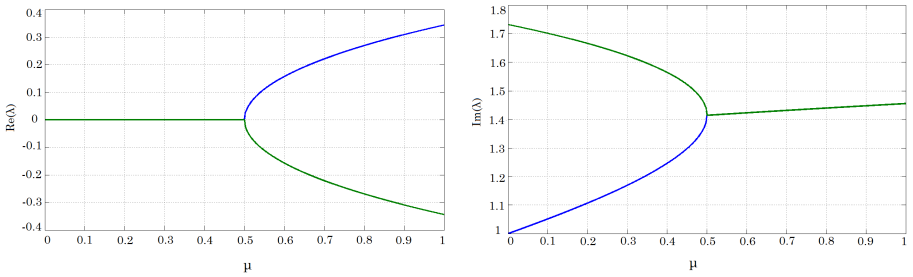

(a) Evolution of the real part of the eigenvalue with μ

(b) Evolution of the imaginary part of the eigenvalue with μ

Figure 2.7: Mode coupling caused by friction

2. The tangencial forces that appear in the contact because of friction produce in–plane vibrations in the disk. The combination of these in–plane vibrations together with the deformation of the surface alter the contact area changing the initially constant friction force. Besides, even though the normal force remains constant, the friction force causes a torque respect the support of the pads which leads to vibration in the pads.

3. Both effects excite the bending modes (out–of–plane) of the rotor and the pads.

The result is that the system vibrates at one of its natural frequencies and the pertinent harmonics [20]. Certain modulation in time can also appear due to temporal variations in the friction force [21].

From the mode coupling point of view, squeal can be divided into two categories: the one due to the coupling of modes of different components of the systems and the one known as rotating squeal, due to the coupling of a doublet mode [22,23].

Nowadays mode coupling is accepted by the majority of the scientific community as the explanation for squeal — the rest of the theories are used as auxiliary mechanisms.

2.2.5 Hammering

Hammering is one of the most recent theories for explaining squeal noise generation, it appeared for the first time in 1989 [24]. It claims that the imperfections in the surface of the rotor cause a hammering action that excites the natural frequencies of the disk and produces squeal [9]. It came out because nor negative damping neither sprag–slip could explain satisfactorily the excitation process, they only describe the conditions under which squeal would arise [12,24]. As with these two last theories, according to hammering squeal can happen even if the friction coefficient is constant.

The imperfections that act as excitation mechanism can come from any type of distortion, ranging from non-uniform wear of the surface of the disk to thermal distortion (see Section 2.3.4). Thus, this theory gives an explanation to polishing the disk as a means to eliminate squeal, since this process would remove any possible imperfection and, thus, any chance to excite the system.

2.2.6 Other theories

There are some other theories that are not as widely accepted as an explanation to the squeal phenomenon. Their main features are presented briefly below:

Parametric resonance

It happens when the system gets excited as a consequence of a variation in its parameters. As a result, combination resonances appear, both of the sum and difference type, because of the action of the friction force that can destabilise the system. An example of this mechanism can be found in [25].

Moving loads

Moving loads can put the system under resonance even if they have constant value [9]. In [26], for instance, the friction force is treated as a moving load, reaching the conclusion that it has a destabilising effect. Moving loads are not normally taken into account as they make computation time grow considerably.

Thermoelastic Instability (TEI) and Thermoelastodynamic Instability (TEDI)

The main point of this theory is that friction causes a feedback process that can be unstable: the thermoelastic deformation produces high pressure areas which, then, get hotter originating hot spots that, in turn, deform more... repeating the cycle again [27,28]. In general, the thermal – dynamic interaction is not addressed, supposing that these two effects occur in different time scales, but according to [29], a little coupling between these two responses can destabilise systems that uncoupled were stable

Stick–slip separation waves

In continuous sliding, self-excited waves appear due to the destabilisation of the sliding waves [19]. This phenomenon can be understood as a kind of hammering, since it comprises a series of impulses acting in the friction interface [12]. An analysis of this mechanism can be found in [30].

Chaos

This theory states that squeal arises when the system reaches chaotic conditions, being chaos a sufficient but not necessary condition for squeal to appear, as it can also take place in systems that present linear behaviour [31].

2.3 Approaches for addressing squeal

Squeal is a problem affected by multiple factors and that ranges from the microscopic to the macroscopic scale. This fact makes it a difficult problem to tackle, on the one hand, because the effect of the different factors is not sufficiently known and, on the other, because depending on the approach employed the conclusions reached differ or, worse, conflict.

That said, squeal can be approached from different perspectives, vibratory, tribological, acoustic or thermomechanical points of view can be chosen. Among all the approaches the vibratory one is the most common and for which all the computation methods have been developed.

2.3.1 Linear and nonlinear vibratory approach

Most of the research relating to squeal belongs to this field, specially to the linear case. Mainly the relation between squeal and the system modes and their coupling is studied, both in simulation models and test benches.

A linear analysis consists in a linearising the system around the equilibrium position. This kind of analysis can tell if a system will be unstable or not, but it cannot determine the amplitude of the unstable vibration. Even if a system is unstable it is possible that the limit cycle the system evolves to has such a little amplitude that does not produce audible noise. Thus, it is not possible to decide only using a linear analysis whether the instability in question would be a problem or not [32]. The issue here is that there are not analytical solutions for nonlinear systems — or, incidentally, for systems parametrically excited — so it is inevitable to resort to numerical techniques.

For the nonlinear case, squeal is usually connected to a Hopf bifurcation [33] and the *Averaging Method* [34] and the *Harmonic Balance Method* are used for studying it [35,36].

Both the effect of rotating speed and damping are usually ignored when studying squeal, except for the case that the objective of the work is precisely the analysis of the effect of these factors in the system. The gyroscopic effect is also ignored since the apparition of squeal is related to low speeds, so it is argued that the terms that it would add to the computation would not be meaningful [37]. Giannini offers a different perspective on the subject in [38], as it concludes

that not taking into account the gyroscopic terms overlooks some of the possible instabilities and reduces therefore the quality of the prediction.

Regarding damping, it is assumed that a system with no damping is always more troublesome that a damped one, this way the safety of the results is guaranteed. On the subject of damping it has also to be said that it reduces the amplitude of the vibration but at the same time it increases the frequency range in which two modes can couple [39,40]. In [35] the effect of damping in the coupling of the modes is analysed, reaching the conclusion that whilst increasing damping in the two unstable modes equally reduces squeal, a disproportionate increase of damping raises the risk of instability. The same results are obtained in [32] in a 2 DOF system, in [41] in a beam–on–disk model, in [17] in a simplified test bench and in [42] in a FE model of a real brake.

An aspect that should be taken into account is the double role played by the friction. It introduces a negative damping that cause the destabilisation of the system and, at the same time, includes a positive damping term that stabilises the system and reduces the overprediction when complex modes are computed [43] (see Section 2.4.2).

Besides, the rotation of the disk stiffens the system and thus increases its natural frequencies [7] as shown in Equation 2.8

$$f^2 = f_0^2 + \lambda\,\Omega^2 \tag{2.8}$$

Where f_0 stands for the natural frequency of the system in static conditions, Ω represents the rotating speed and λ is a coefficient.

Moreover, according to [44] the gyroscopic effects can induce mode coupling and reduce the stability of the system.

Both effects are treated together in [45], concluding that if damping is proportional, gyroscopic effect can be neglected. If damping is not proportional this does not apply.

2.3.2 Tribological approach

The main reason to relate squeal to tribology is that the only features that change fast enough and so unpredictably are the surface condition and the friction properties [46].

Hence, squeal is linked to the evolution of the contact surfaces or *contact plateaus* [46–48]. These surfaces are defined as the zones in the pad that show sliding contact signs. Their most distinctive feature is a flat area grooved in the sliding direction. They are created due to the heterogeneity of the friction material, whose components have very different resistances to wear which makes the contact happen in localised areas.

In [46] contact plateaus are classified into *primary* and *secondary* plateaus. The first appear when the less resistant material wears off, these are the areas where only the hardest material remains. The second are created by aggregation starting from the primary plateaus (Figure 2.8). The valleys that surround these contact plateaus are formed by the less wear resistant materials, such as resin and filler material, and get wore by third body abrasion. These particles are, on the one hand, the ones that degrade the contact plateau and, on the other, the ones that will create them when they reach a sufficiently small size.

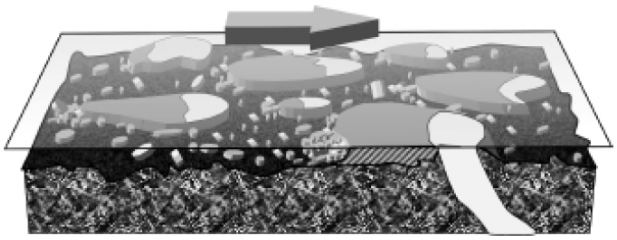

Figure 2.8: Primary and secondary contact plateaus according to the sliding direction [46]

The development and destruction of contact plateaus would explain the changes in the friction behaviour in the system and, thus, would have a major role in squeal generation. According to [47], pads that have many small contact plateaus are more prone to squeal that pads with less contact plateaus but of a bigger size. Following this idea, a *critical plateau area* of $0.01\,\mathrm{mm}^2$ is defined below which squeal would appear.

Besides, a squeal index γ can be defined only based on the superficial features of the disk and that could be used for computing the propensity of a system to squeal [49]:

$$\gamma = \sqrt{\frac{\sigma}{\beta}} \tag{2.9}$$

Where σ stands for the standard deviation of the asperity height and β is the average asperity radius. Then, values of γ higher than 0.1 mean that squeal will not develop under any normal force and relative speed combination. A squeal index lower than 0.1 is related to the possible apparition of squeal, being it more likely when the value is lower.

During the wear process, the average radius of the asperities gets reduced and the standard deviation of the height of the asperities increases so squeal disappears. The explanation to this process according to the author is the tear off process that the low stiffness elastic asperities suffer by action of fatigue [17,49,50] and impact against other asperities.

Despite this, it is possible to cause and suppress squeal only changing the macroscopic parameters of the system, so it could be said that the superficial state is a consequence of squeal rather than its trigger [50]. This goes in line with [19], where it is said that, when the coupling between two components is low, the surface effect is considerable, but when coupling increases, the system moves in one particular mode. The mode in question will vary depending on the geometry, the sliding speed and the normal force, parameters not related to tribology.

2.3.3 Acoustic approach

The first one to study the acoustic radiation of a brake was McDaniel [51] that in 1999 that measured the velocity in a brake under squeal conditions using a laser vibrometer and used these measurements for the computation of the radiation efficiency and sound intensity. The conclusion reached in the aforesaid study is that the disk is the main contributor to acoustic radiation, being transverse speed the culprit even though in–plane force was much larger than out–of–plane force. It can be inferred therefore that a critical factor in the radiation features of the system is the coupling between in–plane and out–of–plane movements.

Besides, Lee represented in his PhD thesis [52] the disk as an annular disk and he studied the effect of structural mode coupling in the acoustic radiation. He concluded that the radiation efficiency changes when coupling occurs, but only if the coupled modes have the same number of nodal diameters.

To finish with the acoustic approach, the work of Oberst and Lai in this field must be highlighted. In [53] they performed the computation of the acoustic power and radiation efficiency of pin–on–disk and pad–on–disk models by both finite elements and boundary elements; in [54] they analysed the effect of pressure and friction coefficient in acoustic radiation and in [55] they compared different acoustic computation methods for squeal application. Apart from this all, in [56] a guide to compute the sound radiation of automotive brakes can be found, where the effect of different contact algorithms, element size and computation methods in the obtained sound pressure are discussed. In spite of this, the acoustic of brake squeal is not a highly developed field.

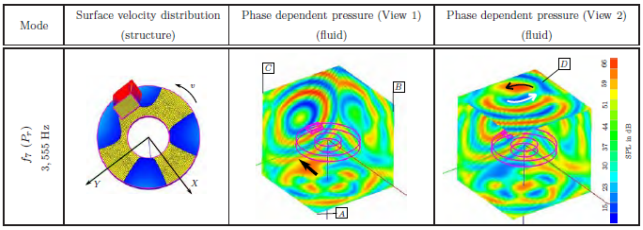

Figure 2.9: Computation of pressure and velocity in [56]

2.3.4 Thermomechanical approach

Thermal distortion is a key feature in the hammering theory [24]. Besides, the generation of hot spots is usually linked to thermoelastic instability (TEI). This instability occurs when the effect of thermal distortion due to friction induced heat and the fact that in real conditions contact happens in a localised area get combined. Thus, the distortion causes the high pressure areas to grow but at the same time as these areas are more prone to wear, they get reduced. In balance, the growth rate of the contact areas due to thermal distortion and the decline rate of the areas by wear are equal, but if wear is not able to balance the growth of the contact area, instabilities may occur. This effect is only taken into account in theoretical or simplified models, such as [57] or [29].

Another way to take account of temperature in squeal computations is by its effects in the rest of the parameters. For instance, in [58] a temperature dependent friction coefficient is introduced in a finite element model and a complex eigenvalue analysis is performed (see Section 2.4.2). The number of unstable modes predicted is reduced in a 60%, so the predictive ability of the model increases thanks to the introduction of temperature as a variable.

Despite this evidence, the effect of temperature is not usually taken into account in squeal modelling due to the high computation time involved [59].

2.4 Theoretical methods

Various theoretical methods exist for the study of squeal. The reason is that they allow to simulate different structures, materials and operative conditions before developing a prototype. In addition, with the help of a theoretical model is easier to understand the results obtained in an experimental bench [59].

With this in mind, in order to tackle the occurrence of squeal in a particular system first a model that precisely expresses the features of the system under study should be developed and, afterwards, the criterion for deciding if a system will suffer or not squeal has to be selected. This section will first describe the types of model found in the literature. A description of the most common criteria for deciding if a system will be prone to squeal or not will follow.

2.4.1 Model types

As stated in [8], the process for developing a model for squeal is the following:

1. Propose a model that adequately represents the real system. it can include damping or not.

2. Write down the equations of movement taking into account all the effectS under consideration

3. Find the parameters that destabilise the system

4. Try to find out the relationship between the effect of a change in the destabilising parameter and the features of the real brake

In general, the models obtain good results when in the first three steps, but are less successful in the last one.

The models can be divided into two categories [18]:**(i)** the ones that are used for understanding the phenomenon, mostly lumped or distributed parameter models and **(ii)** the ones that come from the simplification of the real system and that are usually analysed by finite elements. The first habitually include effects such as a pressure and speed dependent friction coefficient or anisotropic friction material. The latter, on the contrary, are usually limited to constant friction coefficient and isotropic materials (Figure 2.10).

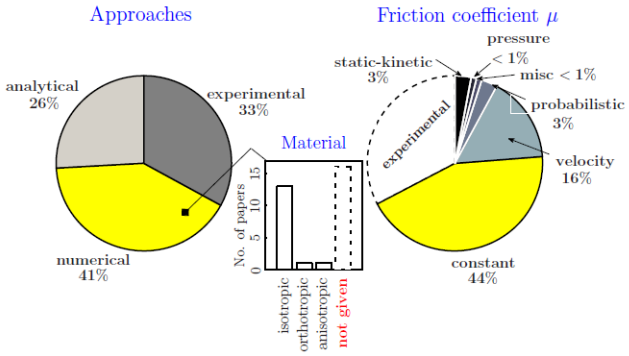

Figure 2.10: Approaches of published papers. Adapted from [56]

Lumped or distributed parameter models

Their fundamental purpose is explaining the origin of squeal and analysing the effect of different parameters in its evolution [16,18,18,20,32,60–62] or trying out suppression techniques [63]. They can also be developed from experimental results as in [64] where an automotive brake is modelled by a 4 DOF system using vibration data from holography.

In [65] a review of 2 and 3 DOF models can be found and in [12] a extensive review of different models is carried out.

Within the distributed parameter models, the circular [51] and annular plates [52] should be highlighted. These models are used as a simplification of the rotor

for understanding mode coupling between in–plane and out–of–plane modes and for computing the radiation efficiency of the system.

As for clutch models, most papers about clutch noise focused on either low frequency noise [66–68] or thermoelastic effects [69,70]. Regarding high frequency noise (up to a few kHz according to [33]), two models can be highlighted: **(i)** the 6 DOF squeal model presented in [71] in which mode coupling instability is studied and which has been validated with experiments (Figure 2.11) and **(ii)** the 2 DOF nonlinear model of a squealing clutch in [33] and [72] in which the effect of friction forces and gyroscopic action in mode coupling is analysed. Despite these efforts, according to [73] nowadays there is no industrial model in the literature for studying squeal in clutch systems.

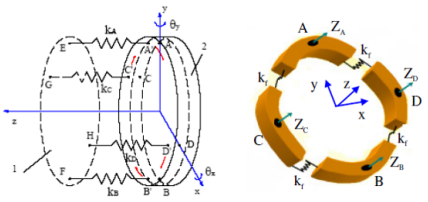

Figure 2.11: 6 DOF clutch model proposed in [71]

In a negative note, the problem of the simplified models is that they can push the simplification process too far and neglect important effects, losing their reliability [74].

Finite element models (FE)

Nowadays Finite Element Analysis is an essential tool for the study of squeal since is the only way to simulate a real system and observe the effects of design changes without producing prototypes. Despite this, it is not possible to introduce every single complexity in a model yet because the computation time required would be unacceptable. In general, the results obtain in FE models are not considered valid without subsequent experimental validation.

For example in [11] and [75] the process of development of a finite element model of the braking system and its validation by experimental modal analysis is described.

There is also the possibility of modelling by FE the simplified test bench as occurs in [76] where a linear and a nonlinear model of a pin–on–disk are developed for comparing numerical and experimental results.

2.4.2 Stability criteria

Once the model has been created, a criterion for deciding whether the model is stable or not has to be selected. The most common are presented below.

Frequency domain: Complex Eigenvalue Analysis (CEA)

Complex Eigenvalue Analysis consist in studying the real part of the eigenvalues of the system. These eigenvalues are complex because friction causes the stiffness matrix to be asymmetric. If any of these real parts is positive the system will be unstable, otherwise, when the real parts of all the eigenvalues are negative, the system will be stable.

An option for computing the complex eigenvalues and eigenvectors is using the so called *Subspace Projection Method* that computes the eigenvectors of the symmetric matrix, i.e. without taking into account the effect of friction, and uses these values for projecting the matrices in the following way:

$$\mathbf{M}\,\ddot{\mathbf{y}} + \mathbf{C}\,\dot{\mathbf{y}} + (\mathbf{K} + \mathbf{K_F})\,\mathbf{y} = \mathbf{0} \tag{2.10}$$

$$(\lambda^2\mathbf{M} + \lambda\mathbf{C} + \mathbf{K})\,\mathbf{y} = \mathbf{0} \tag{2.11}$$

$$\mathbf{M}^* = [\boldsymbol{\varphi}_1, \boldsymbol{\varphi}_2, ..., \boldsymbol{\varphi}_n]^T \mathbf{M}\,[\boldsymbol{\varphi}_1, \boldsymbol{\varphi}_2, ..., \boldsymbol{\varphi}_n] \tag{2.12}$$

$$\mathbf{C}^* = [\boldsymbol{\varphi}_1, \boldsymbol{\varphi}_2, ..., \boldsymbol{\varphi}_n]^T \mathbf{C}\,[\boldsymbol{\varphi}_1, \boldsymbol{\varphi}_2, ..., \boldsymbol{\varphi}_n] \tag{2.13}$$

$$\mathbf{K}^* = [\boldsymbol{\varphi}_1, \boldsymbol{\varphi}_2, ..., \boldsymbol{\varphi}_n]^T (\mathbf{K} + \mathbf{K_F})\,[\boldsymbol{\varphi}_1, \boldsymbol{\varphi}_2, ..., \boldsymbol{\varphi}_n] \tag{2.14}$$

Where $\boldsymbol{\varphi}_i$ stands for the eigenvectors of the symmetric system and $\mathbf{M}^*$, $\mathbf{C}^*$ and $\mathbf{K}^*$ the matrices projected in the subspace defined by the real eigenvectors.

Then, the system $(\lambda^2\,\mathbf{M}^* + \lambda\,\mathbf{C}^* + \mathbf{K}^*)\,\mathbf{y} = \mathbf{0}$ is solved and the complex eigenvalues and eigenvectors are obtained.

This method has the advantage that all the possible squeal frequencies are obtained in only one run — which of them will get activated in reality depends on the conditions the system is subjected to. The method can be considered to be conservative, then. In addition, it allows to study the sensibility of the system to a variation in its features such as damping, friction coefficient or working conditions.

Its main drawback that it does not into account the nonlinearities in the system as it is a linear method and it cannot predict the behaviour of the system after the onset of squeal. But, it can be applied in any of the models described in Section 2.4.1.

This method requires a good modelling of the boundary conditions and joints between elements. It is also heavily dependent on the type of contact introduced, the algorithm for the computation of the eigenpair and to the inclusion of

damping or wear of the friction material [43]. In short, it is a useful tool for the design process as it is capable to identify the possible unstable modes, but it is not valid to study the evolution of the system far from its equilibrium point.

The Complex Eigenvalue Analysis is by far the most extended method for squeal prediction in the automotive industry [6].

Time domain: transient analysis

A transient analysis simulates the behaviour of the system in time. The stability is checked analysing the evolution of the amplitude of the movement. In this case the differential equations of movement are directly solved using numerical techniques. Once the movement of the system is computed, the squeal frequencies can be obtained by the Fourier transform [3].

This methods allows the inclusion of any kind of nonlinearity such as variable contact area, time dependent material laws and friction coefficient or follower forces. In exchange, the computation time is much higher and, therefore, the possibility for trying various designs reduced.

The numerical methods for transient analysis can be either explicit or implicit, as long as it is taken into account that the step size for explicit computation should be very small if high frequencies have to be studied as the method is conditionally stable.

Energetic analysis

Feed–in energy

When the system gets stuck in a unstable mode, part of the friction energy is transformed into vibration energy. This energy, called *feed–in energy* [77], is added to the system due to the relative movement in the friction interface during a cycle. It is computed as the integral of the work undertaken by the friction force in a cycle. Then, if the feed–in energy is positive, the vibration energy in the system increases and, therefore, the system is unstable.

The feed–in energy for any pair of points (a, b) involved in a frictional contact in a period and in a given direction is computed by:

$$E_{abi} = \int_0^T F_{ia} \left(\dot{x}_a - \dot{x}_b \right) \mathrm{d}t \quad / \quad i = x, y, z \tag{2.15}$$

Where F_{ia} stands for the friction force in point a. The total value of the feed–in energy is the summation of this value for every point and every direction.

A similar energetic criterion can be found in [61] where the squeal is linked to the growth of the kinetic energy in a cycle:

$$E_k = \oint \dot{\mathbf{X}}^{\intercal}\,\mathbf{M}\,\ddot{\mathbf{X}}\,\mathrm{d}t \;>\; 0 \tag{2.16}$$

Strain energy

Strain energy is the energy stored by a system undergoing deformation. It shows how much of the vibration belongs to a particular element [75,78]. For an element i in a finite element model strain energy is computed as:

$$U_i = \frac{1}{2}\,\mathbf{X}_i^{\intercal}\,\mathbf{K}_i\,\mathbf{X}_i \tag{2.17}$$

Where $\mathbf{K}_i$ stands for the stiffness matrix and $\mathbf{X}_i$ for the displacement vector.

The energy of a component is the summation of the energy of the elements that comprise it:

$$U_{component} = \sum_{i=1}^{N} U_i \tag{2.18}$$

Knowing the value of the strain energy, it is possible to identify the most active element in a particular mode shape. It has the problem, though, that when comparing the energy of the components their dimensions and their material properties have to be taken into account.

Modal participation

Indicators such as MPF (*Modal Participation Factor*) serve as tool for identifying the elements that participate the most in the movement of the system [75]. MPF is defined as:

$$\mathrm{MPF}(\boldsymbol{\varphi}_1, \boldsymbol{\varphi}_2) = \frac{|{\boldsymbol{\varphi}_1}^T {\boldsymbol{\varphi}_2}^*|}{({\boldsymbol{\varphi}_1}^T {\boldsymbol{\varphi}_1}^*)({\boldsymbol{\varphi}_2}^T {\boldsymbol{\varphi}_2}^*)} \quad / \quad \mathrm{MPF} \in [0, 1] \tag{2.19}$$

Where $\boldsymbol{\varphi}_1$ and $\boldsymbol{\varphi}_2$ are two movement vectors whose similarity is object of study. The higher the similarity of the movement vectors the closer the MPF to unity.

Using the MPF the components that form a unstable complex mode of the system can be identified. This way, the properties or the geometry of the most critical element can be modified so as to avoid coupling.

Wavelets

If the squeal frequencies change in time the Fourier transform does not give good results. In this case, another possibility is using the wavelet transform, in which frequency variations are shown as local maxima in the transform.

A wavelet is a wave that spans a particular range in both time and frequency. The amplitude and phase difference of this kind of waves can be adapted to generate any other function, in a similar way to the Fourier transform, with the advantage that they are useful for transient processes.

Using the wavelet transform figures like Figure 2.12 are obtained where the colour scale stands for the coefficient for a given time and frequency.

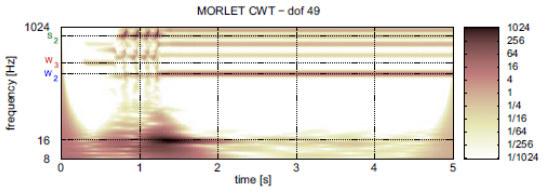

Figure 2.12: Wavelet transform

The wavelet transform is applied to the study of squeal in [79] and [80].

Stochastic methods

Stochastic methods appear in the study of squeal in two contexts. On the one hand, they are used for creating distributions of different parameters (roughness of the surface [81,82], porosity [83], material properties [84],...) and resorting to Monte Carlo methods for the interpretation of the results. A procedure for introducing uncertainties in squeal modelling can be found in [85].

The main drawback of this kind of analysis is the huge amount of data and computation time required, but they allow an improved correlation between experimental and numerical methods. For example, in [84] the dispersion in material properties, damping and pad surface topography are taken into account in a CEA analysis with the outcome of a dramatical improvement in prediction (Figure 2.13). A way to reduce the computation time is reducing the model using the methods proposed in [86] or [87] that are designed specifically for squeal.

The other context in which uncertainty appears in squeal modelling is in its relation to chaos (see Section 2.2.6). If squeal is identified as a chaotic process, small changes in the initial conditions can cause completely different responses. For this reason, the uncertainty in the input parameters should be taken into account in the computations to achieve accurate results [31].

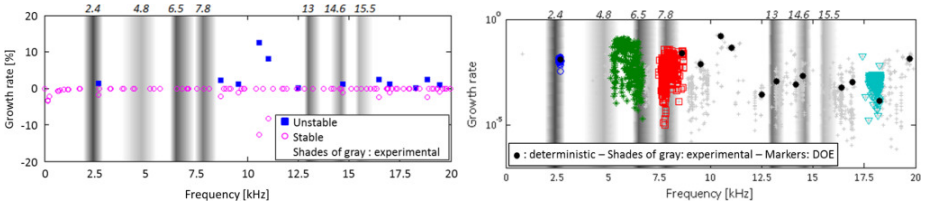

(a) CEA before introducing uncertainties (b) CEA after introducing uncertainties

Figure 2.13: Effect of uncertainties in CEA [84]

The objective in both cases is to develop a robust theoretical model that is not affected by uncertainty [88]. In Figure 2.14 a design cycle to obtain a robust model is shown.

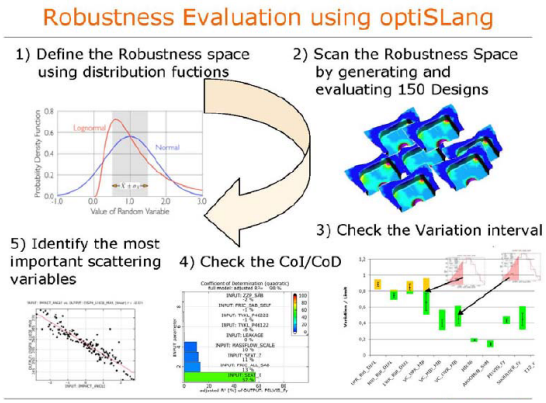

Figure 2.14: Robustness analysis cycle according to [88]

2.5 Experimental methods

Experimental methods are widely used for the study of squeal despite their many drawbacks. This methods are expensive, based on trial a error, can only reach limited solutions and the conclusions drawn are not translatable to other geometries. Still, the results obtained by experimental means are more useful than the ones reached by theoretical methods, even if these methods are becoming more advanced [8]. The impossibility of including the effect of all the factors involved in squeal generation together with the lack of understanding of them implies that experimental methods have to be used, leaving the theoretical methods for a first stage of design [3].

This said, the main types of experimental setups for squeal will be described.

The test benches for squeal can be divided into two groups:

- The *simplified benches*, in which the different parts of the system are represented by simple elements. Pin–on–disk, beam–on–disk and tribometer test belong to this group
- The *dynamometer* test setup in which the real system is used and the effect of the surrounding elements is modelled as inertia. It is specially used in the automotive brake industry.

2.5.1 Simplified test benches

The main motivation for designing a simplified test bench is reducing the number of the variables that can affect the system.

Simplified test benches have the advantage that as their geometry is simple, the problem with joints disappear and the measurements are more repetitive. Besides, a test bench is specifically designed for studying certain aspect of squeal so placing the transducers for measuring the variables of interest is easy. In turn, the drawback is that the results are not directly translatable to a real system.

In short, simplified test benches do not reproduce all the causes of squeal but at least some of them can be studied. In addition, as always is possible to design a system that reproduces the features to study, this kind of test benches is useful for verifying design changes.

The following sections describe the most typical simplified test benches for squeal analysis: the pin–on–disk, the beam–on–disk and the tribometer [17].

Pin–on–disk

Pin–on–disk test benches have the advantage of generating squeal in a simple configuration. They are comprised of a rotating disk that supports the pin (Figure 2.15). The first pin–on–disk for squeal applications was designed by Jarvis and Mills in 1963 to explain sprag–slip (see Section 2.2.3).

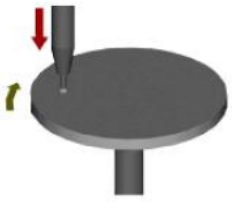

Figure 2.15: Pin–on–disk [89]

From then on that configuration has been used multiple times for explaining different features of squeal. For example, in [90] and [91] it is used to verify the hypothesis of mode coupling and in [89] the effect of 4 parameters — applied force, rotating speed, roughness and Young modulus — in squeal generation is studied using a DOE.

The main finding relating squeal in pin–on–disk setups are summarised in Table 2.1

Table 2.1: Summary of the main findings in pin–on–disk setups. Adapted from [92]

Author	**Main findings**
Earles & Soar	Confirmation of sprag–slip
Earles & Badi	Abrupt changes in acceleration Fugitive nature of squeal High parameter sensitivity
Earles & Chambers	Damping does not eliminate instability Nonlinear behaviour Intuitive predictions impossible
Tworzydlo et al.	Verification of mode coupling mechanism Influence of dynamic characteristics and friction coefficient No dependency of μ – v negative slope Harmonics due to limit cycle Surface damage
Chen et al.	Squeal due to negative slopw μ – v curve No mode coupling
Chen et al.	Time delay between normal and friction force responsible for squeal
Neis et al.	Stick–slip Increase of stiffness and rotating speed: increases vibration frequency but decreases vibration magnitude Effect of damping is stiffness dependent

Beam–on–disk

The beam–on–disk setup is the natural evolution of the pin–on–disk test bench. It opens the way to mode coupling by adding a new flexible element: the

beam. A beam–on–disk bench consists in a beam supported in a rotating disk (Figure 2.16). The normal force, attack angle and the length of the beam can be changed.

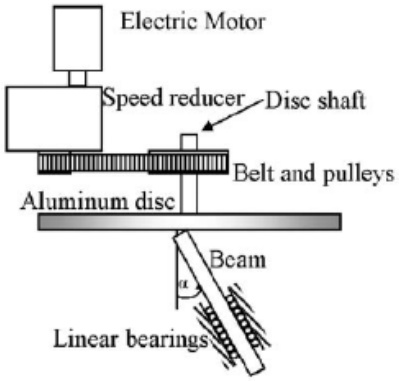

Figure 2.16: Beam–on–disk [17]

Friction force, that acts tangential to the surface of the disk, will excite the in–plane modes. At the same time, bending waves will be appear in the beam due to friction. As a consequence, the disk will be excited by a fluctuating normal force that will excite its bending modes. This process can cause instabilities. The effect is amplified when the contact angle between the beam and the disk is acute against the direction of movement. In addition, if the in–plane and out–of–plane frequencies of the disk are near it is easier to transfer energy from a mode to another and that the bending modes are excited because of friction [19].

Beam–on–disk benches for studying squeal are used, for example, in [81], [7] and [41]. The main findings are summarised in Table 2.2.

Table 2.2: Summary of the main findings in beam–on–disk setups. Adapted from [92]

Author	**Main findings**
Jarvis & Mills	Sprag–slip with constant μ due to geometrical coupling Amplitude of oscillation controlled by contact loss
Tarter	Slotted rotor for squeal suppression Importance of pad material and geometry
Suganami et al.	Squeal due to in–plane vibrations
Akay et al.	Squeal frequency related to natural frequencies of the parts

Author	Main findings
Tuchinda et al.	Response classified into 3 categories: stable, damped and unstable mode Type of response depends on the phase difference between the frictional force and response
Allgaier et al.	Determination of excitation energy per cycle the unstable amplitude growth Amplitude growth rate dependent on the normal load and low dependence on the disc speed
Cantone & Massi	Homogeneous damping reduces system response and propensity to generate squeal Non-homogeneous damping increases the propensity to generate squeal

Tribometers

The tribometer test benches are halfway between beam–on–disk setups and a real brake systems. They are useful for studying the dynamic and tribological features of squeal. A good example of a tribometer is the *TriboBrake* described in [93] shown in Figure 2.17. The main conclusions reached in that setup can be found in Table 2.3.

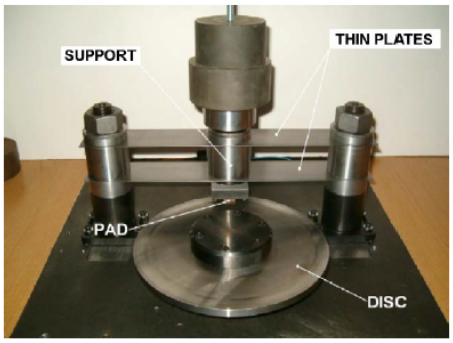

Figure 2.17: TriboBrake

Table 2.3: Summary of the main findings in tribometer setups. Adapted from [92]

Author	Main findings
Massi et al.	Dynamic instability due to a phase relationship between the exciting force and the response of the system Possible couplings: Disc–Pad, Disc–Support Squeal vibrations characterised by a 90º phase difference between in–plane and out–of–plane acceleration of pad Damping reduces modal response but increases the coupling range Squeal happens near less damped mode frequency. Squeal frequency close to in–plane frequency of pad Cracks in friction material due to axial load fatigue Squeal causes exfoliations

2.5.2 Dynamometer test setup

The objective of dynamometer tests is performing tests in a controlled environment but as similar as possible to the real system. The rest of the elements of the system are replaced by inertias. In Figure 2.18 the test bench for a automotive brake is shown [94]. The main findings reported in dynamometer test setups are summarised in Table 2.4.

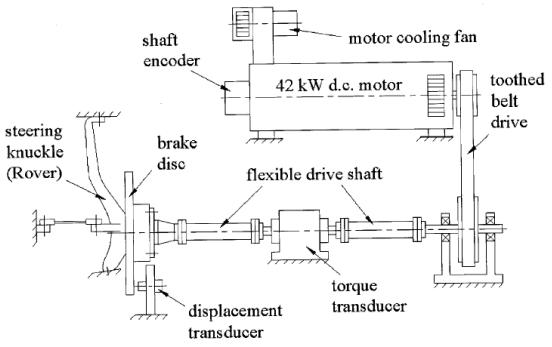

Figure 2.18: Test bench for a real brake [94]

The test bench where the performance of the brake–clutch in operation is simulated is of this kind (Figure 2.19).

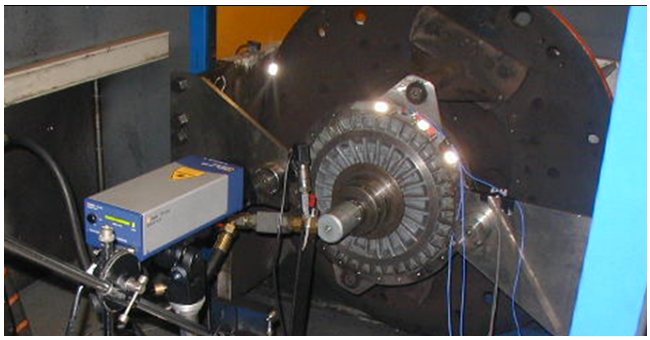

Figure 2.19: Test bench for the brake–clutch [95]

Table 2.4: Summary of the main findings in dynamometer setups. Adapted from [92]

Author	**Main findings**
James	No squeal found when brake assembly was cold, squeal appeared above 100ºC
Majcherzak & Dufrenoy	Pressure fluctuation can excite components at squeal frequency
Renaud et al.	Leading edge is more involved than trailing one in squeal
Eriksson et al.	Increasing pressure squeal propensity increases due to the increase of plateaus contact size
Ishihara et al.	Increasing pressure linear stiffness of pad increases and squeal shifts to higher frequencies
Hetzler & Willner	At low pressure small variations between pressure and contact stiffness lead to instabilities
Yang & Afaneh	Higher clamping force result in stronger coupled vibration
Fieldhouse & Newcomb	To have a pure travelling wave, two stationary waves must have same amplitude and a 90º phase difference

2.5.3 Measuring systems

An important factor when analysing squeal noise experimentally is the correct choice of the measuring systems. The transducers for squeal measurements must have two essential specifications [7]:

- The possibility of measuring in moving components, such as the disk. This, focuses upon contact less devices.
- Ability for measuring responses in a short period of time, since squeal is not stationary.

Apart from the measurement of different parameters during squeal tests, two measuring techniques are widely used for gaining understanding about the squeal generation process: Experimental Modal Analysis and optical techniques.

Experimental modal analysis (EMA)

Experimental Modal Analysis is useful in several ways:

- It can be used to link squeal frequencies to natural frequencies of the system and thus see if the noise has structural origin.
- The information collected in the modal analysis — specially the values of the natural frequencies and the modal shapes [96] — can be used to update the simulation model for it to resemble the most the real system [97].
- Thanks to EMA a map of the system's natural frequencies can be obtained and possible couplings can be identified.
- A simple model can be developed from AME data that is close to the real system but whose computation time is lower [98].

Optical techniques

Optical techniques are used to experimentally identify the shape of the squealing mode. Three optical techniques are described below: *Holographic Interferometry*, *Electronic Speckle Pattern Interferometry* (ESPI) and *Laser Doppler Velocimetry* (LDV). The three of them are non-contact techniques so they do not alter the system and are not affected by operation temperatures. Holographic interferometry (Figure 2.20) and ESPI measure the vibration in the whole component so they have the advantage of avoiding the problems related to the selection of a single point.

Holographic interferometry

Holography allows to record all the information contained light wave emitted by certain object in a medium: the intensity and the phase. The measurement of the wave front requires comparing the value of each point to a standard wave front knows as *reference light beam*. The light source has to be monochromatic and coherent, conditions that are met by a laser beam, either continuous or pulsed.

As two light beams are compared, movements smaller than the wave length cannot be detected. In addition, measurement time should be short to fulfil stability requirements.

Holographic interferometry consist in creating an image by constructive or destructive interference of two light beams. Depending on their phase difference, these two beams will create another light beam of greater or smaller intensity that will represent the relative displacement between two images. By increasing the relative displacement between two points (the initial and the deformed) the number of stripes grows.

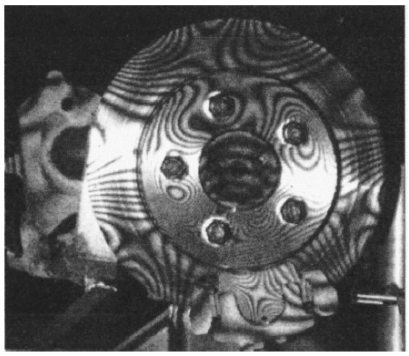

Figure 2.20: Holographic interferometry example

These fringes represent contours of equal displacement and are the sum the rigid body movement in very direction, i.e. absolute displacement is measured. It is necessary, thus, to split up the components to obtain a valid displacement value taking into account that the movement of the disk itself implies in–plane displacement, that will also appear in the stripe pattern [22]. This can be difficult to accomplish in practise. There is also the possibility of creating 3D images interpolating through the images in time. Its main advantage is that the vibration modes can be seen during squeal.

Electronic–speckle pattern interferometry (ESPI)

In this case, a light beam from a ruby laser is spread by a lens to light the surface under study. The reflected light is combined with the reference beam and the result is recorded using a CCD camera (Figure 2.21).

Even though its resolution is lower, it avoids the problems of holography (difficulty of application, time consumption, need for optical and experimental knowledge) and provides a simple way contactless way for measuring displacement.

For the quasistatic case a continuous laser beam is enough, but the dynamic case requires a pulsed laser that emits two light beams separate from each other a specific time interval. Then, it is possible to obtain a snapshot of the deformed shape in two times. This technique is known as *Pulsed–laser electronic speckle pattern interferometry.*

Unlike holography, ESPI has the advantage that it is possible to set apart in–plane and out–of–plane displacements [99].

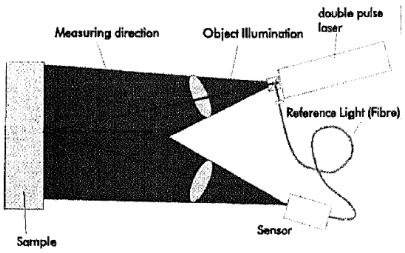

Figure 2.21: Fundamental of ESPI [100]

Laser Doppler Velocimetry (LDV)

In Laser Doppler Velocimetry a laser lights up an object in movement. This object in turn reflects light that gets to a photodetector where it is combined with a reference beam and creates a signal because of the frequency shift caused by Doppler effect (Figure 2.22). This displacements depends on the speed of the object. The principle of this technique is the same that governs ESPI, but for a single light beam.

Scanning Laser Doppler Velocimetry (SLDV) allows measuring the response in different points since the focus point of the laser moves throughout the surface of the object under study. The problem with SLDV is that it requires squeal to last a minimum amount of time for all the points to be scanned [101].

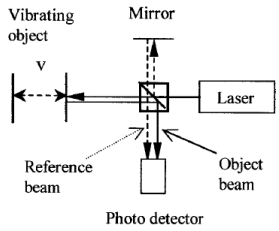

Figure 2.22: Fundamental of LDV [101]

2.6 Suppression methods

Nowadays there is no method to completely suppress squeal. The most effective measure would be reducing friction coefficient since there is a threshold below which squeal rarely occurs ($\mu = 0.3 - 0.4$) [10], but as this step would also reduce the performance of the brake, in general adding damping or changing the design is preferred.

The methods for squeal suppression found in the literature will be presented below, classified into three groups: design changes, antisqueal products and active control. These methods pursue three objectives [102]:

- Reduce the vibration produced by friction. A change in the geometry of the pad is an example.
- Alter the vibratory behaviour of the system, for example optimising its weight or stiffness or using asymmetric rotors.
- Soften the vibration by the addition of damping.

2.6.1 Design modifications

If mode coupling is accepted as the mechanism that generates squeal, noise can be suppressed changing the design so as to avoid coupling.

According to [9], squeal will not appear either if the excitation or the sensitivity of the system to it is reduced. The following strategies are proposed:

- **Design a system less sensitive to vibration**, with this in mind it is necessary to:
  - Uncouple in–plane and out–of–plane modes
  - Uncouple in–plane modes
  - Reduce out–of–plane movement

  - Increase bending stiffness of the rotor

- **Design a system that has lower impulsive excitation at the most sensitive frequencies of the system**. This requires to:

  - Ensure a uniform distribution of contact pressure
  - Ensure that the pad has enough damping
  - Uncouple the modes of the different elements

- **Move the unstable frequencies out of the audible range**. This can be done by:

  - Increasing the stiffness of the rotor
  - Coupling the in–plane or out–of–plane modes with modes of other components at higher frequencies

These objective can be achieved by different means: studying the shape of the modes and changing the geometry of the system to inhibit the movement of certain parts [12,103]. These modifications are generally performed following an iterative scheme mostly by trial and error until a suitable solution is found [104]. Recently, optimisation techniques such as shape optimisation have also been applied [105].

Another option in modifying the surface of the disk [10,106] as shown in Figure 2.23 or carving grooves of different geometries in the friction material [107] or the disc [108], but the results do not last long due to wear.

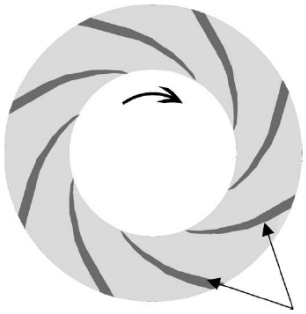

Figure 2.23: Grit blasting pattern in a disk for squeal suppression [106]

Point modifications

A way to suppress squeal is by a point structural modification, either by point masses or springs or a combination of both. In [7], for example, squeal is suppressed in a numerical simulation of beam–on–disk set up by the addition of point masses. Nevertheless, the objective of the work is not squeal elimination

but analysing the effect of a mass mistune in the evolution of squeal frequencies in time — squeal suppression is only a by-product.

Another way to determine a modification for squeal suppression is using the receptance method. This method has been successfully applied in other fields to solve the inverse problem of structural modifications on a simple laboratory structure and simple simulated examples [109,110]. Regarding squeal, only the direct problem has been solved this way. This means that the effect of a modification on the squeal frequencies can be predicted but not the needed modification to achieve a certain change in the behaviour of the system. In [93], for instance, experimental receptances were used to compute the effect of the addition of a single–DOF system in a simplified test bench (Figure 2.24)..

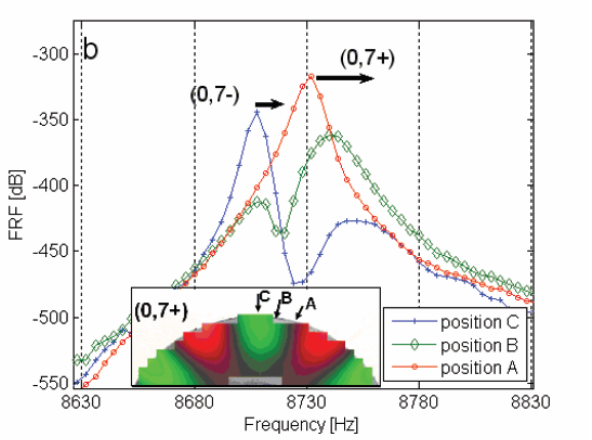

Figure 2.24: Effect of mass in the frequencies for different positions [93]

Receptance method is widely applied for structural modifications in other areas [111] but in general in cases without friction. An example of the use of receptance method in a lumped system with friction can be found in [112].

In a system that presents squeal, being able to shift natural frequencies allows to avoid mode coupling since two modes that are close enough in frequency to coalesce due to friction can be taken apart from each other. This makes the receptance method a possible strategy for squeal suppression. In addition, as the needed modifications are local, the design of the system is not compromised. The main drawback of the method is obtaining accurate experimental receptances from the system but if a reliable finite element model is first developed, simulation receptances can be used as they already include the effect of friction [113].

Mode based design modifications

The information collected by any of the previous numerical techniques about the unstable modes can be used to redesign the problematic component with

the objective of increasing the distance between natural frequency so as to avoid coupling in a trial and error fashion.

Some typical solutions exist such as using a prime or odd number of cooling fins to avoid the movement of the symmetric modes of the disk [12] or breaking the symmetry of the rotor [103,104].

Optimisation

The process described above can be automatised applying a optimisation technique (Figure 2.25). For instance, a shape optimisation can be carried out defining as objective function the minimisation of mass [114] and the split of coupled modes as restrictions. Another possibility is selecting as objective function the minimisation of the real part of the eigenvalue related to squeal and the volume of the pad as a restriction [115]. More examples can be found in [116] and [117] or [118], where the shape of a damping shim is subject of a optimisation process (see Section 2.6.2). Topology optimisation can also be used for defining the best distribution of material so as to avoid squeal, but this field is still under development.

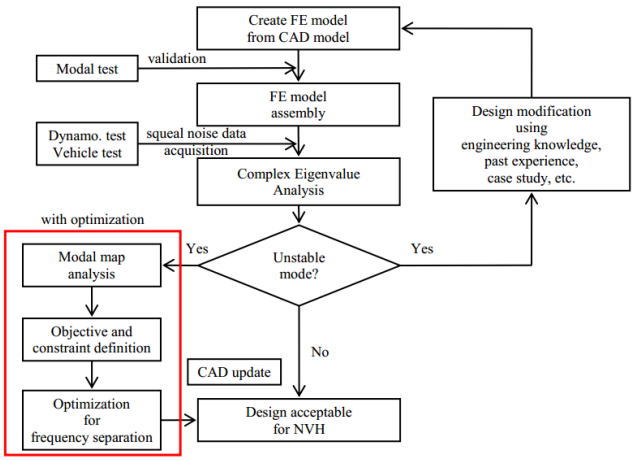

Figure 2.25: Design cycle including optimisation based design modifications [114]

As for point modifications, the same objective can be achieved by discrete optimisation adding several masses with the goal of avoiding mode coupling. A example of this kind of optimisation based on the receptance method but unrelated to squeal can be found in [119].

2.6.2 Antisqueal products

The main commercial solutions for squeal supression in automotive brakes are the application of copper grease in the back part of the pad (Figure 2.26) and the addition of damping shims, a combination of layers of viscoelastic material and steel that have to be attached to the backplate (Figure 2.27). It has not been found any reference that shows the efficacy of the first one, but the contrary has not been proved either.

Figure 2.26: Copper grease application on a automotive brake

As for the shims, some analysis about their function can be found in the literature such as in [120], [121] or [122], in which it is concluded that they are beneficial for the stability of the system as they add damping and split the doublet modes, but this increase in stability is limited [120] and, according to [121], the damping shims are not able to suppress in–plane vibration, so they will not eliminate squeal that occurs for this reason.

These two solutions could be translatable to the context of the brake–clutch, but there is no information available.

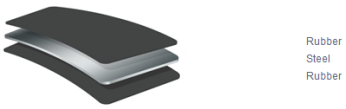

Figure 2.27: Damping shims

2.6.3 Active control

Another way for suppressing squeal is the active control of either the vibration or noise of the system. Different possibilities exist, such as *dither*, *Smart Pads* or *Active Force Control*. Even though different kinds of systems exist and research is carried out in this direction, nowadays active control does not represent a feasible solution for both its size and its prize.

Dither

The noun *dither* refers to high frequency vibration — in general higher than 20 kHz so as to not to be detected by the human ear. It is used for taking out the system from a mode coupling configuration by substituting this unstable vibration with a vibration at the dither frequency. In [123] a system using dither used to suppress rotor mode squeal in a brake squeal dynamometer (Figure 2.28). Its main drawback is the generation of heat because, at the end it does not eliminate the vibration [124].

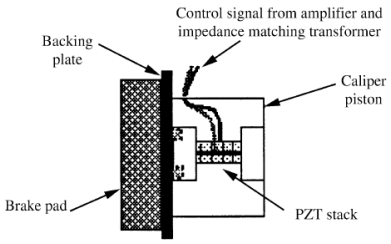

Figure 2.28: Dither system [123]

Smart Pads

Smart pads are pads with implemented piezoceramic that get activated when vibration in the system is detected in order to suppress it (Figure 2.29). The intention is to transform mechanical energy into electrical energy thanks to the piezoelectric material and then dissipate the energy in a circuit. This way the mechanical vibration is reduced. The circuits can be passive (a resistance) or active (LRC type), the latter allows the system to be an actuator and a sensor at the same time.

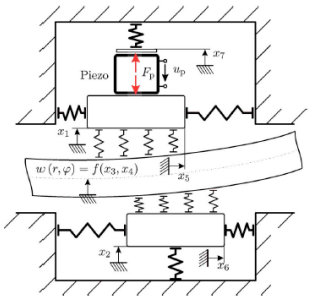

Figure 2.29: Brake with a piezoceramic actuator [125]

In [125] this type of control is used in a brake test rig in order to reduce squeal noise, the results are shown in Figure 2.30. The heating is not considered in the study — this is the main disadvantage of the system as the temperature changes the capacitance of the piezoceramic and thus the performance is reduced.

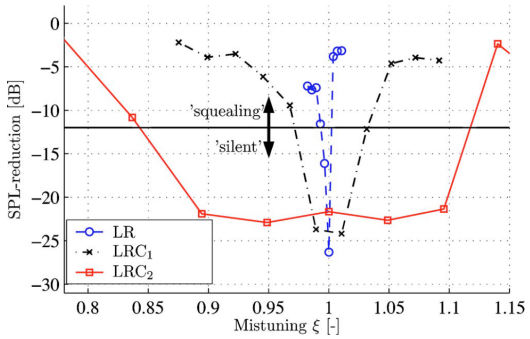

Figure 2.30: Effect of smart pad in squeal noise

Active Force Control (AFC)

In [126] a PID controller is used for active force control and in [127] a PID controller that uses fuzzy logic, but they are only applied to discrete models.

2.7 Critical analysis

The main point to highlight in this critical analysis is that it has not been possible to find any work devoted to industrial brake–clutch squeal in the available literature.

Resorting again to the literature about brake squeal, the following can be identified as accepted knowledge in the field:

- Squeal is linked to a dynamic instability caused by mode coupling
- There is a threshold of friction coefficient below which squeal does not appear
- Symmetric rotors are more prone to squeal since they have doublet modes or two modes at near frequencies.
- The addition of damping reduces the amplitude of vibration, which is beneficial, but increases the range of frequencies in which two modes can couple.

- If damping is added it should be added homogeneously since differences in damping increase squeal risk
- Both thermomechanical coupling and the gyroscopic effect tend to destabilise the system

The main conclusion that can be drawn after analysing the literature is that the squeal related knowledge can be divided into two categories: on the one side, the ones devoted to understanding the phenomenon, that are based on simplified models and compare theoretical results with experimental results obtained in simplified test benches; on the other, the ones focused on the simulation of real systems, specially using finite elements, and the comparison with dynamometer tests.

The objective of the first group is analysing the effect of introducing new elements into the computation such as nonlinearities, gyroscopic effect, uncertainties in the parameters or roughness, or the design of new suppression systems. These works are usually linked to academia and rather far from the real application.

As for the second group, they are dedicated to squeal elimination in a particular system irrespective of its origin. With this in mind, they perform design changes and verify them by simulation or experimentation in a trial and error basis. Lately considerable amount of effort is devoted toward the automation of this task.

Hence, there is a need of an intermediate approach that tries to explain the squeal phenomenon taking into account the different effects but which does not put aside the real application. A work that includes different views of the phenomenon without centring its attention into a single aspect of squeal will be interesting, considering that it is not clear whether a factor should be taken into account or not for some given conditions. This problem arises because the models and test benches are designed to study a particular aspect (damping, mode coupling...) and are not modified for adding variables that correspond to another approach.

Besides, an accepted methodology for squeal suppression does not exist, only some guidelines for design changes can be found, most of which are based on experience. For this reason, it would be useful to develop a process for verifying the behaviour of the system concerning squeal and for changing its design if necessary. A method based on the receptance function appears to be a plausible candidate since the structural modifications derived are local and can be computed theoretically without the need for a prototype.

Chapter 3

Simple model of the brake–clutch

3.1 Introduction

This chapter is devoted to the description of the design of the simple model of the brake–clutch under study. As it has been previously stated, nowadays there is no model for brake–clutch squeal so it is necessary to develop one to gain further understanding of the phenomenon.

The structure of the chapter goes as follows: first, the simple model of the brake–clutch is described, highlighting its distinctive features; then, the finite element model developed is presented and, at the end, its validation process is shown.

3.2 Description of the model

The model developed has three distinct features:

- *Experiments conducted on a commercial tribometer* because of its integrated sensors and control.
- *Simple geometry* of the theoretical model to avoid unnecessary details.
- *Representation of the particularities of the brake–clutch* such as the ring shaped contact area and the asymmetric boundary conditions.

The commercial tribometer used was the *Falex High Performance* which presents disk–on–disk configuration. Its main features are shown in Table 3.1. This

equipment allows control over the rotation and the pressure in its pneumatic cylinders. Different combinations of these two parameters leads to the generation of squeal noise.

Table 3.1: Features of the Falex High Performance tribometer

Maximum speed	10000 rpm
Maximum power	8.16 kW
Minimum measurable torque	250 Lb
Minimum applicable force	253 N
Maximum applicable force	10000 N

In order to fulfill the objectives, two parts were designed taking as a starting point the original components of the tribometer (Figure 3.1): the **fixed part**, made of GG25 cast iron and which assumes the role of the rotor in the brake—clutch, and the **moving part**, made of steel and which represents either the clutch or the brake side and to which the friction material is attached.

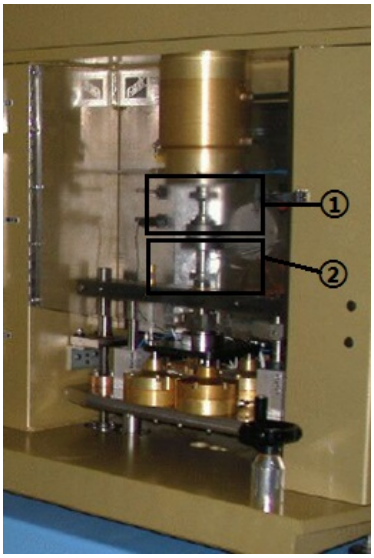

Figure 3.1: Falex High Performance tribometer with its original components. (1) Moving part (2) Fixed part

The fixed part was designed in order to confine the unstable modes in the study range (1 kHz – 20 kHz) in its upper part (Figure 3.2). By doing so, independence to the boundary conditions in the base of the fixed part can be achieved. The moving part was intended to be as simple and robust as possible. Having one part fixed and the other mobile permits a relative rotation between the two of them keeping boundary conditions simple but representative of the real system.

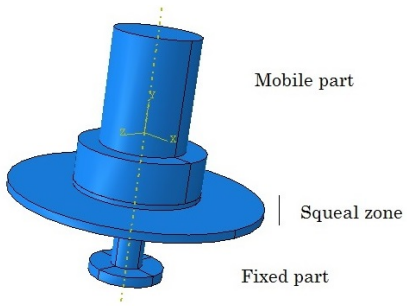

Figure 3.2: Design of the simple brake–clutch model

3.3 Finite element model

A finite element model of the designed system was also developed using the ABAQUS software. First, the individual parts were studied in order to check the possible mode couplings and, after, a model of the complete system including friction was created. This last model will serve as a tool for squeal prediction at first (see Chapter 4) and for squeal suppression later on (see Chapter 5).

3.3.1 Possible mode couplings

First of all, the natural frequencies of the two instances on their own but with boundary conditions applied were compared to check the possible mode couplings. For the fixed part its natural frequencies were obtained with its base clamped. For the moving part the boundary conditions were applied in its upper part, where it is attached to the structure of the tribometer, only displacement along the vertical axis u_z and rotation around the vertical axis ω_z were permitted (Figure 3.3).

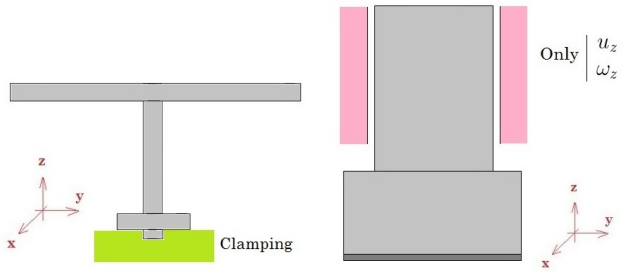

(a) (b)

Figure 3.3: Boundary conditions used for study possible mode couplings (a) Fixed part (b) Moving part

Looking at Figure 3.4 it can be concluded that apart from the possible coupling of a mode of the fixed part with one of the moving part at 10–11 kHz, rotating squeal is more likely to happen since only doublet modes in a single component can couple [23].

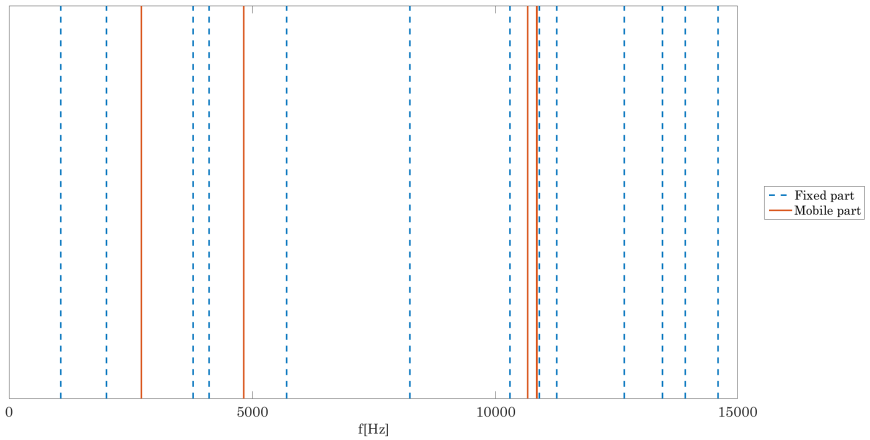

Figure 3.4: Coupling possibilities blue bars denote the natural frequencies of the fixed part and orange bars the ones of the moving part.

3.3.2 Complete model

The finite element model of the complete system had 83.217 degrees of freedom. Incompatible mode linear hexaedra elements were used because of their good response to bending and their moderate computation time [128].

All movement was blocked in the base of the fixed component and in the moving component only vertical displacement and rotation around vertical axis were allowed.

For contact simulation *Hard Contact* allowing contact separation was used for the normal behaviour and *Penalty* for the tangential. *Penalty* method was chosen over *Lagrange multipliers* as it obtains similar results but in less time, since the former has to solve a smaller system of equations.

In the contact interface, the fixed part was selected as master surface and the friction ring as slave since the less stiff part and/or the one with a finer mesh should be selected as slave according to the ABAQUS documentation [129].

Small sliding was preferred to finite sliding for its suitability to the application and easier convergence. In small sliding, as suggested by its name, only a relative small sliding in contact is assumed so the same node in the slave surface will interact with the same area in the master surface throughout the analysis. This

way, the contact state is not recalculated in each step and the process is less time-consuming.

It should be pointed out that the options selected for contact simulation follow the advice given in [56], [75] and [11] for squeal modelling.

The main features of the finite element model are shown in Figure 3.5.

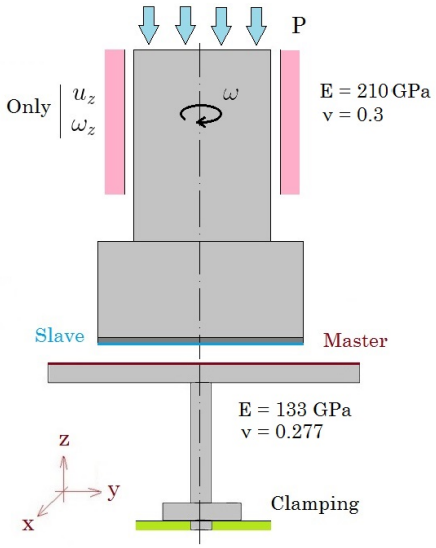

Figure 3.5: Summary of the main features of the FE model

3.4 Validation of the model

The model validation was done in two steps. First, the model of the individual parts was validated. For the fixed part an Experimental Modal Analysis (EMA) was performed in free conditions first and after FRFs were measured with the component mounted in the tribometer. Comparing the results from the EMA to the simulation modes served the purpose of checking the accuracy of the mesh and the material properties. Comparing the measured FRFs to the simulation data allowed to confirm the validity of the boundary conditions.

The idea of performing also a EMA test for the moving part was discarded because only a couple of modes were in the study range and, among them, the ones that can couple have too high frequency for this kind of test. Besides, squeal is related to a very specific zone of the fixed part which is isolated from the rest from the design. Anyway, some FRFs of the system mounted in the tribometer were obtained in order to validate the model of the moving component.

Finally, the ability of the complete model to predict squeal frequencies was adopted as a final validation. The parts of this two step validation are shown in Figure 3.6. This section focuses on the validation tests for the first step, the second step is described in Chapter 4.

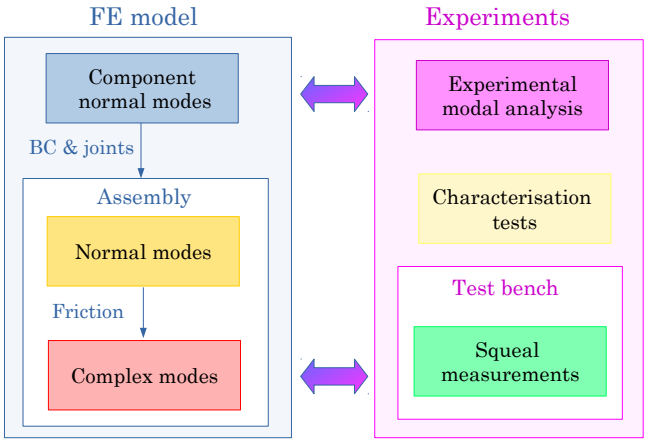

Figure 3.6: The simulation and experimental paths and the two stages of validation

3.4.1 Fixed part

First, an EMA of the fixed part was carried out in order to see the divergences between the computed vibration modes and the experimentally measured ones.

The experiment was performed hanging the element in a structure using elastic bands as shown in Figure 3.7. This way, it can be assumed that the element is in free conditions as the stiffness of the elastic bands is much lower than the one of the element under study.

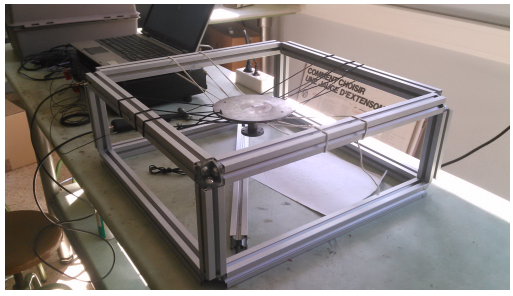

Figure 3.7: Setup for EMA test

For improving the correlation between experimental and simulation modes a asymmetry was introduced in the system — the accelerometer itself — that would fix the position of the nodal lines. The MAC matrices for the cases with and without added asymmetry are shown in Figure 3.8.

Thanks to this strategy, correlation was good enough as 13 modes were correlated in the study range with MAC values higher than 0.6 and with an error in frequency lower that 7.5% (Table 3.2). The discrepancies may be related to limitations of the experimental setup.

Table 3.2: Comparison between simulation and experimental modes

Frequencies[Hz]			**MAC**
EMA	**Simulation**	**Error [%]**	
2007.7	1983.7	1.19	0.752
2031.2	1992.8	1.89	0.742
3525.3	3769.3	6.92	0.744
3985.8	4085.4	2.49	0.855
5421.2	5206.7	3.96	0.674
5438.6	5230.8	3.82	0.632
5615	5624.3	0.17	0.701
7703	7263.6	5.7	0.753
7850.3	7296	7.06	0.805
8311.4	8049.2	3.16	0.623
8436.2	8054.7	4.52	0.656
10192.3	9585.9	5.95	0.701
10388.5	9625.6	7.34	0.798

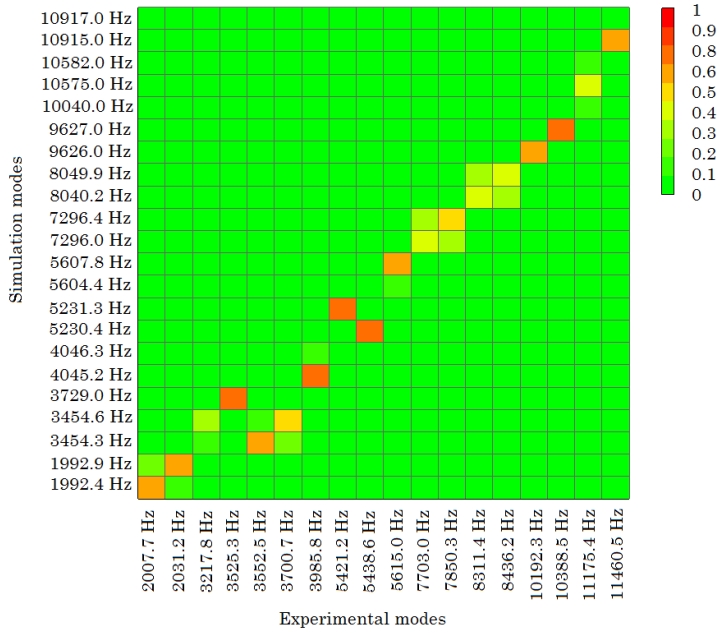

(a)

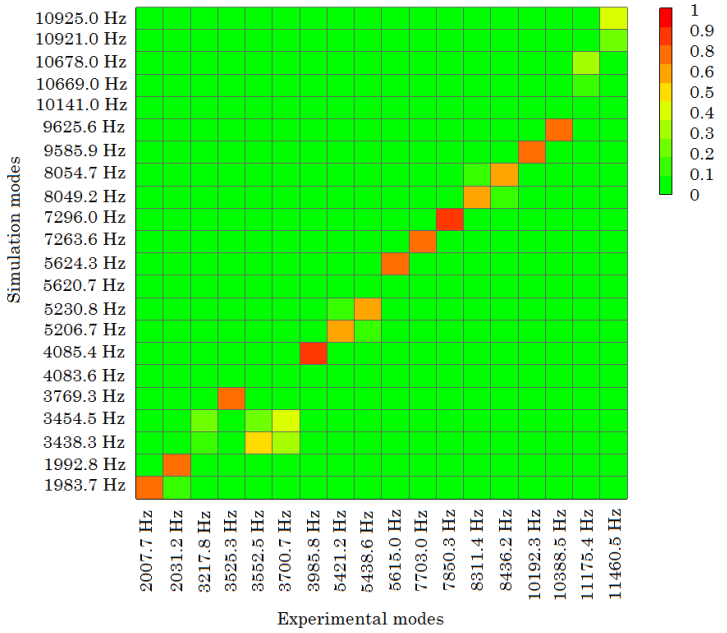

(b)

Figure 3.8: MAC matrix without added asymmetry (a) and with it (b)

Then, some FRFs were measured with the part mounted in the tribometer in order to verify the validity of the boundary conditions. Figure 3.9 shows the position of the accelerometers and the impact point and direction for the hammer. An example FRF ($\frac{\ddot{x}}{F}$) can be seen in Figure 3.10.

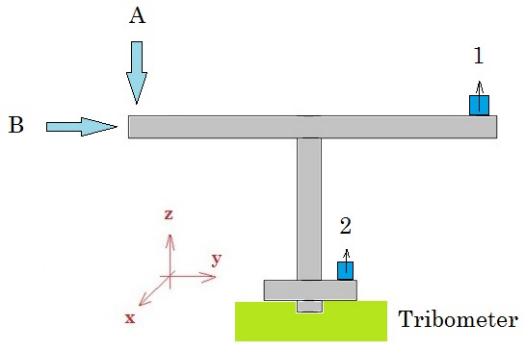

Figure 3.9: Setup for measuring FRFs of the fixed part mounted in the tribometer

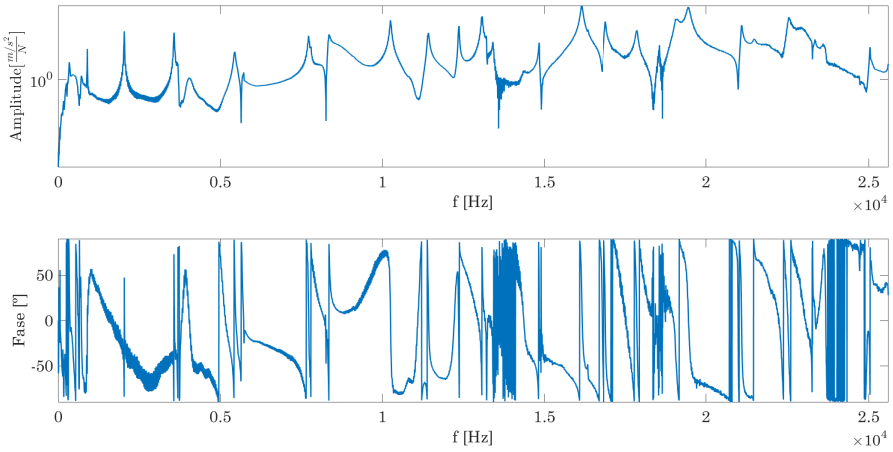

Figure 3.10: Example FRF for the case of the fixed part

A FE model of the fixed part alone with the boundary conditions applied was created and its natural frequencies were computed. The boundary conditions in the FE model were the ones shown in Figure 3.5. In Table 3.3 the frequencies obtained from the FE simulation and the ones from the FRFs are compared. As the maximum deviation in frequency is around 5 % it can be said that the modelling of the boundary conditions is right.

Table 3.3: Comparison between simulation and experimental frequencies for the fixed part

Simulation f [Hz]	Experimental f [Hz]	Error [%]
664	668	0.53
896	896	0.04
2000	2036	1.75
3773	3576	5.51
4105	4072	0.80
5287	5440	2.82
5700	5724	0.42
7402	7720	4.12
8235	8364	1.54
10270	10260	0.10
10887	11280	3.48
11254	11420	1.45
12476	12360	0.94
13443	13080	2.78
13887	13410	3.56
14597	14840	1.64
16555	16140	2.57
16848	16900	0.31

3.4.2 Moving part

As previously said, for the validation of the model of the moving part some FRFs were measured with this part mounted in the tribometer. The point and directions of both the hammer impacts and the accelerometers are shown in Figure 3.11.

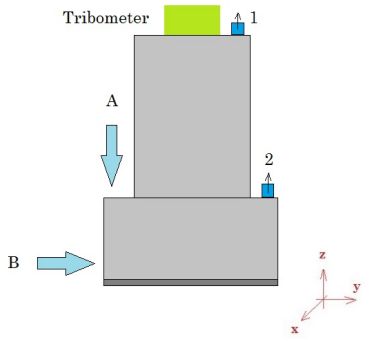

Figure 3.11: Setup for measuring FRFs of the moving part mounted in the tribometer

As done in the previous section, the peaks in the FRFs were then compared to the frequencies computed in the FE simulation. The boundary conditions in the FE model were the ones shown in Figure 3.5. An example FRF is shown in Figure 3.12.

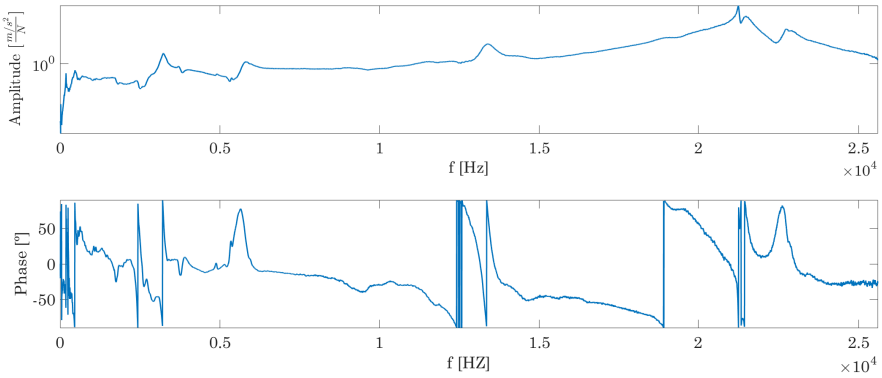

Figure 3.12: Example FRF for the case of the fixed part

A comparison of the simulation frequencies and the ones extracted from the FRFs are shown in Table 3.4. The model of the moving part was accepted as correct since the maximum error in frequency was 2.52%.

Table 3.4: Comparison between simulation and experimental frequencies for the moving part

Simulation f [Hz]	Experimental f [Hz]	Error [%]
12532	12612	0.64
13400	13317	0.62
21236	21018	1.03
21476	21533	0.27
22716	23288	2.52

3.5 Conclusions

This chapter has gone through the creation and validation process of a simple model for brake–clutch modelling. This model was based on a commercial tribometer to take advantage of its integrated sensors and control. Apart from being the first model for brake–clutch model for squeal noise prediction, the model has the particularity of confining squeal to a particular zone and component of the system and, thus, isolating it from the effect of the boundary conditions.

A FE model of the system was also developed which will be used in later chapters for squeal prediction and suppression. To validate the FE model, an EMA test has been performed for the fixed element, with the peculiarity of the addition of an asymmetry to improve correlation in the axisymmetric element. The correlation was satisfactory since 13 modes were correlated with a MAC value higher than 0.6 and a error in frequency lower than 7.5%.

In addition, FRFs of the parts mounted in the tribometer were measured. This had as objective the verification of the modelling of the boundary conditions. A maximum deviation in frequency of 5.51% for the fixed part and of 2.52% for the moving part was obtained so it can be said that the model represents properly the real system.

Chapter 4

Squeal simulation in the simple model

4.1 Introduction

This chapter describes the simulation of squeal in the brake–clutch model presented in Chapter 3. The work can be divided into two distinct parts: on one side, the computation of the complex modes of the system in order to predict instabilities and, on the other, squeal tests performed in the experimental setup. The results obtained in both parts are compared in order to quantify the capability for squeal prediction of the finite element model.

At the beginning the most simple finite model is presented and afterwards new complexity is added to the model, including pressure and velocity dependent friction coefficient, anisotropic elastic properties for the friction material and friction damping. In all cases, experiments carried out for characterising each property are described. The effect of each property in the correlation with experimental squeal frequencies and in the stability of the system is analysed.

4.2 Simulation model

First of all, a Complex Eigenvalue Analysis is performed in the finite element model presented in Chapter 3 to identify the unstable vibration modes of the system. The process is described in [130] and summarised in [6] as:

1. *Nonlinear static analysis* for applying pressure and establish the contact area

2. *Nonlinear static analysis* to impose rotational speed on the disk so that friction is developed on the contact interface
3. *Normal mode analysis* to extract natural frequency of the undamped system
4. *Complex eigenvalue analysis* that incorporates the effect of friction coupling and produces the system eigenvalues

In this system all unstable modes are doublet modes due to the axisymmetry of the system, specially the upper part of the fixed part to which unstable modes belong. Therefore, the system will present rotating squeal [131].

4.3 Squeal tests

To verify the validity of the simulation results, squeal tests were performed in the tribometer setup. In this section the experimental procedure followed and the results obtained are presented.

4.3.1 Experimental procedure

Squeal tests were conducted in low, medium and high conditions in terms of speed and pressure (Table 4.1). Each test was repeated 4 times to ensure repetitiveness. These conditions were decided after a preliminary test in which pressure and speed ramps were applied to the system and squeal conditions were registered. For all the conditions, if the friction material was new a running-in time was needed to produce squeal [23].

Table 4.1: Conditions of the squeal tests

	Test #	**Normal force [N]**	**Rotation speed [rpm]**
LOW	1	470	50
MEDIUM	2	940	90
HIGH	3	1440	110

Measurements of rotation speed, normal force, torque, temperature, acceleration and noise were taken at a sampling speed of 65,536 Hz to properly represent frequency components up to 25,000 Hz. Measurements of rotation speed, normal force, torque and temperature were provided by the tribometer itself whereas acceleration and acoustic pressure measurements were taken using external transducers (Figure 4.1).

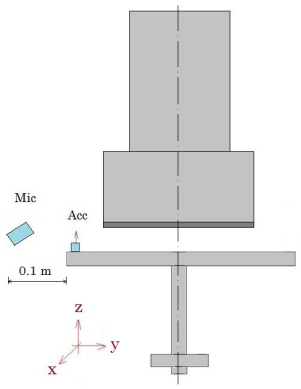

Figure 4.1: Position of the accelerometer and the microphone in the experimental setup

4.3.2 Results

First, the relationship between squeal frequency with normal force, rotation speed and friction coefficient was analysed. This required checking first if the tests were repetitive enough. As seen in Figure 4.2, the same squeal frequencies were obtained for the tests performed under the same working conditions. It was also observed that the test under high conditions showed more squeal frequencies than the rest. This can be linked to the activation of more unstable modes to the higher level of excitation these last tests meant. Regarding the low frequency range, low and medium conditions also show some frequency content in that range, but its amplitude is much more lower than in the high conditions.

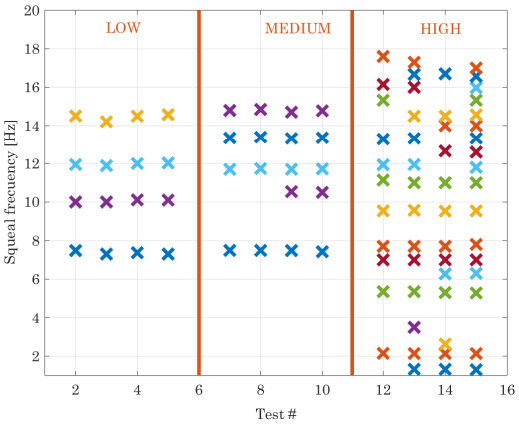

Figure 4.2: Squeal frequencies in tests. Vertical lines divide tests in different conditions and colours track frequencies through tests

After, the changes in squeal frequencies related to the aforementioned three parameters were studied. In Figure 4.3, squeal frequencies in function of the values of the parameters at the starting point of squeal are plotted. Two conclusions can be drawn from these results:

- There is a threshold of friction coefficient of approximately $0.3 - 0.35$ under which the likelihood of squeal to occur is very low. The presence of squeal events under the threshold can be attributed to measuring errors.
- Normal force is the most influential parameter: it fixes the value of the squeal frequencies.

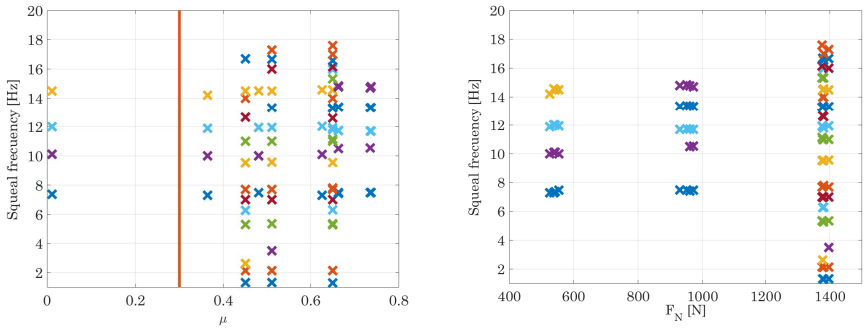

Figure 4.3: Conditions at the onset of squeal vs squeal frequencies (a)Friction coefficient (b)Normal force (c) Rotation speed. Colours track frequencies through tests

These facts match the conclusions reached in the literature for automotive brake squeal, for instance in [46].

The evolution of the measured variables in time was also studied. An example of this temporal variation can be found in Figure 4.5 (a), where the cyclic variation of the variables can be noticed, being this period T equal to the period related to the nominal rotation speed for each test (Figure 4.4).

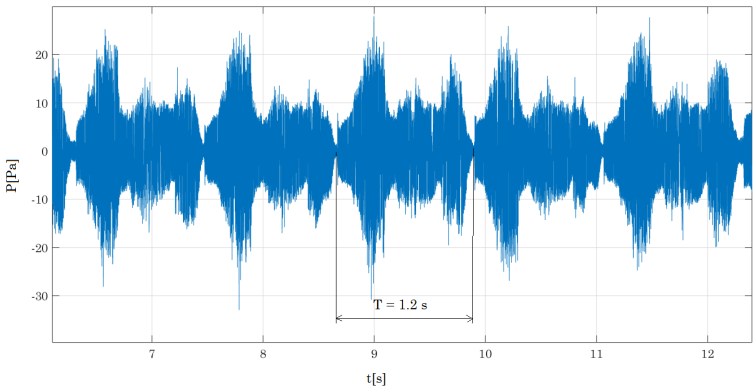

Figure 4.4: Squeal presented a cyclic modulation in time related to rotation speed. For example, for the tests at 50 rpm $T = \frac{2\pi}{\omega} = 1.2\,\mathrm{s}$

If attention is focused in a single squeal cycle (Figure 4.5 (b)), it can be observed that the onset of squeal is linked to an increase in oscillation in normal force and a drop in torque. This effect can be most clearly seen if the zone between 5.05 s and 5.08 s is magnified (Figure 4.5 (c)). This finding is in line with [132].

This phenomenon can be explained in two different ways:

1. Contact between the friction element and the fixed component is lost making the torque drop and causing the vertical vibration in the fixed element.
2. Oscillations in normal force provoke the lost of contact and therefore the drop of torque.

In either case, squeal appears when a drop in torque is accompanied by a greater oscillation in normal force. These results suggest the possibility of sprag–slip being the triggering mechanism for mode coupling.

After analysing the variation in time of squeal the effect of friction coefficient, rotation velocity and normal force in squeal generation was studied. In Figure 4.6 the values of friction coefficient, rotation velocity and normal force at the onset of squeal are plotted. Two conclusions can be reached from there, the first one is that the tests with less demanding conditions show lower variation in rotation speed. The second is that tests with different normal force values present different friction coefficient thresholds.

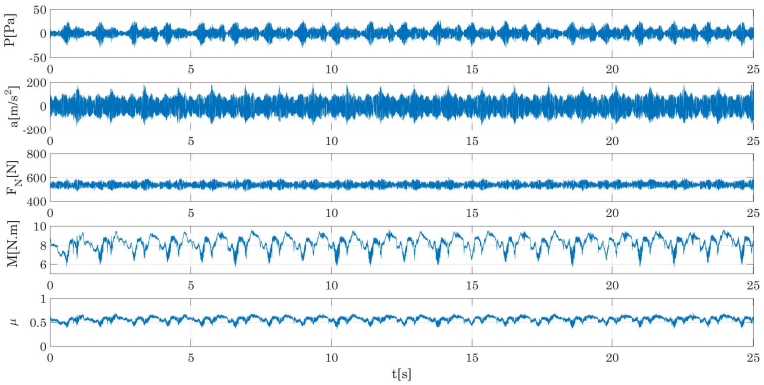

(a)

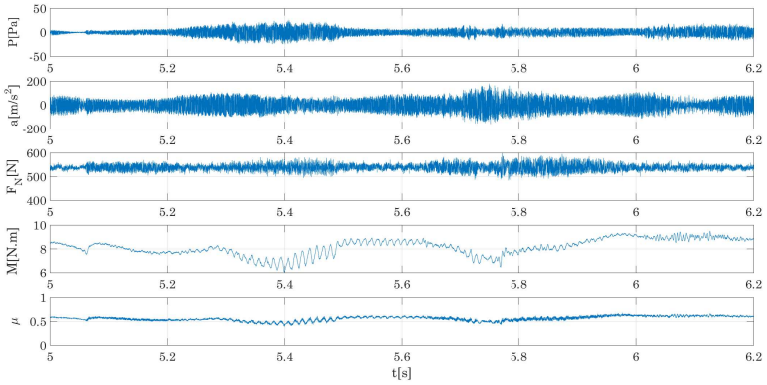

(b)

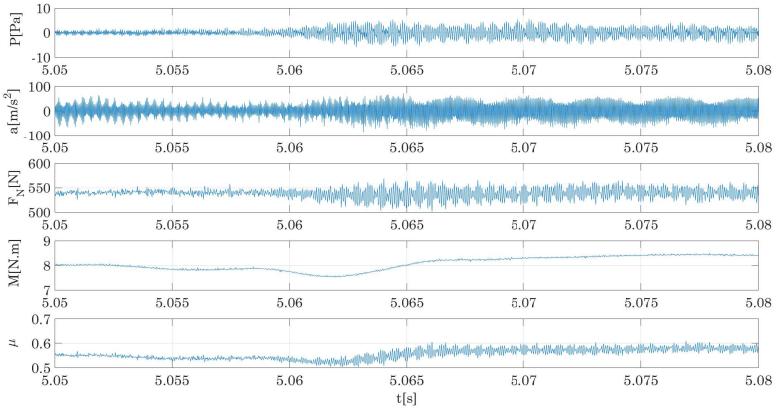

(c)

Figure 4.5: Variation of variables in time. From top to bottom: sound pressure, acceleration, normal force, torque and friction coefficient (a) During the test (b) Zoom into one squeal cycle (c) Further zoom

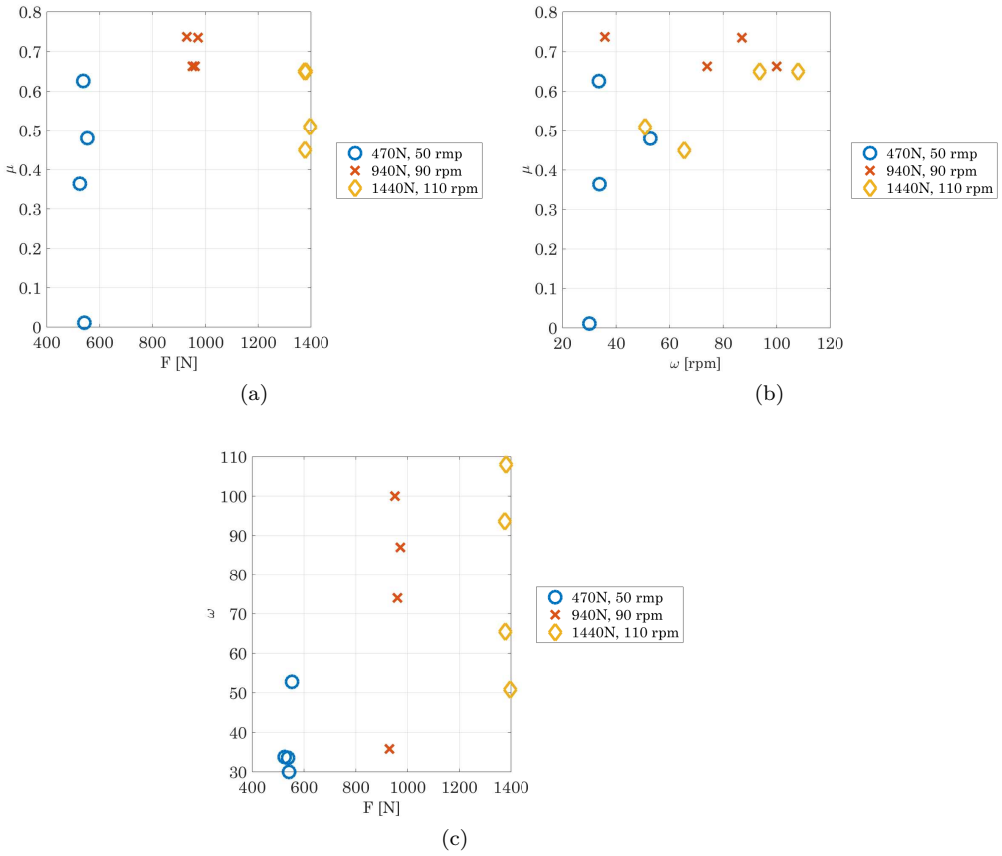

Figure 4.6: Conditions at the onset of squeal (a) Normal force vs friction coefficient (b) Rotation speed vs friction coefficient (c) Normal force vs rotation speed

4.4 Comparison of simulation with experimental results

Once the experimental results had been analysed, the squeal frequencies obtained in the tests were compared with the frequencies of the unstable modes from the FE model. In Figure 4.7 this comparison for the three test conditions is presented. Only one instance for each testing category is displayed due to the similarity that exists between the noise spectra for the same testing conditions (see Figure 4.2)

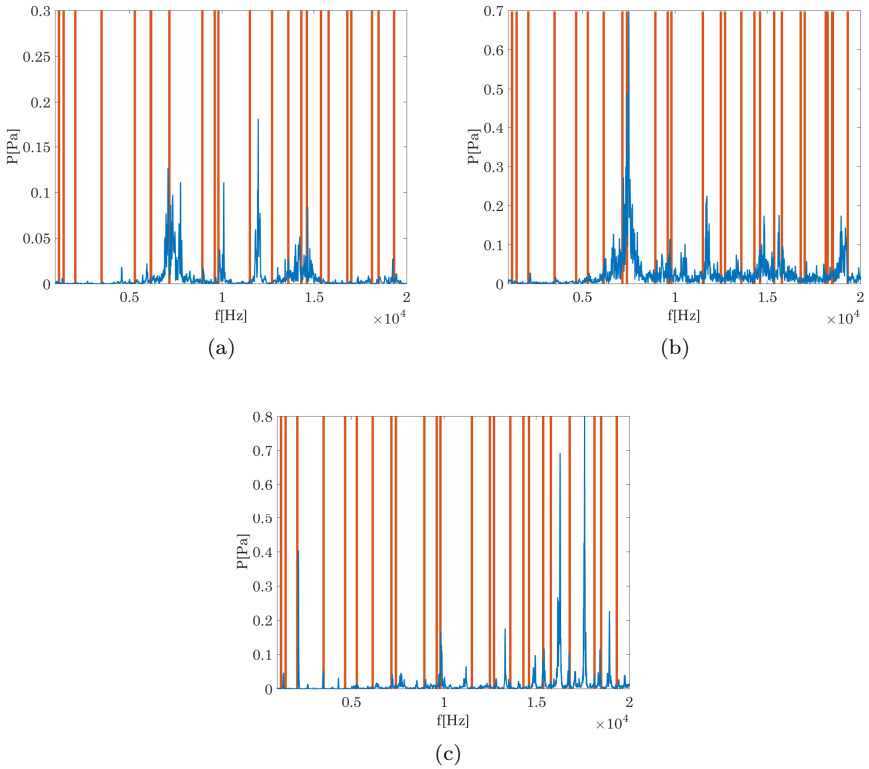

Figure 4.7: Comparison between noise spectra from squeal tests and frequencies of the unstable modes (vertical lines) for the three testing conditions (a) Low (b) Medium (c) High

All the experimental squeal frequencies can be found among the unstable modes of the system with a maximum deviation of 10%, but the number of squealing frequencies is overpredicted. This overprediction is probably linked to the simplifications of the model such as the constant friction coefficient, the instantaneous application of both force and rotation speed and the lack of damping. This issues will be addressed in the following sections.

4.5 Added complexity to the model

In order to reduce overprediction, some improvements were added to the FE model. First, the elastic properties of the friction material were obtained. After, pin–on–disk tests were carried out in order to obtain a pressure and speed dependent friction coefficient and, finally, friction damping was added to the

model. In this section the cumulative effect of these modifications will be studied — focusing in particular on the effect in stability and in correlation of each of them.

4.5.1 Anisotropy of friction material

The friction material is an anisotropic material whose chemical composition and material properties are unknown. It is known, however, that its elastic properties vary with applied normal force and frequency, so different properties can be obtained depending on the test used to that purpose [133]. Because of this reason elastic properties were deduced from an Experimental Modal Analysis (EMA) and a subsequent optimisation process, this way the elastic properties obtained correspond to the frequency range where squeal occurs (1–20 kHz). This is also the process that the SAEJ3013 standard [134] suggests.

Description of the tests

First of all, the test specimen was manufactured. It consisted in a 300 x 40 x 2 mm steel base that functioned as a backplate and to which a segment of friction material of the same dimensions but a thickness of 4 mm was glued. The steel base is necessary due to the damping of the friction material, if the EMA analysis were carried out without it the level of the response obtained would not be high enough for the results to be reliable.

A roving hammer test of the element in free conditions[1] was performed impacting in 48 points and measuring the response in the three directions in a single point with a triaxial accelerometer (Figure 4.8).

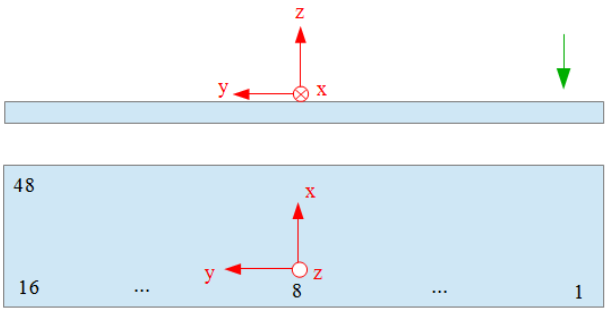

Figure 4.8: Diagram of the roving hammer test. The axes mark the position of the accelerometer and the arrow the impact direction

[1]The beam was supported by elastic bands in a metallic structure, as the beam was much stiffer than the bands the hypothesis of free boundary conditions could be accepted.

Simulation model

A FE model of the specimen was also developed. In the absence of more appropriate properties, data for automotive brake pads from literature [135] was used a starting point since the data provided by the manufacturer considered the friction material isotropic (Table 4.2).

Table 4.2: Properties of the friction material according to the manufacturer and from literature [135]

Manufacturer		Literature	
E	1.89 GPa	E_1	12.75 GPa
ν	0.3	E_2	12.75 GPa
		E_3	3.11 GPa
		$\nu_{12} = \nu_{21}$	0.11
		$\nu_{13} = \nu_{23}$	0.09
		$\nu_{32} = \nu_{31}$	0.22
		$G_{13} = G_{23}$	2.81 GPa
		G_{12}	4.45 GPa

It is important to point out that the differences between elastic properties are due to two facts:

- The composition of the friction materials used in automotive brakes is different to the one of the materials for industrial applications.
- The data supplied by the manufacturer correspond to compression tests while the ones from literature have been obtained from ultrasonic test. Elastic moduli are higher at higher frequencies.

Therefore, values higher than the ones provided by the manufacturer but lower than the ones from literature are expected.

Optimisation process

Once the simulation and experimental modes had been obtained, the optimisation process started. It consisted in updating the elastic properties of the friction material so as to improve the correlation between the experimental and simulation data. To this end, for mode i with shape $\boldsymbol{\varphi}$ the following was sought:

$$|f_{i\ exp} - f_{i\ sim}| \to 0 \quad / \quad i = 1, ..., n$$

$$\mathrm{MAC}(\boldsymbol{\varphi}_{i\ exp}, \boldsymbol{\varphi}_{i\ sim}) \to 1 \quad / \quad \mathrm{MAC}(\boldsymbol{\varphi}_1, \boldsymbol{\varphi}_2) = \frac{|\boldsymbol{\varphi}_1{}^{\mathsf{T}} \boldsymbol{\varphi}_2{}^*|}{(\boldsymbol{\varphi}_1{}^{\mathsf{T}} \boldsymbol{\varphi}_1{}^*)(\boldsymbol{\varphi}_2{}^{\mathsf{T}} \boldsymbol{\varphi}_2{}^*)} \tag{4.1}$$

(4.2)

The software itself (*Virtual Lab*) modifies the properties until the two relationships in Equation 4.2 are accomplished as well as possible for the selected modes, in this case the first 6 bending modes and the first 6 torsional modes. After this process, the properties presented in Table 4.3 are obtained.

Table 4.3: Elastic properties after the optimisation process

E_1	6.43 GPa
E_2	6.92 GPa
E_3	2.42 GPa
ν_{12}	0.27
ν_{13}	0.309
ν_{21}	0.291
ν_{23}	0.296
ν_{31}	0.117
ν_{32}	0.104
G_{12}	4.87 GPa
G_{23}	2.15 GPa
G_{13}	2.39 GPa

It can be noticed that the typical approximation of orthotropy is reasonable, since the behaviour of the material in the two direction in the plane is similar. In fact, there is only a deviation of 10% in natural frequencies if the material is considered orthotropic instead of anisotropic.

Finally, in Figure 4.9 the differences between the experimental natural frequencies, the frequencies from simulation for both the initial values given by the manufacturer and ones from literature, and the frequencies after the optimisation are shown. The error was reduced from a 25% to a 5%.

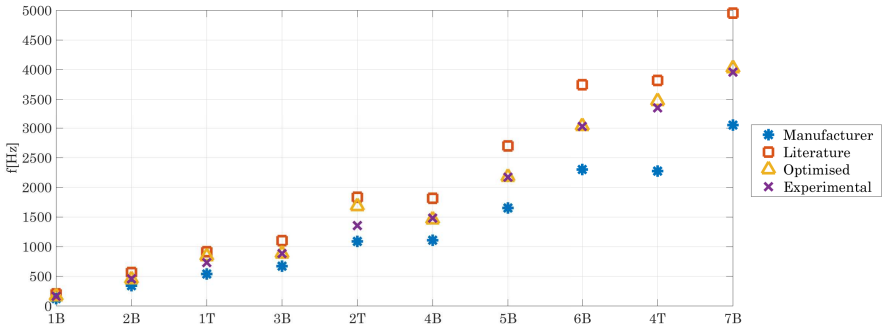

Figure 4.9: Natural frequencies for different cases. The horizontal axis denotes the type of mode: T, torsional; B, bending

Effect in stability

First, the effect of taking into account the anisotropic elastic properties in stability was studied. In Figure 4.10 the real parts of the complex eigenvalues in the range of frequency from 1 kHz to 20 kHz are plotted for both the isotropic case, using the values from the manufacturer, and the anisotropic case, using the values after the optimisation. For most of the eigenvalues, the real parts are bigger if anisotropy is considered, i.e. the system is more unstable. This means that taking into account the anisotropy of the material can lead to the detection of a unstable mode otherwise unnoticed.

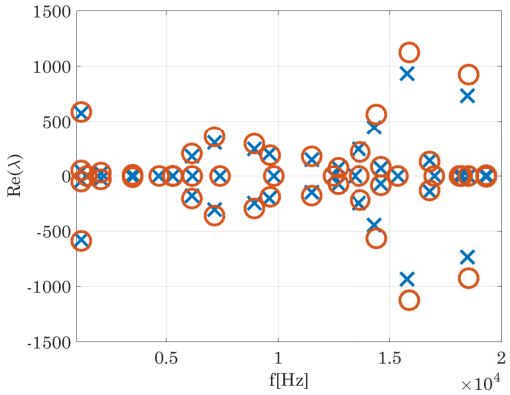

Figure 4.10: Stability diagram with isotropic elastic properties from the manufacturer (blue crosses) and taking into account anisotropy (red circles)

Effect in correlation

Then, the frequencies of the unstable modes predicted after updating the elastic properties were compared to the experimental squeal spectra (Figure 4.11). The differences in frequencies are small since the proportion of friction material in the system is little. Even though overprediction is not reduced, thanks to the introduction of anisotropy some peaks that could not be identified in the simple model could be detected.

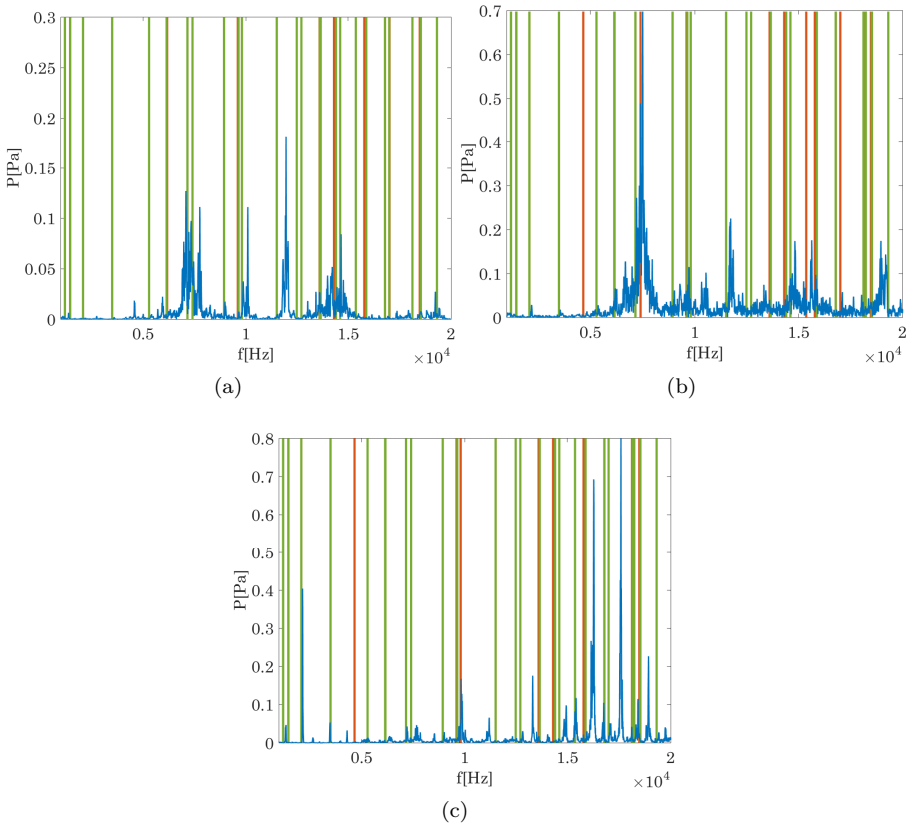

Figure 4.11: Comparison between noise spectra from squeal tests and frequencies of the unstable modes (vertical red lines) and adding anisotropy (vertical green lines) for the three testing conditions (a) Low (b) Medium (c) High

4.5.2 Pressure and speed dependent friction coefficient

The next effect taken into account was the pressure and speed dependent friction coefficient. First, the effect of its introduction in stability was studied and, then, the differences in correlation were observed. In both cases the base case included anisotropy.

Description of the tests

In order to obtain the pressure and speed dependent friction coefficient, pin–on–disk test were carried out in the same tribometer used for the squeal tests. The methodology consisted in a initial running-in to stabilise the properties of the friction material followed by three consecutive tests under the same conditions.

The test conditions were the following:

- **Speed**: 46, 139, 231 y 462 rad/s that correspond to 0.1, 0.3, 0.5 y 1 m/s
- **Normal load**: 154, 253, 505, 760 y 1014 N that correspond to 1.22, 2, 4, 6 y 8 MPa

This values were selected because they directly correspond to the normal force and speed values in operation, either in the test performed in the tribometer or in the real brake–clutch application.

The typical evolution in time of the variables measured in the pin–on–disk tests is shown in Figure 4.12.

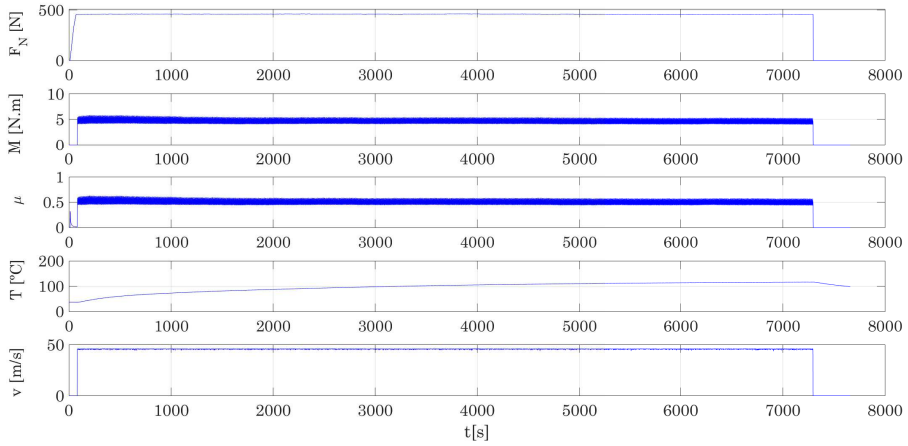

Figure 4.12: Typical evolution in time of the variables measured in the pin–on–disk tests

From these signals the following parts were rejected:

– The normal force is zero, negative or its deviation from the mean value is greater than the standard deviation

– The speed is zero, negative or its deviation from the mean value is greater than the standard deviation

– The torque is zero, negative or its deviation from mean value is greater than the standard deviation

From the processed data the mean friction coefficient for each test was computed. As the values for the friction coefficient were similar for the test under the

same conditions (Figure 4.13), the mean value for all the test under the same conditions was computed.

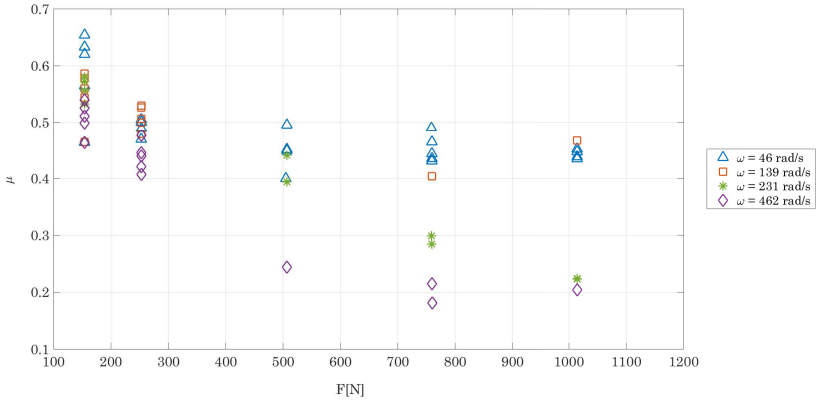

(a) Friction coefficient vs normal load

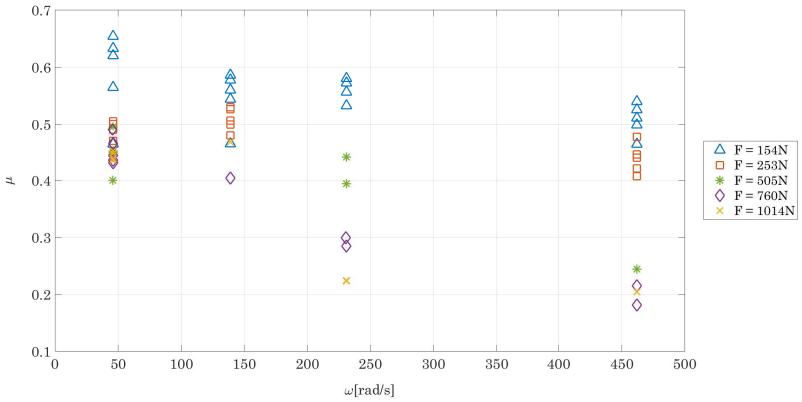

(b) Friction coefficient vs rotation speed

Figure 4.13: Values of the mean friction coefficient for different conditions

Afterwards, the experimental data were fitted to a second grade polynomial for the normal force and a third grade polynomial for the speed (Equation 4.3) that represents the surface shown in Figure 4.14.

$$\mu(P,v) = c_0 + c_1 P + c_2 v + c_3 P^2 + c_4 P v + c_5 v^2 + c_6 P^2 v + c_7 P v^2 + c_8 v^3 \quad (4.3)$$

$c_0 = 0.4531$ $c_1 = -1.425 \cdot 10^{-4}$ $c_2 = 3.204 \cdot 10^{-3}$ $c_3 = 1.042 \cdot 10^{-7}$
$c_4 = -2.91 \cdot 10^{-6}$ $c_5 = -1.47 \cdot 10^{-5}$ $c_6 = 1.078 \cdot 10^{-9}$ $c_7 = 1.95 \cdot 10^{-9}$
$c_8 = 1.89 \cdot 10^{-8}$

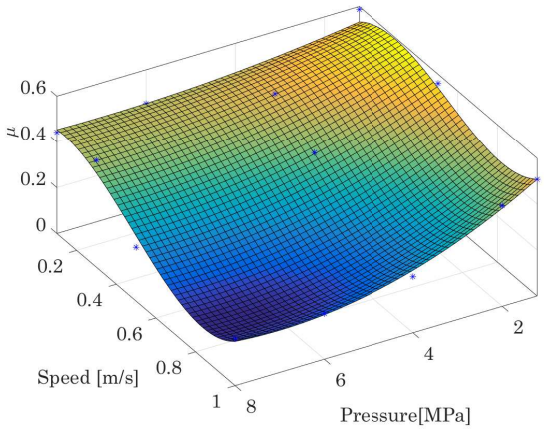

Figure 4.14: Fitting of the friction coefficient

This fitting was used to introduce a speed and pressure dependent friction coefficient in the finite element model.

Introduction of pressure and speed dependent friction coefficient in the EF model

As previously done for anisotropy, for the non constant friction coefficient both the effect in stability and in correlation with the experimental results was studied. The base case for the comparison are the results after the optimisation process performed for the elastic properties.

In Figure 4.15 the eigenvalues obtained by CEA are shown for the constant case of $\mu = 0.32$ provided by the manufacturer and for the $\mu = \mu(P,v)$ case, specifically for the squeal tests in low force and speed conditions. In this case, if the friction coefficient is considered constant for every force and speed, the degree of instability of the system is underestimated. Exactly the same occurs for the rest of the cases.

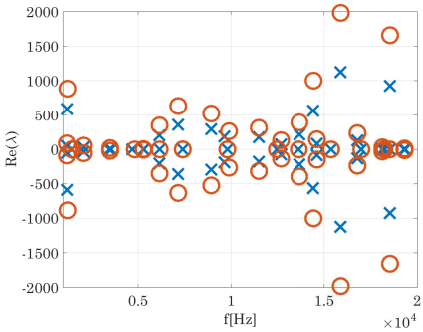

Figure 4.15: Stability diagram with constant friction coefficient(blue crosses) and pressure and speed dependent friction coefficient (red circles)

This happens because of the difference between the nominal pressure and the real one: since the element deforms, the contact pressure is not uniform in the whole surface, but the high pressure area (low friction coefficient) is located in the internal side of the ring whereas the rest works under much lower pressure (high friction coefficient) (Figure 4.16). This way, in most of the surface friction coefficient has a value around 0.6, much higher than the value of 0.32 given by the manufacturer (Table 4.4).

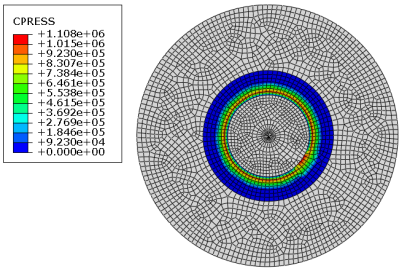

Figure 4.16: Pressure distribution for Test #1

Table 4.4: Pressure, speed and friction coefficient ranges for the three test types

	Test #1	**Test #2**	**Test #3**
P_{min} [MPa]	0.1	0.15	0.24
P_{MAX} [MPa]	1.1	1.8	3
v_{min} [m/s]	0.14	0.25	0.31
v_{MAX} [m/s]	0.21	0.38	0.46
μ_{min}	0.59	0.55	0.44
μ_{MAX}	0.6	0.65	0.65

On the other hand, the effect of the introduction of a variable friction coefficient in the correlation was studied. As shown in Figure 4.17, overprediction is not reduced but squeal frequencies are better fitted.

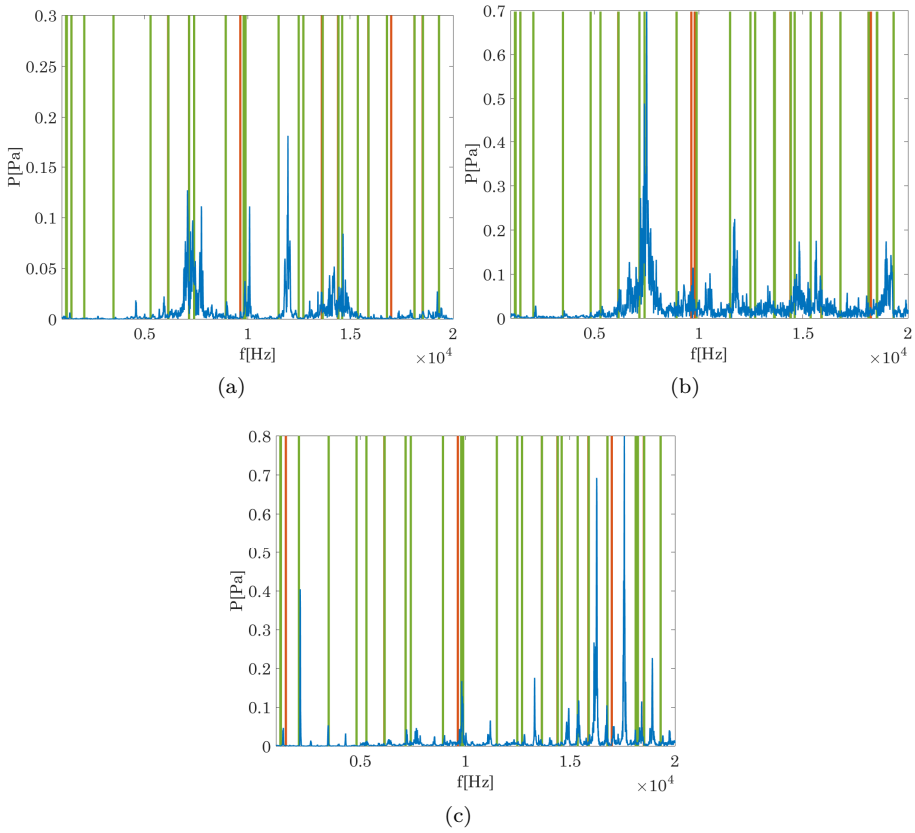

Figure 4.17: Comparison between noise spectra from squeal tests and frequencies of the unstable modes taking into account anisotropy (vertical red lines) and adding variable friction coefficient (vertical green lines) for the three testing conditions (a) Low (b) Medium (c) High

4.5.3 Friction damping

As explained in Section 2.3.1, there are two factors that help to reduce the system's response: the damping of the system itself, that comes from both the material and the geometry, and friction damping. The second one was introduced to the simulation since Abaqus takes it into account directly introducing stabilising and destabilising terms in the damping matrix **C**. An explanation of the introduction of friction damping in the finite element model can be found in

Appendix A.

In Figure 4.18 it can be seen that the introduction of friction damping reduces the real parts of the unstable modes, so it is useful for reducing instabilities.

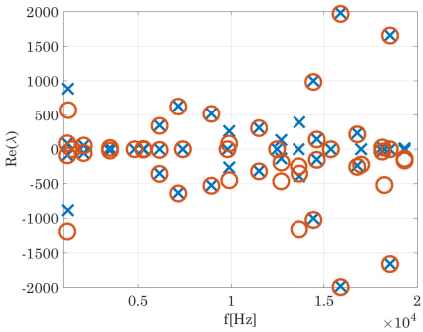

Figure 4.18: Stability diagram without friction damping (blue crosses) and with friction damping(red circles)

On the other hand, the effect of the addition of friction damping in overprediction was studied. Since friction damping reduces the value of the real parts of the eigenvalues, introducing it helps to predict more accurately squeal frequencies (Figure 4.19).

4.5.4 Final model

To sum up, a comparison between the initial and the final model is presented in this section. As seen in Figure 4.20, correlation has been improved whilst overprediction has been reduced.

Two aspects should be highlighted regarding correlation between experimental and simulation frequencies:

- Peaks that appear to be non detected are either:
  - System modes
  - Modes on the verge of instability
  - Harmonics of unstable modes
- Simulation frequencies appear under experimental frequencies because of less stiff boundary conditions in the simulation model — the moving part was completely free to move vertically and rotate

Apart from the aforementioned details, it can be stated that the final model represents accurately the behaviour of the experimental setup, being the maximum deviation in frequency of a simulation frequency to an experimental one less than 4 %.

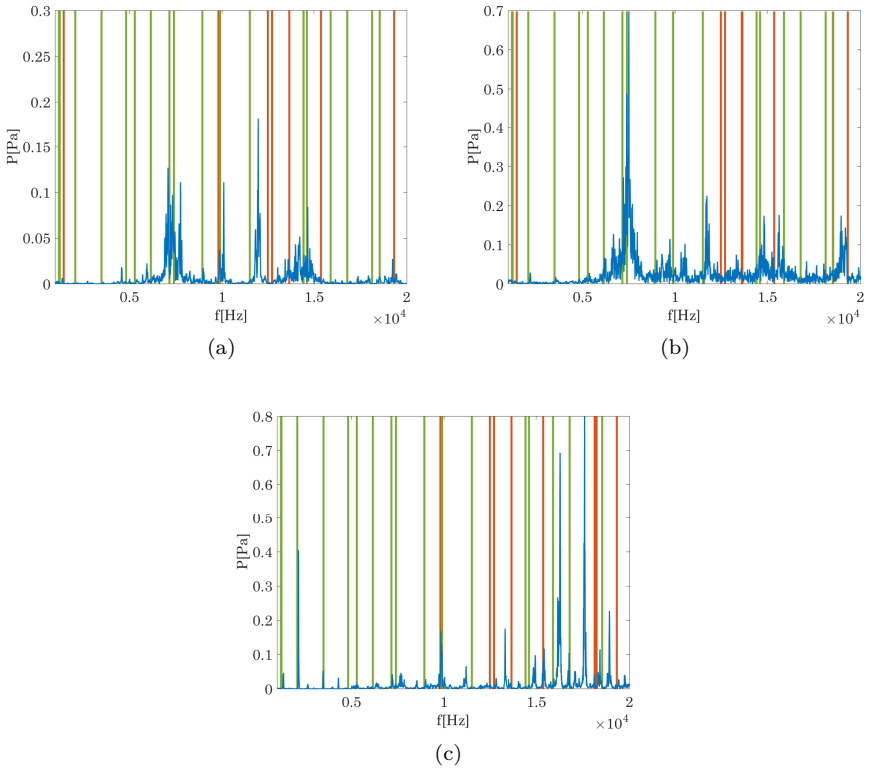

Figure 4.19: Comparison between noise spectra from squeal tests and frequencies of the unstable modes taking into account anisotropy and variable friction coefficient (vertical red lines) and adding friction damping (vertical green lines) for the three testing conditions (a) Low (b) Medium (c) High

4.6 Conclusions

This chapter describes the development of a simple model for brake–clutch squeal prediction. The model is able to reproduce squeal without the drawback of the complexity of a real system.

Regarding test results, several facts should be highlighted. The first one is the good repetitiveness that squeal test in the experimental setup showed, the same squeal frequencies appear for the same test conditions. As for the parameters influencing squeal, among the parameters under study, normal force is the decisive one as it sets squeal frequencies. Friction coefficient is also important, since squeal only emerges if friction coefficient is higher than a threshold level of 0.35. Finally, attention should be called to the fact that squeal is related to a drop in torque and an increase in normal force oscillation, which suggests

sprag–slip as the triggering mechanism for mode coupling and, thus, squeal.

As for simulation, fair correlation between experimental and simulation results was obtained, even with the most simple simulation model, squeal frequencies could be predicted with an error lower than 10%. The degree of correlation can be improved to a maximum deviation of 4 % by adding more complexity to the model. This implies that the methodology followed for automotive brake squeal can be extended for brake–clutch squeal, which was not obvious at the first stages of this work.

With the idea of reducing overprediction, anisotropic properties for the friction material, pressure and speed dependent friction coefficient and friction damping were introduced to the system. It was found that taking anisotropy into account can make the difference between detecting an unstable mode or not.

Using a pressure and speed dependent friction coefficient the distribution of pressure on the surface is considered and, as most of the surface is under low pressure due to deformation, friction coefficient is much higher than expected, so the system is much more unstable than anticipated.

Last, the effect of friction damping was studied. It is useful to reduce overprediction as it takes down the real parts of the eigenvalues, moving modes that were previously thought as unstable to the stable zone.

As a general conclusion, it can be stated that friction coefficient is a determinant parameter in the stability of the system. This is because the effect of friction coefficient in squeal is twofold: on the one hand, it is the parameter that determines whether a mode will be unstable or not in CEA; on the other, the most helpful effect to reduce overprediction in the system is the introduction of friction damping.

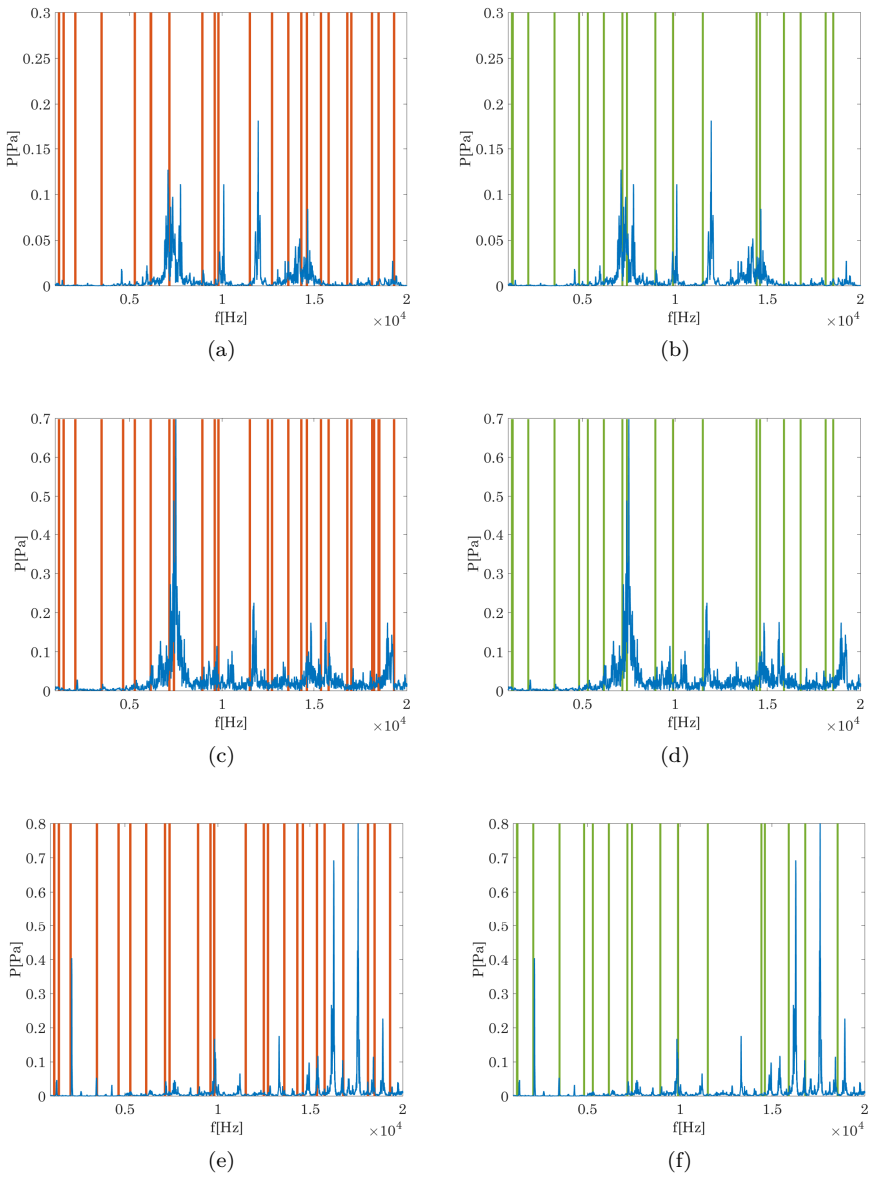

Figure 4.20: Comparison between prediction of the original FE model (left) and the model with added complexity (right) for the three test conditions:(a)–(b) Low (c)–(d) Medium (e)–(d) High

Chapter 5

Structural modification in the simple model

5.1 Introduction

This chapter is dedicated to the description of the structural modification conducted in the simple brake–clutch model with the aim of suppressing squeal noise.

A novel methodology for deciding over point structural modifications was explored. This was achieved using the receptance function with the idea of being able to compute the value of a point modification for a existing squealing system. The methodology used is described and applied to suppress squeal in the simple brake–clutch model.

5.2 The receptance method for squeal suppression

After identifying the squeal frequency, a receptance-based inverse dynamic method was explored to determine a point structural modification for squeal suppression. Two possibilities were analysed: a point mass modification and a ground connected spring modification. In the case of the simple model, the additon of either a point mass or spring to the fixed part implies fixing the position of the nodal lines and separating the frequencies of the doublet mode [131]. With this in mind, a point in the periphery of the fixed part (point A in Figure 5.1) was selected and the needed mass or stiffness for shifting the frequency of the mode with an antinode in the position A was computed. The

idea underneath is to obtain enough separation between the frequencies of the two modes so as to avoid mode coupling due to friction.

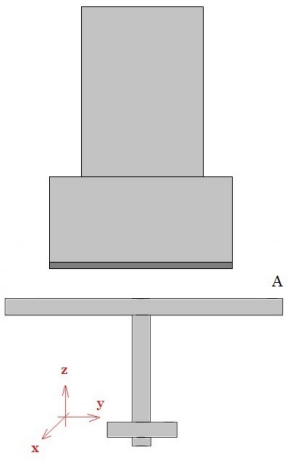

Figure 5.1: Position of the point structural modification

The amount of mass or stiffness was determined using the receptance similarly to the method proposed by Ouyang in [112] for structural modifications. The procedure is formulated below. The key is to express the receptance of the modified system by means of the receptance of the original system.

The equation of motion of the modified system in the Laplace domain can be written as follows:

$$\left[(\mathbf{M}+\mathbf{\Delta M})s^2+\mathbf{C}s+(\mathbf{K}+\mathbf{\Delta K})\right]\mathbf{X}(\mathbf{s})=\mathbf{0} \tag{5.1}$$

where $\mathbf{M}$, $\mathbf{C}$ and $\mathbf{K}$ are the mass, damping and stiffness matrices of the original system; $\mathbf{X}$ is the Laplace transform of the the nodal displacement vector of the system; $\mathbf{\Delta M}$ and $\mathbf{\Delta K}$ are respectively the modifications to the mass and stiffness matrices.

Taking into account that the receptance matrix is defined as $\mathbf{H}(s)=(\mathbf{M}s^2+\mathbf{C}s+\mathbf{K})^{-1}$, then Equation 5.5 can be rewritten as:

$$\left[\mathbf{I}+\mathbf{H}(s)(\mathbf{\Delta M}s^2+\mathbf{\Delta K})\right]\mathbf{X}(\mathbf{s})=\mathbf{0} \tag{5.2}$$

where $\mathbf{I}$ stands for the identity matrix. For N point masses, $\mathbf{\Delta M}$ can be expressed as:

$$\mathbf{\Delta M}=\sum_{i=1}^{N}\Delta m_i\mathbf{e}_i\mathbf{e}_i^{\intercal} \tag{5.3}$$

where $\mathbf{e}_i$ is a vector whose elements are zero except the ith element that is 1 and corresponds to the degree of freedom affected by the point modification and Δm_i is the ith added point mass.

Similarly, for M ground connected springs, $\mathbf{\Delta K}$ can be expressed as:

$$\mathbf{\Delta K} = \sum_{i=1}^{M} \Delta k_i \mathbf{e}_i \mathbf{e}_i^{\intercal} \tag{5.4}$$

where Δk_i is the ith added grounded spring.

Introducing this two terms in Equation 5.2 yields:

$$\left[\mathbf{I} + \mathbf{H}(s) \left(s^2 \sum_{i=1}^{N} \Delta m_i \mathbf{e}_i \mathbf{e}_i^{\intercal} + \sum_{i=1}^{M} \Delta k_i \mathbf{e}_i \mathbf{e}_i^{\intercal} \right)) \right] \mathbf{X}(\mathbf{s}) = \mathbf{0} \tag{5.5}$$

This system will only have a solution other than the trivial if:

$$\det \left(\mathbf{I} + \mathbf{H}(s)(s^2 \sum_{i=1}^{N} \Delta m_i \mathbf{e}_i \mathbf{e}_i^{\intercal} + \sum_{i=1}^{M} \Delta k_i \mathbf{e}_i \mathbf{e}_i^{\intercal}) \right) = 0 \tag{5.6}$$

If a mass modification is conducted at a degree–of–freedom A, Equation 5.6 becomes:

$$\begin{vmatrix} 1 & 0 & \cdots & 0 & s^2 h_{1A} \Delta m & 0 & \cdots & 0 \\ 0 & 1 & \cdots & 0 & s^2 h_{2A} \Delta m & 0 & \cdots & 0 \\ \vdots & \vdots & & \vdots & \vdots & \vdots & & \vdots \\ 0 & 0 & \cdots & 0 & 1 + s^2 h_{AA} \Delta m & 0 & \cdots & 0 \\ \vdots & \vdots & & \vdots & \vdots & \vdots & & \vdots \\ 0 & 0 & \cdots & 0 & s^2 h_{nA} \Delta m & 0 & \cdots & 1 \end{vmatrix} = 0 \tag{5.7}$$

from where the needed point mass for shifting an existing natural frequency to a desired one ω_h can be computed as:

$$\Delta m = -\frac{1}{s^2 \, h_{AA}(\omega_h)} \tag{5.8}$$

Similarly, the needed ground connected spring will be:

$$\Delta k = -\frac{1}{h_{AA}(\omega_h)} \tag{5.9}$$

where $h_{AA}(\omega_h)$ stands for the point receptance at the degree–of–freedom A for the desired frequency.

In the case under study, simulation receptances were used as they already include the effect of friction in the stiffness matrix [113]. The process for computing them was equivalent to the one used for complex modes in Chapter 4 but substituting the two last steps of the simulation with the computation of the response to an impulse force in the frequency domain:

1. *Nonlinear static analysis* for applying pressure and establish the contact area
2. *Nonlinear static analysis* to impose rotational speed on the disk so that friction is developed on the contact interface
3. *Direct steady state analysis* to compute the response of the system in the frequency domain when a impulse force is applied. The previous two steps make it possible to include the effect of contact and friction in the response.

The complete process is shown in Figure 5.2. It consists in an iterative method, first selecting a possible point for the structural modification, then, computing the receptance at this point for the desired frequency and, finally, obtaining the needed value for either mass or stiffness. This modification should be applied to the finite element model so as to study the stability of the modified system: if it is stable the process is finished; if it is not, a different frequency or point has to be selected and the process starts again.

The main limitation of this method is choosing the ω_h frequency as it is not possible to know in advance how much separation in frequency between two eigenvalues is needed for the modes not to couple when friction is applied. This implies that several iterations must be performed until the required frequency shift is achieved.

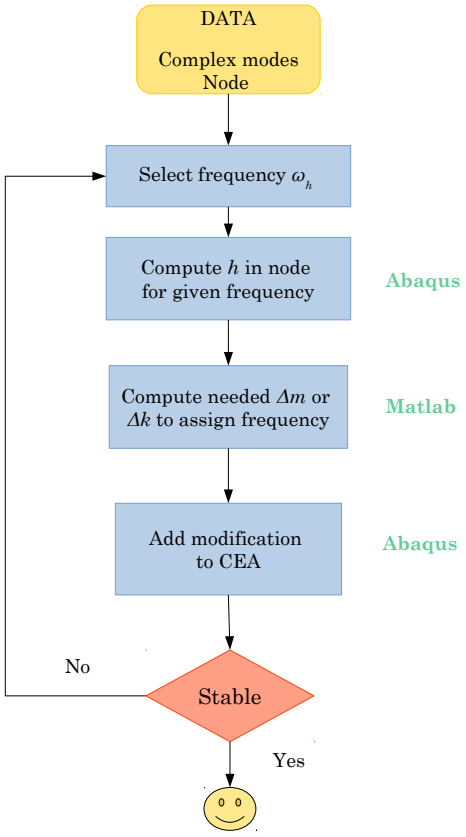

Figure 5.2: Process for computing a point structural modification to stabilise the system

5.3 Proposed methodology

In view of the above, the following methodology was proposed to suppress squeal in the simple model to avoid iteration when assigning frequencies:

1. Select a point for the point structural modification
2. Compute the receptance around the squealing frequency
3. Use Equation 5.8 and Equation 5.9 to compute the needed mass or stiffness to assign each frequency in the range

4. Perform a parametric study to check the effect of the modification in the stability of the system

5. Decide over the value of the point modification

This methodology is summarised in Figure 5.3.

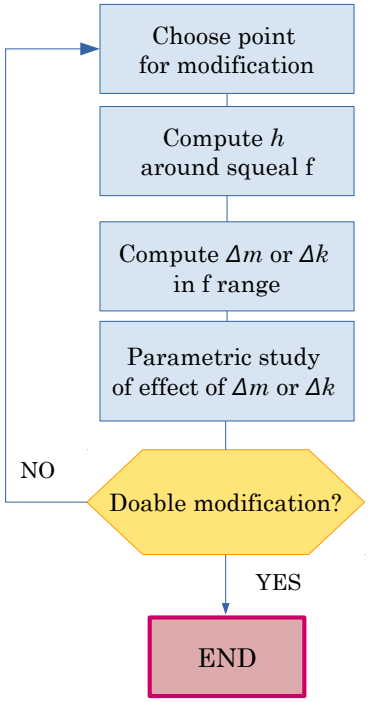

Figure 5.3: Proposed methodology for squeal suppression

For the practical implementation of this methodology see Appendix C.

5.4 Case study

The test with the lowest conditions was selected (see Section 4.3.1) as a case study as it presented the fewer squeal frequencies. The study focused in the first squeal frequency that occurred at 7.5 kHz and corresponded to the simulation mode that has six nodal diameters and a frequency of 7.4 kHz (Figure 5.4).

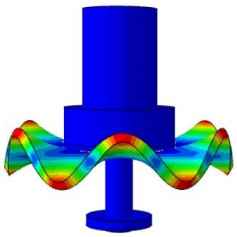

Figure 5.4: Shape of the unstable squealing mode

Receptance was computed in the vicinity of the squealing mode, from 7 kHz to 8 kHz, and using Equation 5.8 and Equation 5.9 the amount of mass or stiffness needed to assign a frequency in the range was obtained (Figure 5.5).

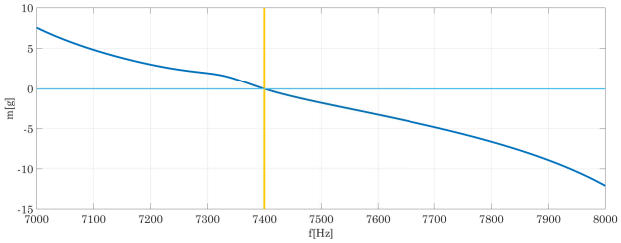

(a) Needed mass

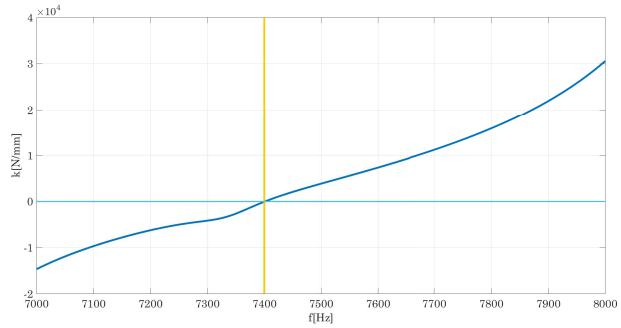

(b) Needed stiffness

Figure 5.5: Needed point modification to assign a certain frequency

The imaginary part of the mass or stiffness modification was neglected for both options because in this case it represents the amount of negative damping needed to shift the eigenvalue along the real axis of the complex plane [109], as only frequency and not real part of the eigenvalue had been assigned.

Once the range of the parameters was obtained, two parametric studies were performed to check the effect of the modifications in complex modes: one for the case of adding a single point mass shown in Figure 5.6 (a) and the other for the case of adding a ground connected spring shown in Figure 5.6 (b). In this case, a point mass cannot be used to avoid coupling since it causes another unstable mode to appear. The addition of a ground connected spring, by contrast, seamed to be able to uncouple the doublet mode.

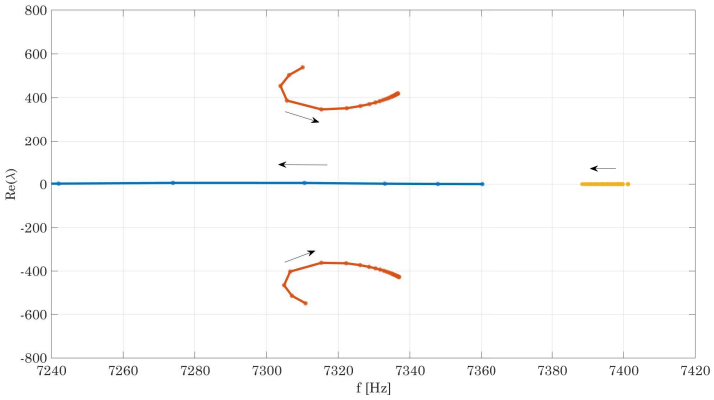

(a) Stability diagram for different values of mass (0 – 8g)

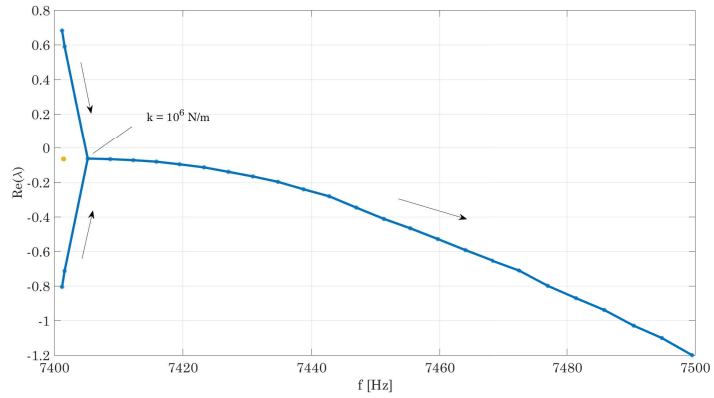

(b) Stability diagram for different values of stiffness (0 – $3{\cdot}10^7$N/m)

Figure 5.6: Stability diagrams from the parametric studies. The arrows show the evolution of the eigenvalue in the complex plane when increasing the parameter under study

According to the simulation, a k value greater than 1000 N/mm is enough to suppress squeal, but adding such a small value of stiffness is challenging from the point of view of design. With this in mind, a stiffness value of approximately

7000 N/mm was selected for the ground connected spring since such a value did not cause other modes to coalesce to result in a new unstable mode.

The desired value of stiffness was accomplished by means of a 0.8 mm diameter steel wire of length of 14.6 mm, that added 6890 N/mm to the system. The setup is shown in Figure 5.7 and simply consists in a support for the steel wire. This tool was firmly fixed to the structure of the tribometer, which in this case serves as the ground. The steel wire could be preloaded by tightening the screw on top so it was also effective under compression. The damping introduced to the experimental system by this tool was not taken into account.

Figure 5.7: Setup including a ground connected spring

This value of stiffness separates the doublet mode at 7.4 kHz into two different modes, one at 7.4 kHz and the other at 7.58 kHz. The mode with lower frequency stays at 7.4 kHz since for this mode the spring is located on a nodal line. This happens because introducing a perturbation to an axisymmetric system fixes the position of the nodal lines. The aforementioned effect can be seen in Figure 5.8 where simulation FRFs in point B with and without the ground connected spring are shown. For both cases an impulse force was applied in point B and the response was computed also in point B.

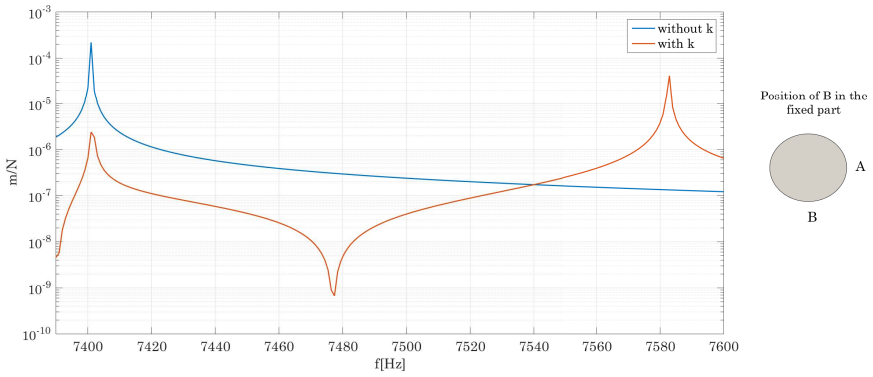

Figure 5.8: Comparison of the FRFs in point B with and without the added ground connected spring

Squeal tests were repeated on the modified system. As expected, the addition of the spring to the system caused the squeal to disappear and its removal (t=3232 s) took squeal back as it can be seen in the spectrogram in Figure 5.9.

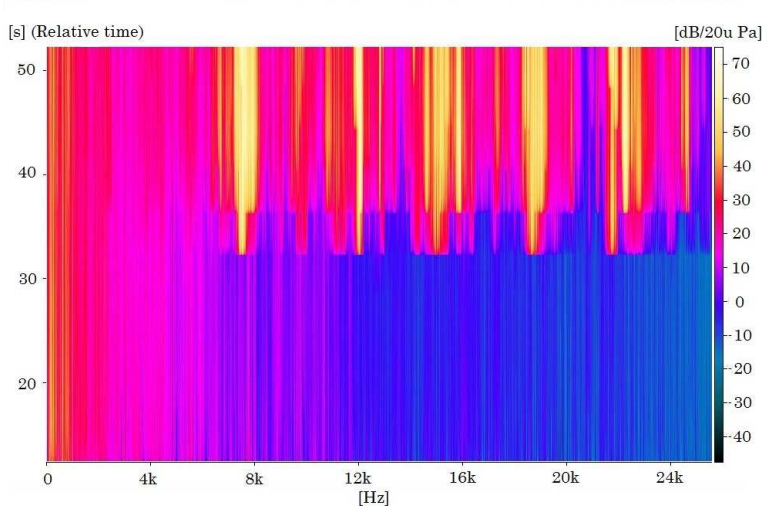

Figure 5.9: Spectrogram of squeal test with added ground connected spring.

If the spectra before and after the addition of the spring are compared (Figure 5.10) a difference greater than 50 dB in sound pressure can be noticed.

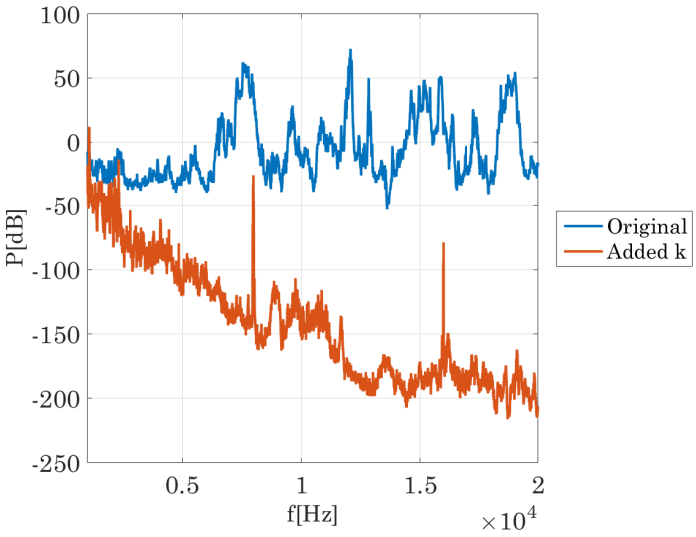

Figure 5.10: Spectra for the case with and without the added spring

5.5 Conclusions

In this chapter a methodology for squeal suppression in the brake–clutch simple model is proposed and applied in the experimental setup. The methodology is based in simulation receptances including contact and obtains the needed point mass or ground connected spring that should be added in a specific point in order to uncouple modes.

Using this method the needed ground connected spring to suppress squeal in the simple model was computed and experimentally tested with the outcome of eliminating actual squeal noise.

This work is thought to be the first one to suppress squeal in a using a theoretically derived structural modification.

Chapter 6

Real brake–clutch model

6.1 Introduction

Once the simple model had been designed and studied, the analysis of the real system started. The same process followed for the simple model was adopted for the brake–clutch. First, a finite element model was created and its validity was checked in two steps: the natural frequencies and mode shapes obtained from EMA were compared with simulation results and, after, experimental squeal frequencies and frequencies of unstable modes from CEA were compared. The real brake–clutch model includes anisotropic properties for the friction material and friction damping.

In summary, this chapter covers the creation and validation process of a simulation model for squeal prediction for a real brake–clutch system.

6.2 Description of the model

In this section the finite element developed for the real brake–clutch will be described. For the brake–clutch model anisotropic material properties for the friction material and friction damping. Below the main features of the FE model will be addressed.

Boundary conditions and joints

The boundary conditions and joints can be condensed in the three following points:

- The two covers are tied together and to the axis

- The rotor can move along and around the axis
- The lining–holders in either side1 are clamped to each correspondent support

These interactions may be better understood if the schematic in Figure 6.4 is considered.

Contact

As done for the simple model, the tangential behaviour was modelled with the *Penalty* method and the normal behaviour with the *Hard Contact* option allowing separation. For all the contact interactions the surface made of friction material was the slave surface and brake or clutch cover, both of the made of cast iron, the master surface.

Unlike the rest of the factors, for contact simulation in the real model the constant friction coefficient of $\mu = 0.32$ given by the manufacturer had to be used because the limitations of the pin–on–disk setup for the low pressure range (under 1 MPa) did not permit to have a more accurate value. Anyway, as seen in Section 4.5.2, even though the inclusion of a speed and pressure depend friction coefficient results in a better prediction, the results do not differ too much from the ones obtained using a constant friction coefficient.

The contact areas for the elements involved in the clutch–engagement manoeuvre are shown in Figure 6.1 and the ones for the braking manoeuvre are shown in Figure 6.2.

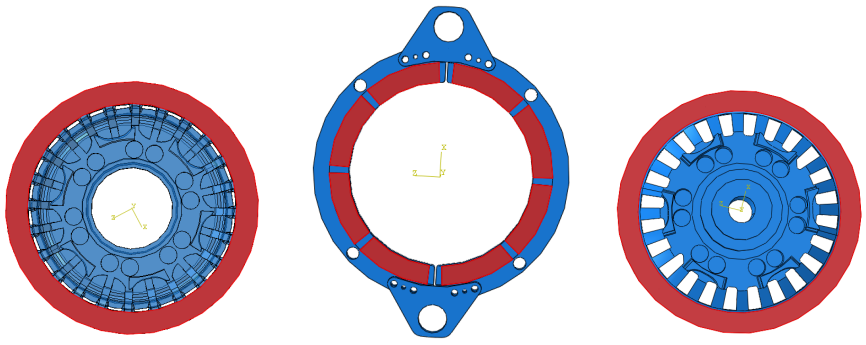

(a) (b) (c)

Figure 6.1: Contact in clutch–engagement simulation (a) Contact area in rotor (b) Contact area in the lining–holder, only one side is shown but contact happens equally in both sides (c) Contact area in the clutch side cover

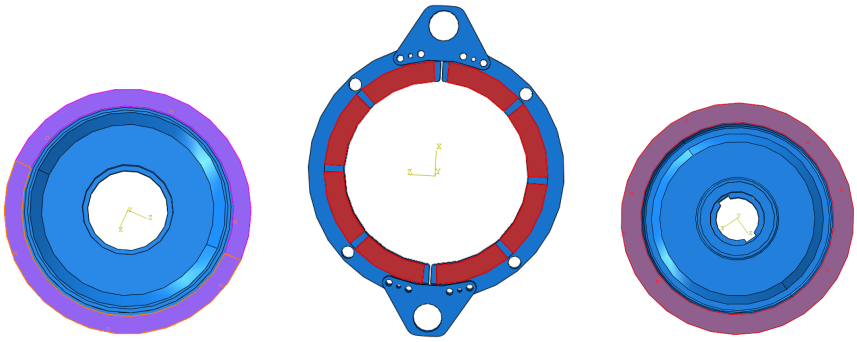

(a) (b) (c)

Figure 6.2: Contact in braking simulation (a) Contact area in rotor (b) Contact area in the lining–holder, only one side is shown but contact happens equally in both sides (c) Contact area in the brake side cover

Spring modelling

The springs that serve the purpose of braking were modelled as an applying an uniform pressure in the areas shown in Figure 6.3. This pressure was computed using the springs' data:

- $k = 42.5\,\mathrm{N/mm}$
- $L = 87\,\mathrm{mm}$
- $D = 28\,\mathrm{mm}$

Taking into account that the space for the spring has 62.3 mm in length, the exerted force will be:

$$F = k\Delta L = 42.5 \cdot (87 - 62.5) = 1041.25\,\mathrm{N}$$

Dividing it by the area of the circle where the springs are based gives:

$$P = \frac{F}{A} = 1.691 \cdot 10^6\,\mathrm{Pa}$$

Element type and number of DOF

In this case, unlike the simple model, quadratic tetrahedra elements were used because the difficulty of meshing such a complex geometry with incompatible mode hexaedra. The model has 1,941,501 degrees of freedom.

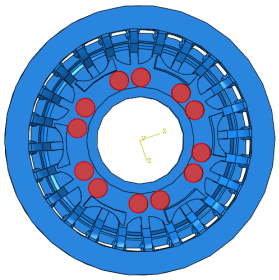

Figure 6.3: Position of the springs in the rotor

The main features of the simulation of both manoeuvres are summarised in Figure 6.4.

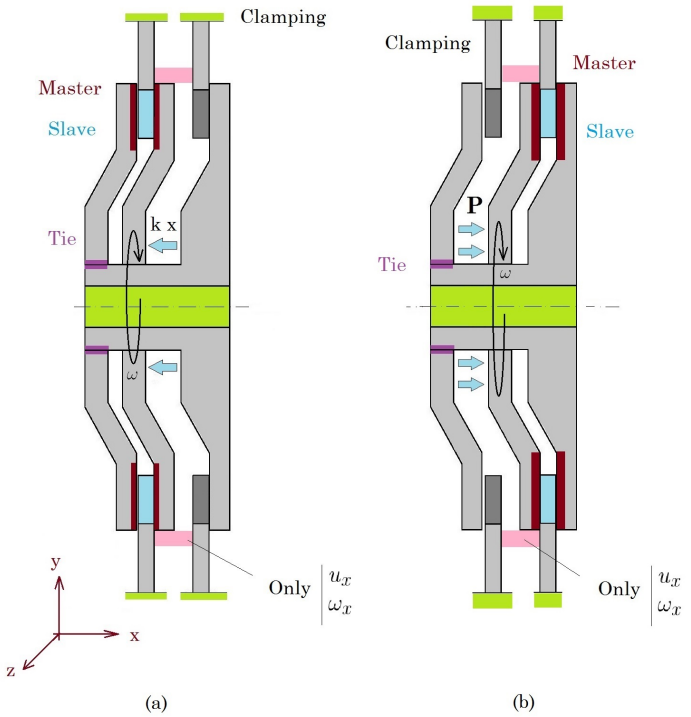

Figure 6.4: Brake–clutch simulation schematic (a) Braking manoeuvre (b) Clutch–engagement manoeuvre

6.2.1 Validation

In order to validate the accuracy of the mesh, the vibration modes of the components were obtained experimentally and then compared to the ones computed via finite element simulation. Good correlation was attained both for the mode shape and frequency since the mean error is 6 % and a fair amount of modes show a MAC value higher than 0.75. The results of the EMA tests are summarised in Table 6.1 but a more detailed description can be found in Appendix B.

Table 6.1: Summary of the results of the correlation of the components

Component	Number of modes MAC > 0.75	Maximum relative error [%]	Mean error [%]
Brake side cover	6	8	4
Rotor	10	4	2.2
Clutch side cover	(6)[1]	15	6
Lining–holder	18	3	1.8

This degree of correlation implies that the elastic properties were properly characterised and that the mesh of the simulation model is acceptable.

6.3 Squeal simulation

The process for squeal simulation in the brake–clutch was equivalent to the one used for the simple model (see Section 4.2). Only the differences will be addressed below.

The process for the computation of complex modes is divided into four steps:

1. *Application of force*: for the clutch–engagement manoeuvre, a pressure is applied in the pressure chamber in order to simulate the pneumatic pressure; for the braking manoeuvre, the force exerted by the springs is applied in the areas described in Section 6.2.

2. *Application of rotation speed*: a rotation speed of 800 rpm is applied to the rotor. The requirement is to have a relative rotation speed between the components and applying it to the rotor is the simplest approach.

[1] For the clutch side cover MAC was not computed because even if correlation was good regarding frequency, it was not possible to successfully correlate the mode shape due to the complexity. In this case this number represents the number of simulation modes that had a error in frequency lower than the maximum error.

3. *Computation of normal modes*: the normal modes in the 1–20 kHz frequency range are computed.

4. *Computation of complex modes*: the complex modes in the 1–20 kHz frequency range are computed to determine the possible instabilities.

After performing the CEA computation the complex modes shown in Figure 6.5 were obtained. It can be seen that the number of unstable complex modes is high specially in around 4000 Hz.

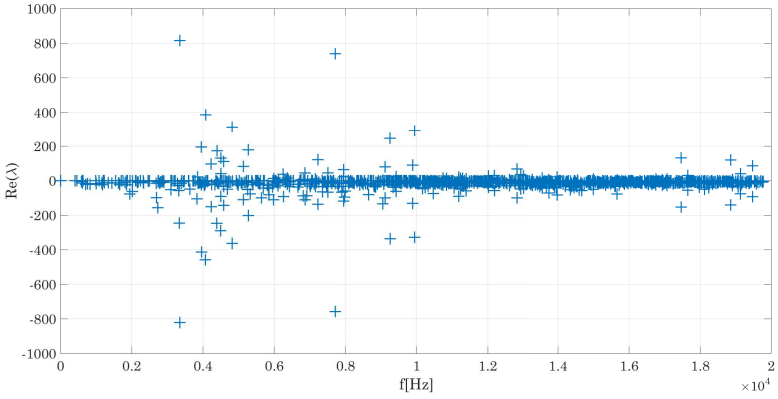

(a)

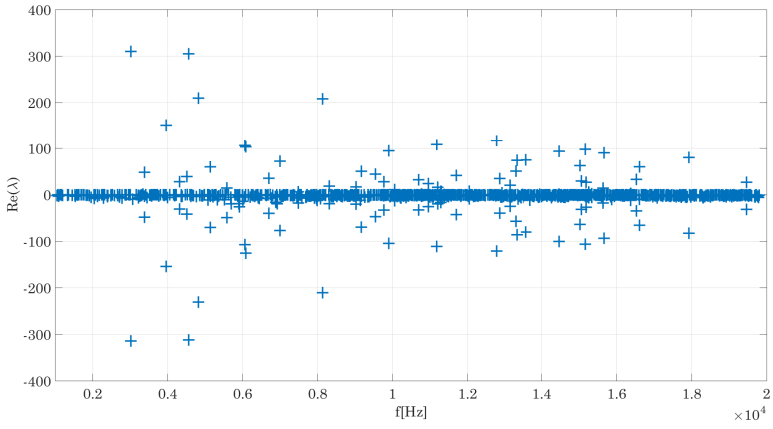

(b)

Figure 6.5: CEA for the brake–clutch system (a) Clutch–engagement (b) Braking

6.4 Experimental tests

Once the simulation model was finished, some experimental tests were carried out with the objective of checking the ability of the model to predict the squeal frequencies. In this section the test bench and the results will be described.

6.4.1 Test bench setup

The test rig simulates the typical application for a brake–clutch: a punch press. It consist in a brake–clutch with its brake side lining–holder attached to a fixed structure and its clutch side lining–holder connected to a flywheel (Figure 6.6). It is equipped with different flywheels in order to reproduce different inertias.

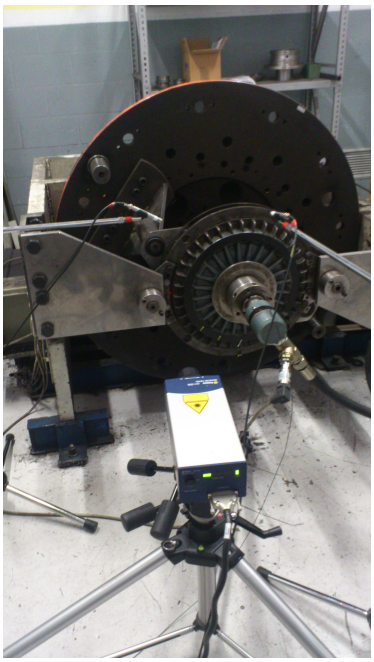

Figure 6.6: Test bench including sensors

The test bench has integrated sensors for applied pneumatic pressure and rotating speed. Apart from these two measurements, sound pressure in radial and axial direction and vibration in the rotor in the out–of–plane direction were measured. Vibration in the rotor was measured using a laser vibrometer through a purpose–built hole in the brake side cover and lining–holder. All these characteristics appear in Figure 6.7.

Tests were performed at a rotation speed of 800 rpm. Each test consist in a series of alternating braking and clutch–engagement manoeuvres lasting around

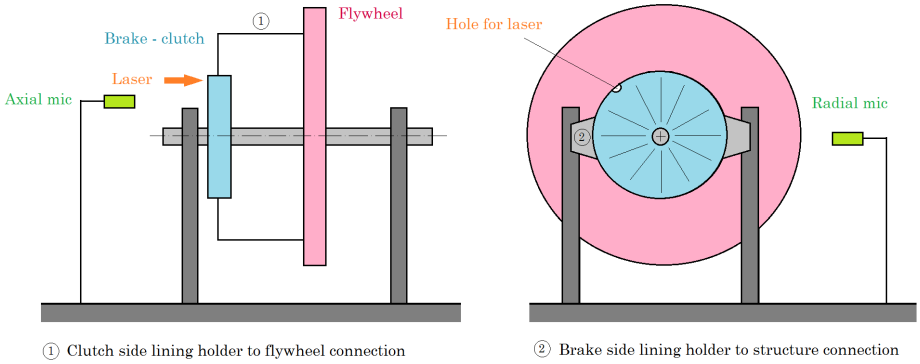

Figure 6.7: Test bench schematic showing sensor position

1 minute total. An example of a typical measurement is shown in Figure 6.8.

6.4.2 Experimental results

The first thing that stands out in the experimental results is that for both cases squeal happens at the beginning of the manoeuvre, when the pressure and rotation speed conditions are changing. Once the working conditions reach a constant value, squeal disappears. This effect can be clearly seen in the sample squeal test in Figure 6.8 and can be confirmed if Figure 6.9 is considered, in which the spectrogram of the sound pressure signal for a full working cycle comprising a clutch–engagement and a braking manoeuvre is shown. This phenomenon reveals the relationship of brake–clutch squeal with transient conditions.

From now on the two manoeuvres will be addressed separately.

Clutch–engagement manoeuvre

In Figure 6.10 the signals obtained in a typical clutch–engagement manoeuvre are presented. It can be seen that in this manoeuvre squeal has transient nature, since it appears during the phase were operation conditions change.

If the noise spectra is considered, little difference can be noticed between the axial and the radial microphone signals, both having a main peak at 4.1 kHz and its harmonics (Figure 6.11)

The same information can be extracted from the laser signal so it is not added here.

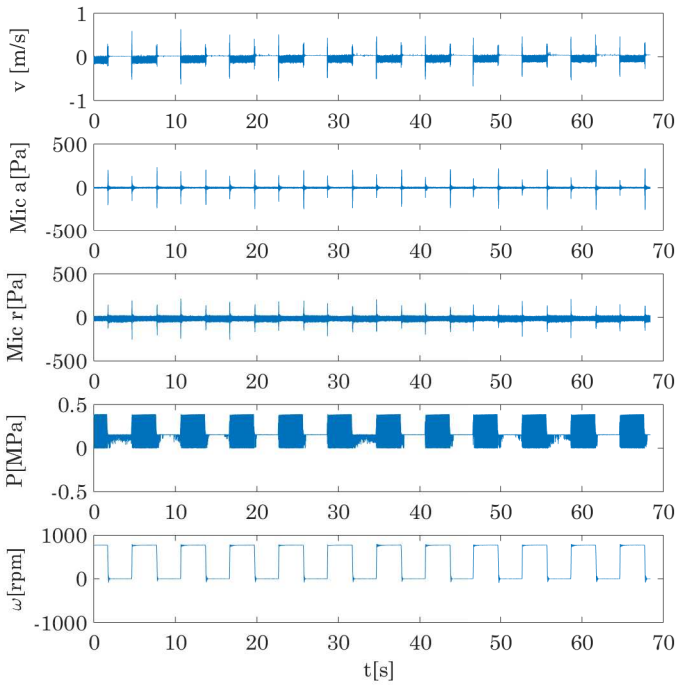

Figure 6.8: Sample squeal test

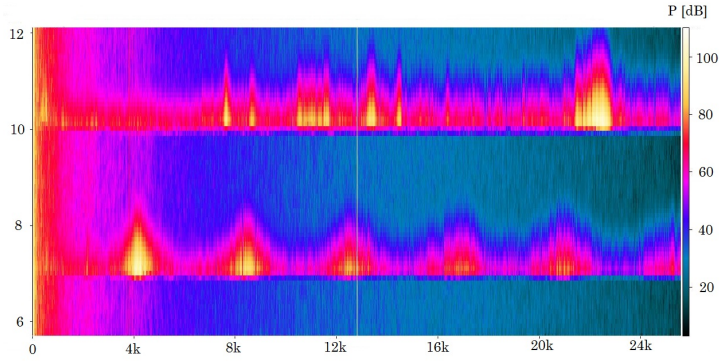

Figure 6.9: Spectrogram of a working cycle containing a manoeuvre of each type

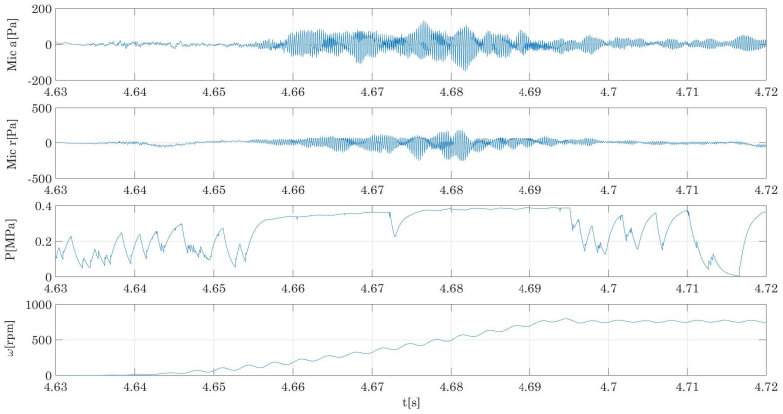

Figure 6.10: Signals measured during clutch–engagement. It can be seen that squeal presents transient nature

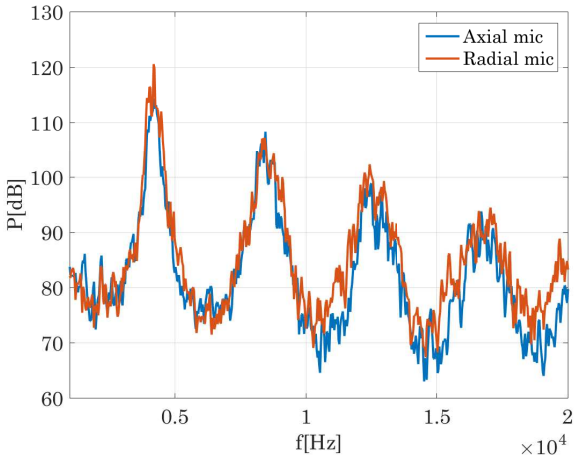

Figure 6.11: Spectra in axial and radial microphones for clutch–engagement manoeuvre

Braking manoeuvre

The braking manoeuvre also presents tranisent nature (Figure 6.12) for the reason mentioned above.

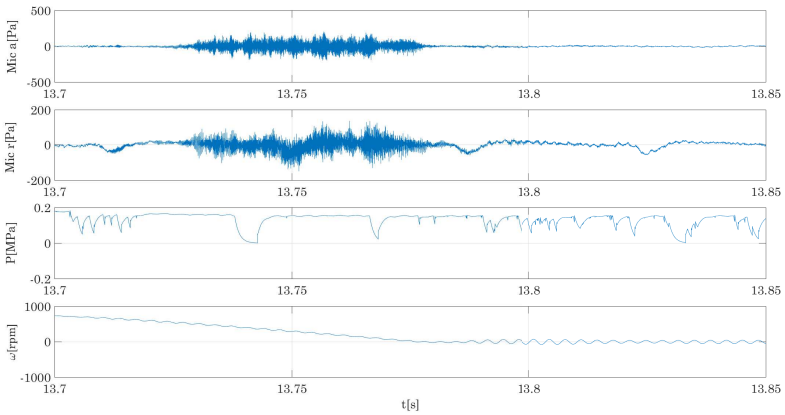

Figure 6.12: Signals measured during clutch–engagement. It can be seen that squeal presents transient nature

In this case the noise spectra do not show a prevailing frequency but some peaks distributed along the measured range. The spectra are more complex, but there is a main peak at 4.2 kHz (Figure 6.13), near to the squeal frequency in clutch–engagement manoeuvre. In addition, the noise level in this case is much lower than for clutch–engagement.

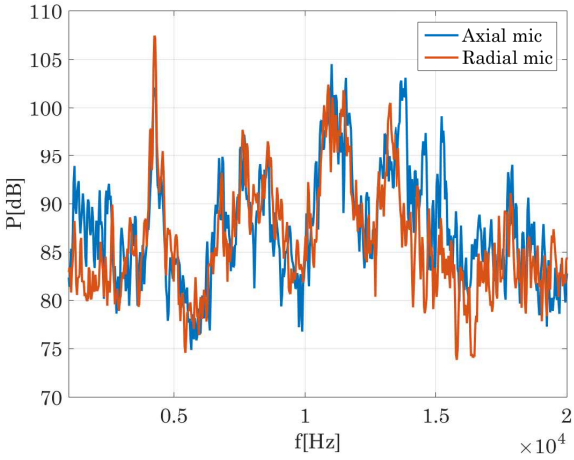

Figure 6.13: Spectra in axial and radial microphones for braking manoeuvre

6.5 Comparison of simulation results with experimental data

In this section the frequencies of the unstable modes obtained in CEA will be compared to the squeal frequencies in the tests.

As previously seen, the brake–clutch has several unstable modes for both manoeuvres, so in this case a Squeal Index [136,137] was used to discard some unstable modes. Squeal Index is defined as:

$$\mathrm{SI} = \frac{\mathrm{Re}(\lambda)}{\mathrm{Im}(\lambda)}$$

The unstable modes with and SI $< 1\%$ (Figure 6.14) are discarded. The high level of overprediction is probably related not only to the impossibility to correctly measure the friction coeffient in the pin–on–disk setup but also to the rest of the simplifications in the modelling process such as the exclusion of material damping.

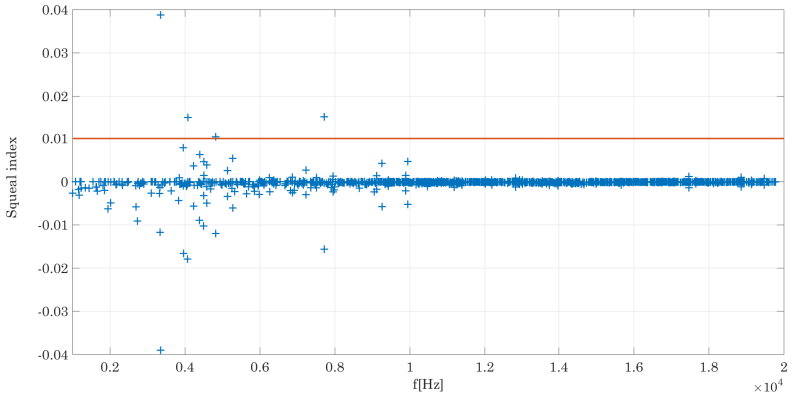

(a)

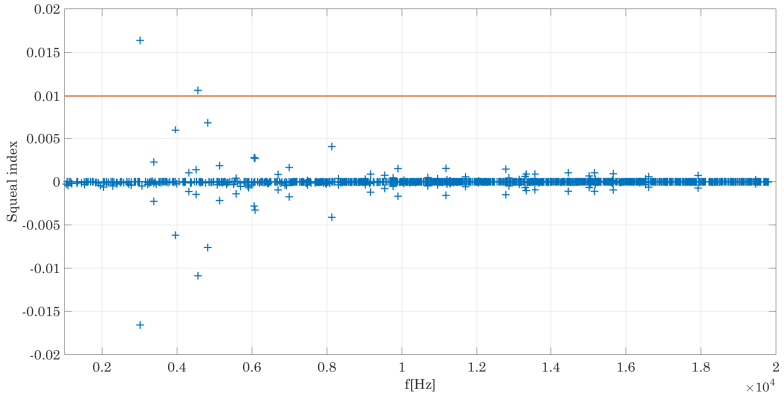

(b)

Figure 6.14: Squeal index applied to CEA results (a) Clutch–engagement (b) Braking

6.5.1 Clutch–engagement manoeuvre

This manoeuvre shows a single squeal frequency that is properly predicted by the CEA but there is some overprediction even after applying the Squeal Index (Figure 6.15).

Experimental squeal occurs at 4100 Hz whilst the closest unstable simulation mode has a frequency of 4076 Hz, which means that the deviation in frequency from the experimental squeal frequency is 0.58 % (Figure 6.15). This mode is shown in Figure 6.19 where it can be seen that mainly the clutch side cover and the rotor participate the most in the movement.

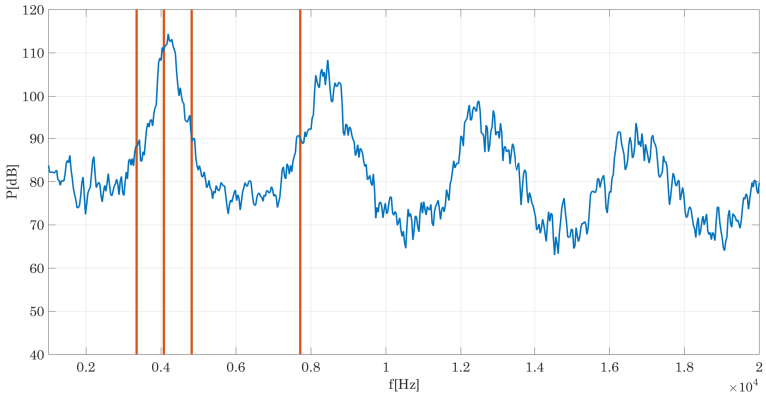

Figure 6.15: Comparison between noise spectrum and CEA for the brake–clutch in clutch–engagement manoeuvre

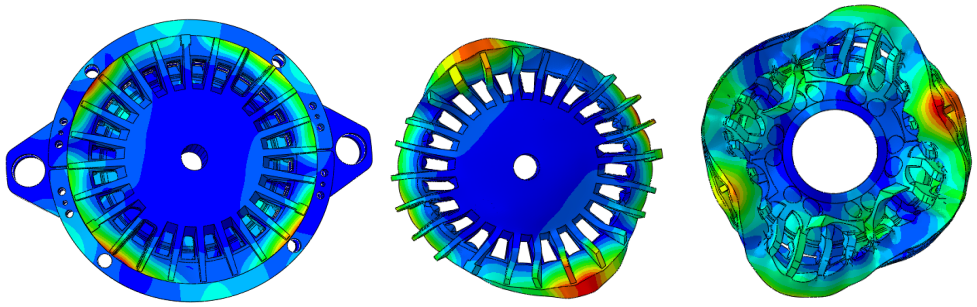

(a) (b) (c)

Figure 6.16: Squealing mode for the clutch–engagement manoeuvre showing the movement of (a) the complete system, (b) the clutch side cover alone and (b) the rotor alone

The squealing mode for the clutch–engagement manoeuvre is a combination of a mode of the clutch side cover together with a mode of the rotor. The cover's mode has two nodal lines and a nodal circumference and occurs at 4139.3 Hz. The rotor's mode has four nodal lines and occurs at 4347.6 Hz. Both modes are shown in Figure 6.17

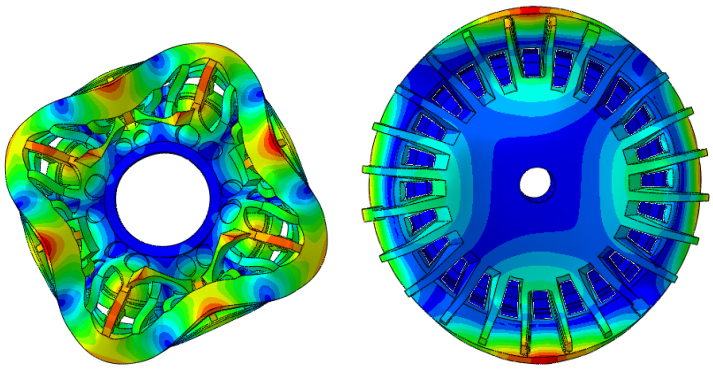

(a) (b)

Figure 6.17: The squealing mode corresponds to (a) the (4,0) mode of the rotor together with (b) the (2,1) mode of the cover. Where (a, b) denotes the number of nodal lines and nodal circumferences

6.5.2 Braking manoeuvre

In this case the results are similar to the clutch–engagement manoeuvre, the main squeal frequency is predicted but not so accurately as in the previous case. Experimental squeal occurs at 4288 Hz whilst the closest unstable simulation mode has a frequency of 4558 Hz, which means that the deviation in frequency from the experimental squeal frequency is 6.3 % which in any case is not a high error (Figure 6.18). The shape of the unstable mode identified as the squealing mode is shown in Figure 6.19 where it can be seen that mainly the brake side cover and the rotor are involved in the movement.

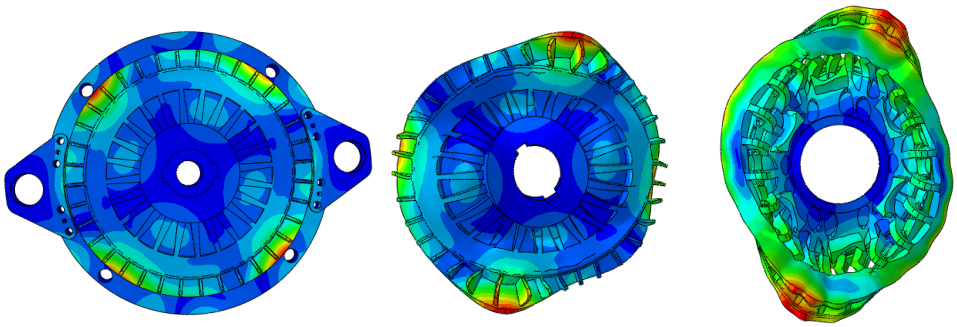

(a) (b) (c)

Figure 6.19: Squealing mode for the braking manoeuvre showing the movement of (a) the complete system, (b) the brake side cover alone and (b) the rotor alone

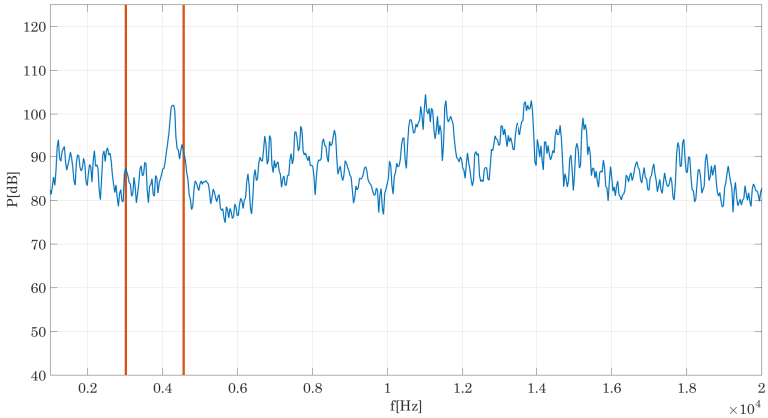

Figure 6.18: Comparison between noise spectrum and CEA for the brake–clutch in braking manoeuvre

The squealing mode for the braking manoeuvre is a combination of a mode of the brake side cover together with a mode of the rotor. The cover's mode has two nodal lines and a nodal circumference and occurs at 4445.3 Hz. The rotor's mode has the same shape but occurs at 4843.7 Hz. Both modes are shown in Figure 6.20

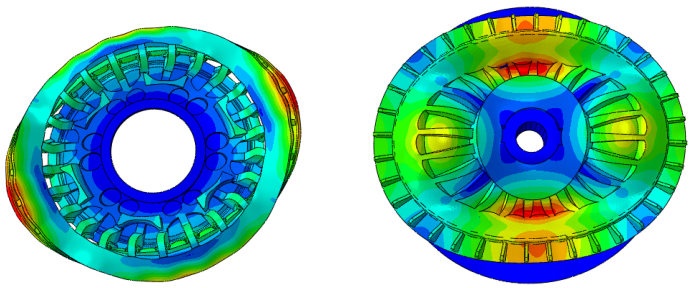

(a) (b)

Figure 6.20: The squealing mode corresponds to (a) the (2,1) mode of the rotor together with (b) the (2,1) mode of the cover. Where (a, b) denotes the number of nodal lines and nodal circumferences

6.6 Conclusions

In this chapter the development and later validation of a finite element model for brake–clutch squeal prediction has been described. When developing the FE model, the insight gained in Chapter 4 was used to ease the modelling process of the real brake–clutch system, so the material properties previously obtained and friction damping were introduced to the model directly. Mesh validation was done by means of comparing simulation modes with EMA results, as well.

After the model had been created, experimental test were performed in a brake–clutch in a test bench and the experimental squeal frequencies were compared to the frequency of the unstable complex modes computed.

To achieve acceptable correlation a Squeal Index was used in the simulation model so as to reduce the level of overprediction, this overprediction if probably related to the failure to characterise properly the friction coefficient in the low pressure range due to limitations in the pin–on–disk setup and to the simplifications inherent to a modelling process.

In any case, after setting the SI to 1 % and disregarding the unstable modes below this value, it was possible to reach a fair correlation between predicted squeal frequencies and measured ones, since maximum frequency deviation was 6.3 % for the braking manoeuvre and 0.58 % for the clutch–engagement manoeuvre.

Chapter 7

Structural modification in the brake–clutch

7.1 Introduction

In this chapter the methodology for structural modification described in Chapter 5 will be applied to the case of the real brake–clutch. As done for the simple model, simulation receptances will be used to compute the amount of mass or stiffness needed to prevent the appearance of the unstable squealing mode.

7.2 Receptance-based point structural modifications

In this section the use of the receptance function for the computation of the needed structural modification in the real system is presented. Both the cases of the addition of mass and stiffness are explored.

Being the clutch–engagement manoeuvre the most noisy one and taking into account that once the process is understood it can be applied to any structure, the clutch–engagement manoeuvre was taken as the working case.

7.2.1 Balanced mass

For the performance of the brake–clutch to be correct, it is necessary to keep the system balanced. The degree of balance needed for the application is 6.3, meaning that supposing the system to be perfectly balanced before the addition of the point mass, the maximum amount of mass that can be added to the

periphery of the brake–clutch is less than 30 g, a negligible value for a system that has a total weight of around 70 kg.

For this reason it is not possible to add a single mass to modify the natural frequencies of the system. Therefore, the methodology presented in Chapter 5 has to be accordingly modified to preserve balance whilst shifting the mode involved in squeal.

Taking as a start point Equation 5.6 and reducing the determinant for the case that a balanced mass modification is applied, yields the following equation:

$$\left| \begin{bmatrix} 1 & 0 \\ 0 & 1 \end{bmatrix} + s^2 \begin{bmatrix} \Delta m & 0 \\ 0 & \Delta m \end{bmatrix} \begin{bmatrix} h_{11} & h_{12} \\ h_{21} & h_{22} \end{bmatrix} \right| = 0 \tag{7.1}$$

Which can also be represented as:

$$s^4 \det(\mathbf{H})\, \Delta m^2 + s^2 \operatorname{tr}(\mathbf{H})\, \Delta m + 1 = 0 \tag{7.2}$$

that, as a second degree equation, has two different results.

Returning to the real system, points A and B in the clutch side cover were selected as the location for the balanced point masses (Figure 7.1).

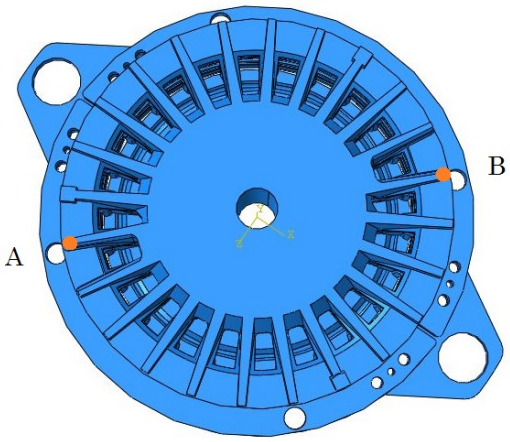

Figure 7.1: Position of the balanced masses in the clutch side cover of the brake–clutch

There were two reasons for this decision:

- Because of the shape of the mode (see Figure 6.16), the points at the periphery have a greater response, so a point mass added here will have more effect

- The cover is easily accessible and does not interact with other elements so making a modification in it does not alter the system

Applying Equation 7.2 for the clutch engagement manoeuvre in the vicinity of the squealing frequency (4050–4170 Hz) and using simulation receptances from points A and B results in Figure 7.2, where for each frequency the greater value of mass obtained from Equation 7.2 has been represented in blue and the lower in orange.

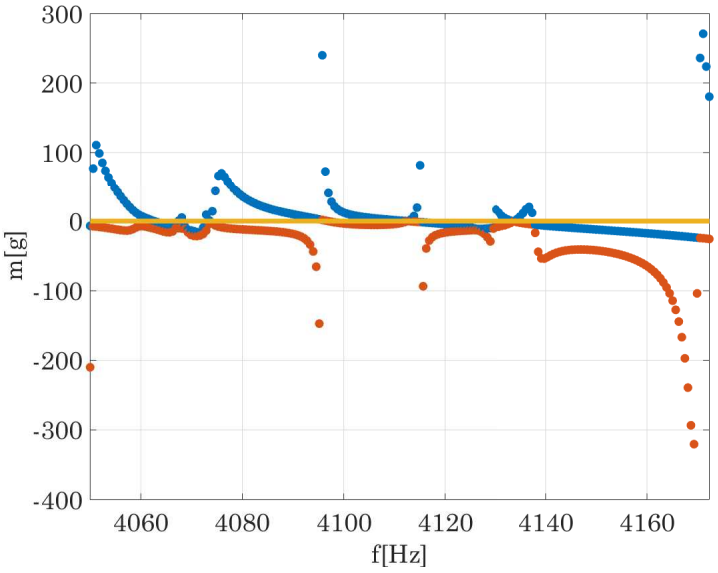

Figure 7.2: Needed balanced mass in frequency

Once the range of the needed balanced mass was computed, a parametric study of the effect of this mass was performed, with the mass ranging from 10 g to 70 g in 10 steps. If instead of the real part the Squeal Index is plotted it can be determined the amount of mass to add in order to reduce the squeal propensity under the threshold of 1 %. As shown in Figure 7.3, adding two balanced masses of 23 g or more is possible to stabilise the system. Care should be taken not to create a new unstable eigenvalue, for example, the eigenvalue at 4400 Hz gets more unstable with the addition of mass and adding 70 g nearly destabilises the system.

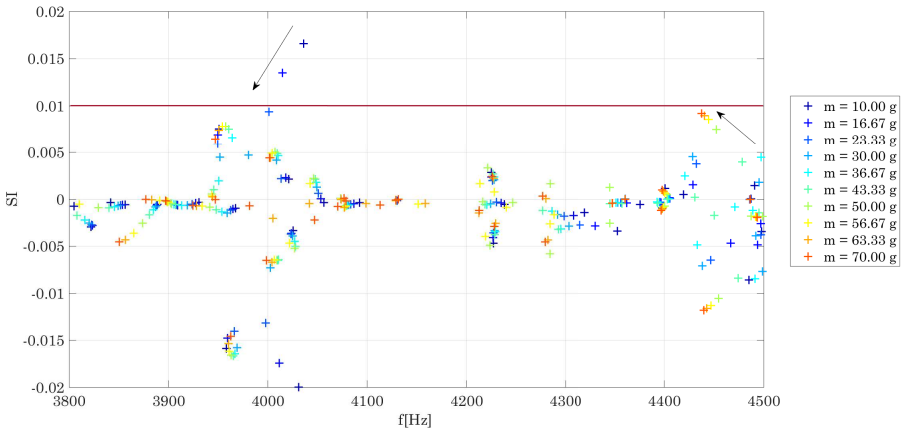

Figure 7.3: Parametric study of the effect of the added masses

7.2.2 Spring between two degrees of freedom

Another possibility is to add a spring between two degrees of freedom i and j. In this case, the modification affects four positions in the stiffness matrix of the system, the values that have to be added are shown in Equation 7.3.

$$\Delta\mathbf{K} = \begin{matrix} \\ i \\ j \end{matrix} \begin{matrix} \begin{matrix} i & \quad j \end{matrix} \\ \begin{pmatrix} k & -k \\ -k & k \end{pmatrix} \end{matrix} \tag{7.3}$$

The $\Delta\mathbf{K}$ matrix can be represented using unitary vectors as:

$$\Delta\mathbf{K} = k\left(\mathbf{e}_i\mathbf{e}_i^\intercal + \mathbf{e}_j\mathbf{e}_j^\intercal - \mathbf{e}_i\mathbf{e}_j^\intercal - \mathbf{e}_j\mathbf{e}_i^\intercal\right) \tag{7.4}$$

Where $\mathbf{e}_p$ stands for a unitary vector with zeros in every position except for position p.

Introducing the value of $\Delta\mathbf{K}$ in Equation 5.2 yields:

$$\left[\mathbf{I} + \mathbf{H}(s)k\left(\mathbf{e}_i\mathbf{e}_i^\intercal + \mathbf{e}_j\mathbf{e}_j^\intercal - \mathbf{e}_i\mathbf{e}_j^\intercal - \mathbf{e}_j\mathbf{e}_i^\intercal\right)\right]\mathbf{X}(\mathbf{s}) = \mathbf{0} \tag{7.5}$$

For this equation to have a solution the determinant of the leftmost matrix must be equal to zero:

$$\left|\mathbf{I} + \mathbf{H}(s)k\left(\mathbf{e}_i\mathbf{e}_i^\intercal + \mathbf{e}_j\mathbf{e}_j^\intercal - \mathbf{e}_i\mathbf{e}_j^\intercal - \mathbf{e}_j\mathbf{e}_i^\intercal\right)\right| = 0 \tag{7.6}$$

Reducing the determinant to is simplest form gives:

$$\begin{vmatrix} 1 + k\,(h_{ii} - h_{ij}) & k\,(h_{ij} - h_{ii}) \\ k\,(h_{ji} - h_{jj}) & 1 + k\,(h_{jj} - h_{ji}) \end{vmatrix} = 0 \tag{7.7}$$

That solving for k and taking into account that $h_{ij} = h_{ji}$ yields:

$$k = \frac{-1}{h_{ii} + h_{jj} - 2h_{ij}} \tag{7.8}$$

This procedure was followed in two different ways:

- Adding a spring between two ribs
- Adding a spring connecting the two covers

The computations and results of these two approaches are described in the following two sections.

Spring between two ribs

The first idea was connecting two ribs in the clutch side cover by a spring (Figure 7.4). The value of the spring was computed using Equation 7.8, the result is shown in Figure 7.5. It is worth noticing the small range of positive stiffness available due to the high number of modes in the frequency range — each zero crossing represents a natural frequency.

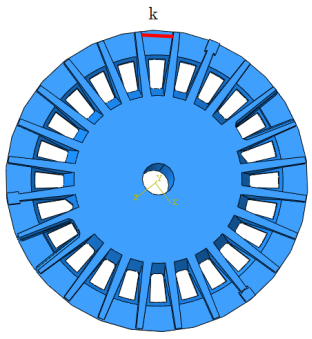

Figure 7.4: Position of the spring in the clutch side cover

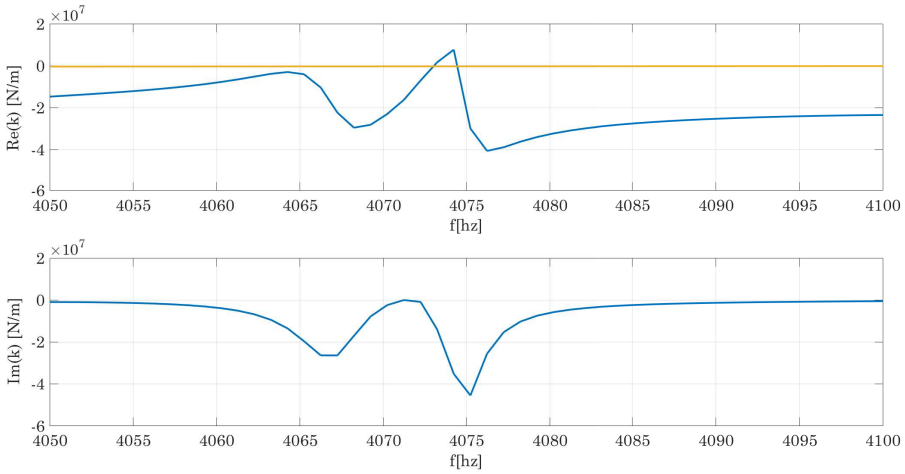

Figure 7.5: Needed stiffness for the spring in frequency

Once the range of the needed stiffness was computed a parametric study was performed with the stiffness ranging from 10^6 to $8 \cdot 10^6$ N/m. As shown in Figure 7.6 the effect of this spring is nearly negligible, presumably because the squealing mode is an out–of–plane mode.

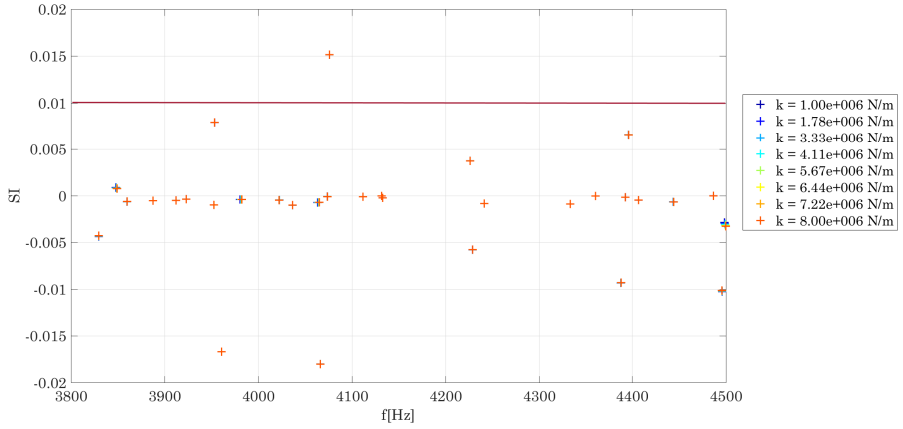

Figure 7.6: Parametric study of the effect of the added spring

Spring connecting two covers

The second idea was connecting the two covers with a spring so as to affect more the out–of–plane direction of the mode (Figure 7.7). As in the previous cases,

the needed stiffness value was computed using Equation 7.8 and the results are plotted in Figure 7.8.

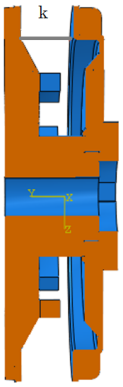

Figure 7.7: Spring connecting the two covers

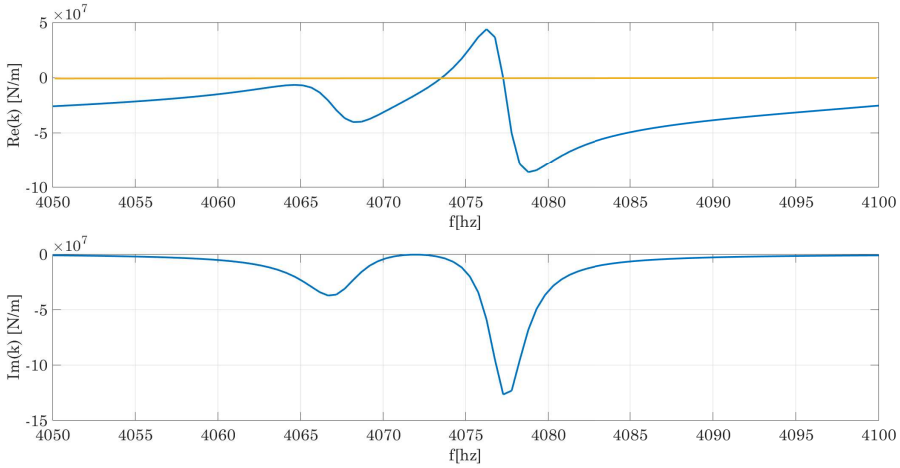

Figure 7.8: Needed stiffness for the spring in frequency

The value of the stiffness in the parametric study for this case ranged from 10^6 to $4.4 \cdot 10^6$ N/m. The evolution of the Squeal Index with frequency is shown in Figure 7.9, in this case the effect is bigger but it is not still possible to take the squealing eigenvalue under the threshold of 1 %.

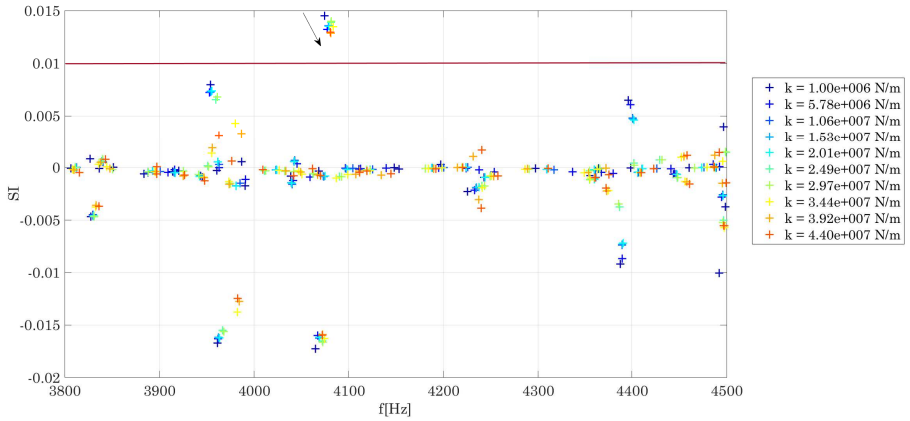

Figure 7.9: Parametric study of the effect of the added spring

7.3 Conclusions

In this chapter the receptance method has been extended and applied to propose structural modifications for suppressing squeal in a real brake–clutch. Two options were considered:

- Balanced point masses
- A spring connecting two points

Thanks to the receptance function the value of the modification to avoid mode coupling was computed. Then, its effect in the complex modes of the brake–clutch was analysed.

For the case of the balanced mass it was possible to reduce the real parts of the eigenvalue of the squealing mode under the threshold of 1 % by the addition of two balanced masses of 23 g each.

For the case of the spring, neither the two possibilities studied were able to reduce the real part of the squealing eigenvalue enough due to the specific features of the mode under study.

To sum up, this chapter offers insight into the different possibilities to modify a brake–clutch to eliminate squeal noise. This methodology is useful to determine the validity of a modification to suppress squeal without the need of an experiment.

Chapter 8

Conclusions

8.1 Main conclusions

The present work consists in the description of the process from a simple model for gaining insight into brake–clutch squeal to the proposal of a design modification for squeal suppression in a real system.

The first step was designing the simple model itself which was based on a commercial tribometer to take advantage of its integrated measuring system and control.

The analysis in the simple model comprised an experimental and a simulation part. On the experimental side, squeal tests were performed and squeal frequencies identified. On the simulation side, unstable modes were computed by means of Complex Eigenvalue Analysis. To improve the correlation between simulation and experimental squeal frequencies the friction material was characterised: its elastic properties and friction coefficient as a function of speed and pressure were obtained. This point is important since, generally, the friction material is assumed to be isotropic and friction coefficient constant whilst in reality neither of these assumptions are strictly right.

This simple model was useful to check the validity of CEA as a tool for brake–clutch squeal prediction (Objective 1) and to confirm that the mechanism responsible for brake–clutch squeal is mode coupling (Objective 2), neither of which were evident at the beginning of the work. These two conclusions were further reinforced in Chapter 6 when the simulation and experimental results for the real system were compared with good correlation.

In addition, the effect in squeal of operation conditions (normal force and rotation) and system properties (friction coefficient, material properties and damping) was examined (Objective 4). Regarding operation conditions the following conclusions were drawn:

- The most influential parameter in squeal is the normal force, since it sets the squeal frequencies.
- There is a friction coefficient threshold under which squeal rarely occurs. This threshold is different depending on the normal force applied.
- Squeal appears when torque drops and normal force oscillation increases.
- Modulation in squeal noise is cyclic being its period related to the rotation speed.

Regarding stability it can be said that:

- The most influential parameter in stability is the friction coefficient as it determines the value of excitation and the amount of damping introduced to the system.
- Proper material properties for the friction material should be included in the model to correctly predict the unstable frequencies.

Once the model had been developed and validated, the effect of point structural modifications in squeal appearance was studied (Objective 3). A methodology for the computation of the needed design modification for squeal suppression was proposed. It comprises the following steps:

1. Prepare a finite element model with a fair correlation to experimental data
2. Choose the points for the structural modification.
3. Compute the required point receptances in a frequency range around the squeal frequency
4. Solve the equation (or system of equations) for the case under study and select the appropiate value for the modification
5. Drop the imaginary value of the modification as the eigenvalue is moving along the real axis
6. Perform a parametric Complex Eigenvalue Analysis with the added modification to determine the effect of the modification in the unstable modes

This methodology can be adapted to the case with one or several point masses or ground connected springs or to the case in which two degrees of freedom are connected with a spring.

After analysing squeal generation and suppression in the simple model, squeal in the real model was tackled. First, a finite element model of a real brake–clutch was developed and the squeal frequencies were identified, thus confirming that

the methodology used is appropriate for the application (Objective 5). Care should be taken when using material properties or friction coefficient values from the automotive industry (or other).

A Squeal Index may be applied to the simulation results if overprediction is too high. This is related to the axisymmetry of the system and may be reduced with the introduction of asymmetry to the system.

Then, having the FE model validated, several options for structural modifications were proposed (Objective 6) including balanced mass and a spring between two points. The methodology proposed in Chapter 5 was proved to be a useful tool when deciding if a structural modification is able to stabilise the system before producing a prototype and performing experiments. In fact, the validity of a balanced mass modification for squeal suppression was theoretically proved.

8.2 Main contributions and publications

The main contributions of the present work and the related publications are listed below:

- Development of a tribometer-based simple model of a brake–clutch for squeal prediction. Published in *On the development of a simple model of a brake–clutch for squeal prediction.* Zarraga, O.; Abete, J. M.; Ulacia, I.; Zabala, B.; Uzkudun, O. EuroBrake 2014 Conference Proceedings. Lille. 13–15 May, 2014
- Squeal suppression by structural modification in the simple model based on the receptance function. *Receptance based structural modification in a simple brake–clutch model for squeal noise suppression* Ondiz Zarraga; Ibai Ulacia; José Manuel Abete; Huajiang Ouyang. 2016 (Under review)
- Development of a FE model of a brake–clutch and validation by experimental squeal measurements. The part about the experimental squeal measurements was published in *Analysis of the Vibration Phenomena in Brake–Clutches. Experimental Measurement of Squeal.* Zarraga, O.; Abete, J. M.; Galfarsoro, U.; Mondragon, M.; Uzkudun, O.; Ulacia, I. EuroBrake 2013 Conference Proceedings. Dresden. 2013
- Theoretical validation of possible structural modifications for brake–clutch squeal suppression.

8.3 Recommendations for future work

The following suggestions for future work are made in order to advance a step further in the understanding of brake–clutch squeal:

- An automated process for testing the structural modifications could be designed so that the most favourable position for the modification could be selected beforehand. With this in mind, the procedure described in Chapter 5 could be extended to include several alternative points and to create a response surface comprising them all.
- The friction coefficient under low pressure conditions should be better measured avoiding the high dispersion found in the pin–on–disk tests performed for this work. This would probably require the design of a specific methodology and specimens for the tests.
- The theoretical modifications proposed for the brake–clutch should be tested experimentally. The design should be as simple as possible for the hypothesis of mass or stiffness point modification to continue being acceptable. The differences derived from manufacturing should be taken into account since a modification that is not robust enough could be overridden by the deviation introduced in during production.
- The modelling of the point modification can be improved by taking into account the amount of damping introduced to the system. This damping could be estimated from the FRFs of the system with and without the modification.

Appendix A

Friction damping

Giving that Coulomb's friction in defined as:

$$\mathbf{F_R} = \mu F_N \hat{\mathbf{t}}$$

where

$$\hat{\mathbf{t}} = \frac{\dot{\boldsymbol{\gamma}}}{\dot{\gamma}}$$

stands for the sliding direction, then the shear stress can be computed as:

$$\int_A \boldsymbol{\tau} \mathrm{d}A = \int_A \mu P \frac{\dot{\boldsymbol{\gamma}}}{\dot{\gamma}} \mathrm{d}A \tag{A.1}$$

where $\dot{\boldsymbol{\gamma}}$ is the sliding velocity, P the contact pressure and $\mu = \mu(\dot{\gamma}, P)$ the sliding speed and pressure dependent friction coefficient.

In an area $\mathrm{d}A$ the shear stress is:

$$\boldsymbol{\tau} = \mu P \frac{\dot{\boldsymbol{\gamma}}}{\dot{\gamma}} \tag{A.2}$$

This shear stress has of course two components τ_1 and τ_2 defined as:

$$\tau_i = \mu P \frac{\dot{\gamma}_i}{\dot{\gamma}} = \mu P t_i \quad / \quad i = 1, 2 \tag{A.3}$$

being:

$$t_i = \frac{\dot{\gamma}_i}{\dot{\gamma}} \quad / \quad i = 1, 2$$

$$\dot{\gamma} = \sqrt{\dot{\gamma_1}^2 + \dot{\gamma_2}^2}$$

Taking the first component as an example and linearising:

$$\mathrm{d}\tau_1 = \frac{\partial \tau_1}{\partial P}\mathrm{d}P + \frac{\partial \tau_1}{\partial \dot{\gamma}}\mathrm{d}\dot{\gamma} = \left(\mu + \frac{\partial \mu}{\partial P}P\right) t_1 \mathrm{d}P + \left(\frac{\partial \mu}{\partial \dot{\gamma}} t_1 + \frac{\partial t_1}{\partial \dot{\gamma}}\mu\right) P \mathrm{d}\dot{\gamma} \quad \text{(A.4)}$$

The first term represents the contribution to the stiffness matrix **K** and the second one the contribution to the damping matrix **C**.

Taking into account that:

$$\mathrm{d}\dot{\gamma} = \frac{\partial \dot{\gamma}}{\partial \dot{\gamma}_1}\mathrm{d}\dot{\gamma}_1 + \frac{\partial \dot{\gamma}}{\partial \dot{\gamma}_2}\mathrm{d}\dot{\gamma}_2 = \frac{\dot{\gamma}_1}{\sqrt{\dot{\gamma_1}^2 + \dot{\gamma_2}^2}}\mathrm{d}\dot{\gamma}_1 + \frac{\dot{\gamma}_2}{\sqrt{\dot{\gamma_1}^2 + \dot{\gamma_2}^2}}\mathrm{d}\dot{\gamma}_2 = t_1 \mathrm{d}\dot{\gamma}_1 + t_2 \mathrm{d}\dot{\gamma}_2$$

and

$$\frac{\partial t_1}{\partial \dot{\gamma}} = \frac{1}{\dot{\gamma}^2}\left(\dot{\gamma}\frac{\mathrm{d}\dot{\gamma}_1}{\mathrm{d}\dot{\gamma}} - \dot{\gamma}_1\right) = \frac{1}{\dot{\gamma}}\left(\frac{\mathrm{d}\dot{\gamma}_1}{\mathrm{d}\dot{\gamma}} - t_1\right)$$

Equation A.4 becomes:

$$\mathrm{d}\tau_1 = \left(\mu + \frac{\partial \mu}{\partial P}P\right) t_1 \mathrm{d}P + \frac{\partial \mu}{\partial \dot{\gamma}} t_1 P (t_1 \mathrm{d}\dot{\gamma}_1 + t_2 \mathrm{d}\dot{\gamma}_2) + \frac{\mu P}{\dot{\gamma}}(\mathrm{d}\dot{\gamma}_1 - t_1(t_1 \mathrm{d}\dot{\gamma}_1 + t_2 \mathrm{d}\dot{\gamma}_2))$$

The same process can be followed for the τ_2 component. Both terms can be expressed together if index notation is used as:

$$\tau_i = \left(\mu + \frac{\partial \mu}{\partial P}P\right) t_i \mathrm{d}P + \frac{\partial \mu}{\partial \dot{\gamma}} P t_i t_j \mathrm{d}\dot{\gamma}_j + \frac{\mu P}{\dot{\gamma}}(\delta_{ij} - t_i t_j)\mathrm{d}\dot{\gamma}_j \quad \text{(A.5)}$$

where:

- The first term represents the effect of friction in the stiffness matrix **K**, it makes the matrix asymmetric.
- The second term represents the effect of having a speed dependent friction coeficient, if the slope of the $\mu - \dot{\gamma}$ curve is negative, negative damping appears.
- The third term represents friction damping, the positive contribution to the damping matrix **C**. This damping depends on the contact pressure P and on the inverse of the sliding speed $\frac{1}{\dot{\gamma}}$

Appendix B

EMA of the brake–clutch components

This appendix serves as a summary of the EMA tests performed in the components of the brake–clutch: the rotor, the brake side cover, the clutch side cover and the lining–holder. All the tests were roving hammer tests keeping the triaxial accelerometer in a single position and hitting with the hammer in perpendicular direction in the rest of the point.

B.1 Rotor

Measurements were taken with the accelerometer in point 1 in three concentric circumferences measuring in 24 points in each (Figure B.1).

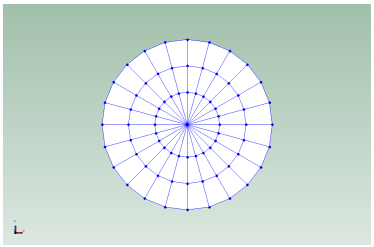

Figure B.1: Measurement points in the rotor

The MAC matrix comparing the simulation modes with the experimental ones is shown in Figure B.2 and the modes with higher MAC values are gathered in Table B.1.

Table B.1: Experimental and simulation frequency comparison for the rotor

Simulation f [Hz]	Experimental f [Hz]	MAC	Error[%]
430	417.6	0.81	2.88
431.2	417.7	0.844	3.13
990.5	965.7	0.765	2.50
1010.6	974.4	0.868	3.58
1391.5	1365.7	0.929	1.85
3320.2	3242.8	0.884	2.33
3607.6	3522	0.864	2.37
3610.3	3523.7	0.85	2.40
4644.4	4621	0.729	0.50
4646.1	4620	0.75	0.56

B.2 Brake side cover

Measurements were taken with the accelerometer in point 1 in three concentric circumferences measuring in 24 points in each (Figure B.3).

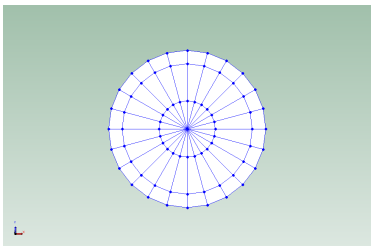

Figure B.3: Measurement points in the brake side cover

The MAC matrix comparing the simulation modes with the experimental ones is shown in Figure B.4 and the modes with higher MAC values are gathered in Table B.2.

Table B.2: Experimental and simulation frequency comparison for the brake side cover

Simulation f [Hz]	Experimental f [Hz]	MAC	Error[%]
480.6	521.1	0.767	8.43
494.3	522.3	0.805	5.66
894	940.7	0.436	5.22
897.6	940.8	0.638	4.81
986.1	1043.8	0.712	5.85
1551.2	1593	0.468	2.69
2378.4	2411.9	0.457	1.41
3300.8	3322.6	0.488	0.66
3308.1	3322	0.584	0.42
4277.1	4263.1	0.556	0.33
5248.2	5180.3	0.432	1.29

B.3 Clutch side cover

Measurements were taken with the accelerometer in point 1 in 48 points in the circumference and another 8 measurements were taken in the protrusion (Figure B.5).

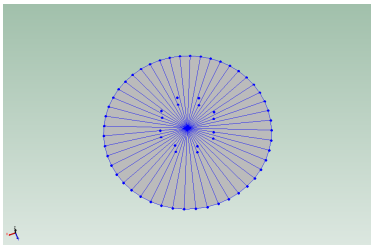

Figure B.5: Measurement points in the clutch side cover

In this case the shape of the modes could not be compared successfully due to the complexity of the geometry of the element. In any case, as the frequency error was not high the correlation was thought as acceptable (Table B.3).

Table B.3: Experimental and simulation frequency comparison for the clutch side cover

Simulation f [Hz]	Experimental f [Hz]	Error
1264.1	1105.61	14.34
1267.8	1116.52	13.55
1591.8	1549.8	2.71
1620.2	1596.2	1.50
1976.9	1931	2.38
1991	1945	2.37

B.4 Lining–holder

Measurements were taken with the accelerometer in point 1 in three concentric semi–circumferences measuring in 20 points in each (Figure B.6)

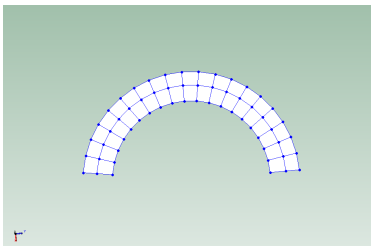

Figure B.6: Measurement points in the lining–holder

The MAC matrix comparing the simulation modes with the experimental ones is shown in Figure B.7 and the modes with higher MAC values are gathered in Table B.4.

Table B.4: Experimental and simulation frequency comparison for the lining–holder

Simulation f [Hz]	Experimental f [Hz]	MAC	Error[%]
256.23	251.0637396	0.99199886	2.06
423.35	429.4541491	0.9581087	1.42
668.06	647.6301113	0.94654526	3.15
794.03	796.242631	0.95897089	0.28
1112	1079.675303	0.95071528	2.99
1460.9	1430.995516	0.9136899	2.09
1696.1	1647.317323	0.90950239	2.96
2206.5	2143.530605	0.93710878	2.94
2339.9	2309.306393	0.89016006	1.32
2936.5	2847.059115	0.90408289	3.14
3148	3118.275054	0.8898082	0.95
3674.2	3576.163825	0.86248611	2.74
3952.3	3884.112724	0.88853176	1.76
4494.4	4404.326571	0.82039728	2.05
4839.9	4760.165193	0.82716854	1.68
5566.1	5479.418212	0.83552982	1.58
5761.1	5687.863441	0.79022003	1.29
6601.5	6491.516326	0.81619207	1.69

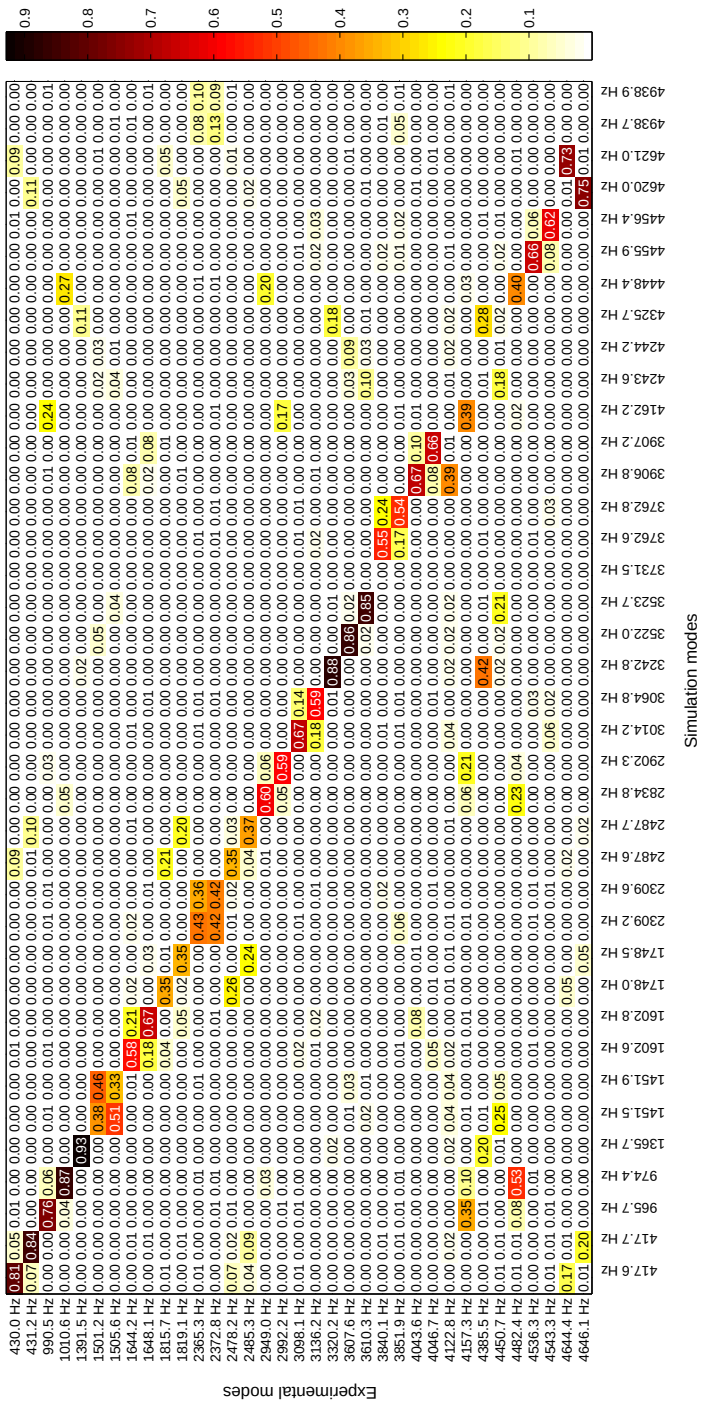

Figure B.2: MAC matrix for the rotor

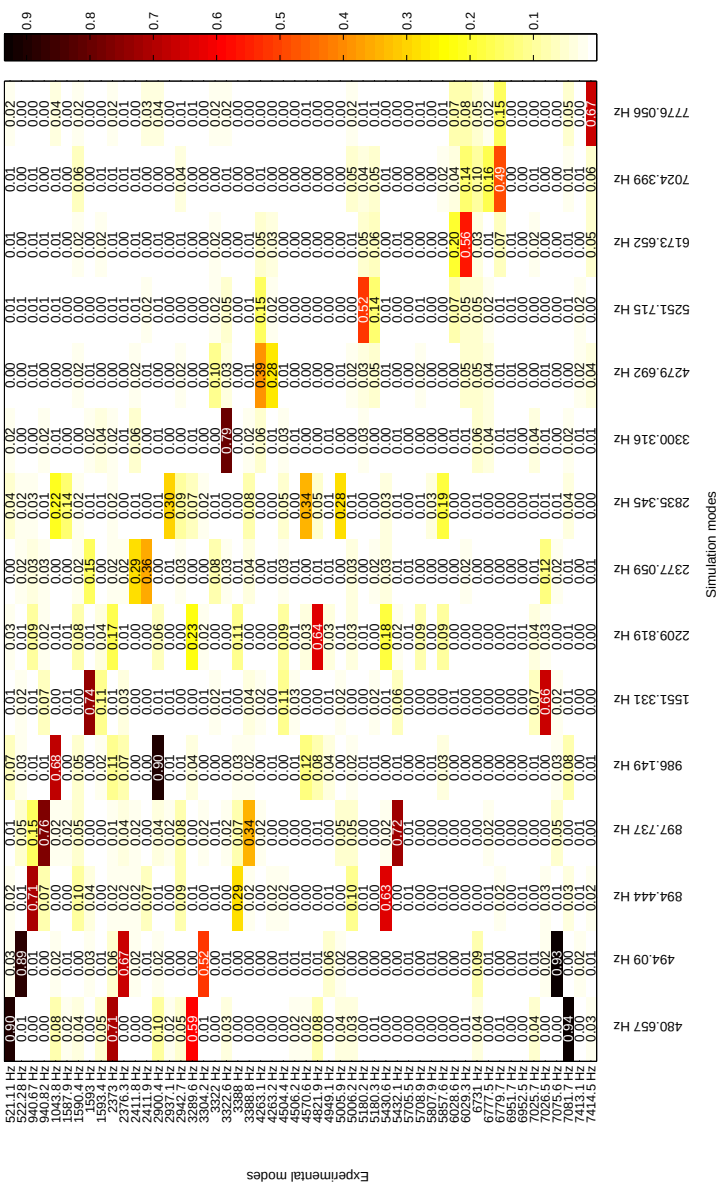

Figure B.4: MAC matrix for the brake side cover

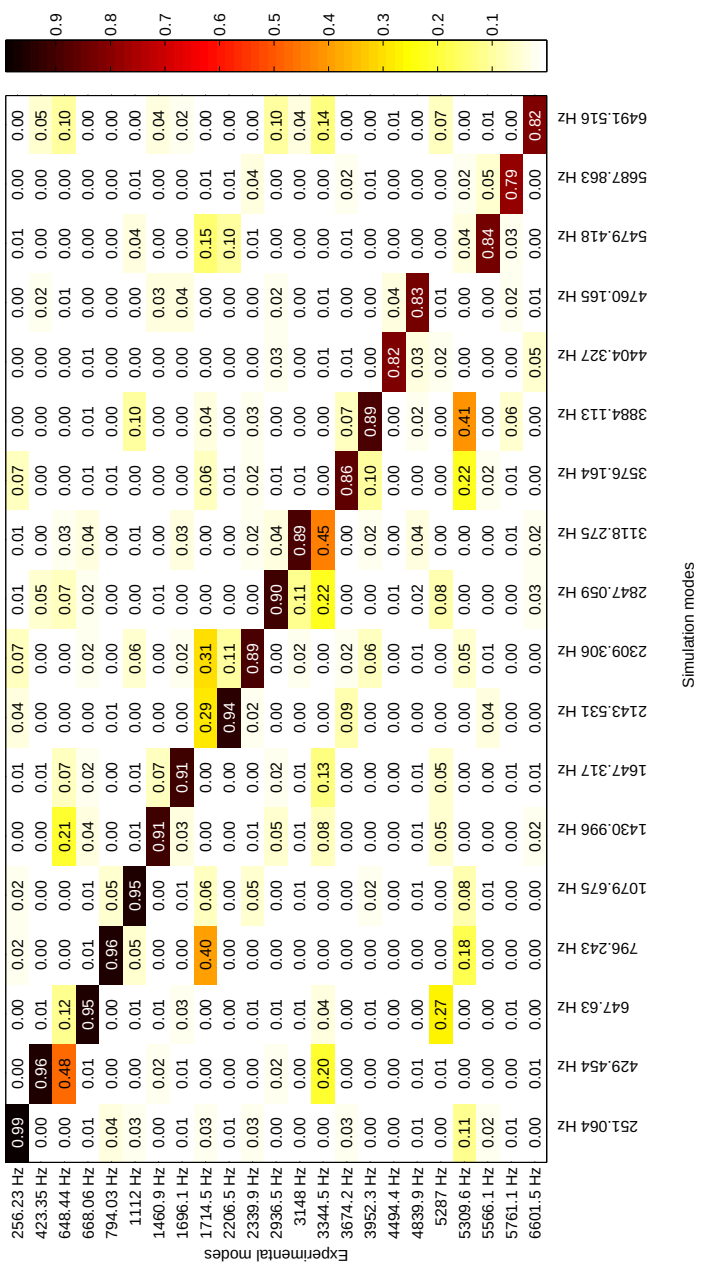

Figure B.7: MAC matrix for the lining–holder

Appendix C

Practical procedure

The objective of this appendix is to tackle the most practical side of the work, explaining the concrete procedure used in Abaqus and Matlab to obtain the results presented in this document. It is divided in three parts, the computation of complex eigenvalues, the computation of receptance and the parametric study.

C.1 Computation of complex eigenvalues

The complex eigenvalues of the system are computed using Abaqus in a four–step procedure comprising:

1. A non linear pressure application step
2. A non linear rotation application step
3. The computation of the normal modes
4. The computation of the complex modes from the normal modes.

A sample input file is provided below (Listing C.1), where the values in between brackets stand for the variables.

The following should be noted:

- During the pressure step stabilisation can be used to aid convergence. This is discouraged during the rotation step because of the damping that it is introduced to the system by this procedure.
- In order to reduce convergence problems, friction coefficient can be applied in the rotation step assuming that in the first step the friction coefficient is zero.
- Both non linear steps have been performed in 10 steps.

- The rotation is introduced with the keyword MOTION that defines the velocity of the material transported through the mesh during a static analysis

```
** STEP: pressure
**
*Step, name=pressure, nlgeom=NO, amplitude=STEP
*Static
0.1, 1., 0.1, 0.1
**
** LOADS
**
** Name: pressure  Type: Pressure
*Dsload
<surface>, P, <pressure>
**
*Contact Output
CDISP, CSTRESS
**
*End Step
**-----------------------------------------------
** STEP: rotacion
**
*Step, name=rotation, nlgeom=NO
*Static
0.1, 1., 0.1, 0.1
**
** BOUNDARY CONDITIONS
** Name: rotation Type: Velocity/Angular velocity
*Motion, rotation, type=VELOCITY
<node_set>, <omega>, <x1>,<y1>,<z1>,<x2>,<y2>,<z2>
** INTERACTIONS
*Change Friction, interaction=<name>
*Friction, slip tolerance=0.005
 <mu>,
**
*Contact Output
CDISP, CSTRESS
*End Step
**-----------------------------------------------
** STEP: modo
**
*Step, name=modo, nlgeom=NO, perturbation
*Frequency, eigensolver=Lanczos, acoustic coupling=↩
   on, normalization=displacement
```

```
, <f1>, <f2>, , ,
*End Step
**----------------------------------------------
** STEP: modo complejo
**
*Step, name="modo complejo", nlgeom=NO, perturbation↩
    , unsymm=YES
*Complex Frequency, friction damping=YES
, <f1>, <f2>,
*End Step
```

Listing C.1: Sample input file

C.2 Computation of receptance

In order to compute the value of the needed modification the point(s) where the modification will be located have to be selected and the receptance computed. With this in mind, the last two steps of the computation performed in the last section are substituted by the one shown in Listing C.2.

```
** STEP: receptance
*Step, name=H, nlgeom=NO, perturbation
*Steady State Dynamics, direct, frequency scale=↩
   LINEAR, friction damping=YES
<f1>, <f2>, <number_of_points>, <bias=1>.
**
** LOADS
** Name: F   Type: Concentrated force
*Cload, real
<point>, <direction=1,2,3>, 1.
**
** OUTPUT
*Output, history
*Node Output, nset=<point>
<direction= U1,U2,U3>,
*End Step
```

Listing C.2: Step for the computation of receptance

The value of the receptance(s) can be exported as a *Report* from the Abaqus Viewer in order to compute the range of values of needed mass or stiffness modification in Matlab using the formulae described in both Chapter 5 and Chapter 7.

C.3 Parametric study

Once the range of values of the modification has been set, a parametric study can be defined to determine the effects of the modification in the system. This can be accomplished in Abaqus by a Python script — a psf file — that is called from the terminal window as:

```
abaqus script=<script_name>
```

The script file has a structure similar to the one shown in Listing C.3

```
# Define the modification

inp = '<TEMPLATE_INPUT>'
rang = (<LIMIT1>,<LIMIT2>)
variable = '<VARIABLE_NAME>'

# Define the study

aStudy=ParStudy (par=variable, name=inp)

aStudy.define(CONTINUOUS, par=variable, domain=rang)
aStudy.sample(NUMBER, par=variable, number=<NUMBER>)
aStudy.combine(MESH)

# Create input based on the template

aStudy.generate(template=inp)
```

Listing C.3: Sample psf file

And has to be accompanied by a template input file where the modification is added but its value is not fixed, this means adding:

```
*PARAMETER
Variable = value
```

to the beginning of the input file and substituting the value of the parameter with when it appears. For example, if the mass of a point mass is the parameter under study, at the beginning of the input file the following should be added:

```
*PARAMETER
m = 1
```

The value of the parameter acts as a starting value and does not matter. Then, when the parameter appears its value is substituted by:

```
*Mass, elset=setName
<m>,
```

In this case the template input file is a computation of complex eigenvalue analysis where the parameter is the value of the modification. This parametric study creates several dat files that have to be analysed to determine if the modification is able to stabilise the system.

The real parts and frequencies of the eigenvalues can be easily extracted from the files using a regexp as shown in Listing C.4.

```
function [re, f] = extractReF(file)

% Extracts the real part and frequency of an ↩
    eigenvalue from a dat file

text = fileread(file);
exp = '\n\s+\d{1,3}\s+(?<re>[0-9.E-]+)\s+[0-9.E+]+\s↩
    +(?<f>[0-9.]{6})\s+[0-9.-]{6}';
data = regexp(text,exp,'names');

clear text

% Convert to number

f = cellfun(@str2num,{data.f});
re = cellfun(@str2num,{data.re});

clear data
```

Listing C.4: Function for extracting eigenvalues from a dat file

Then the pairs of data can be plotted for each value in the parametric study and to check the stability.

It is worth stressing that this whole procedure is susceptible to automation by following these steps:

- Prepare a generic input file to compute receptances and another to perform CEA with added mass or stiffness. After, the points where forces are applied, displacements measured and modifications applied will be modify by a script.
- Select frequency range around squealing frequency.

- Select possible points for the modification.
- For each point compute the needed receptance functions
- Read receptance functions in Matlab with and compute the possible range for the modification.
- Perform a CEA analysis for several values in the range.
- Read and plot the results.

A sample code showing this automatic procedure for the addition of a single point mass modification is shown in Listing C.5

```
% NEEDED DATA

inpH = 'H.inp'; % Generic input file for calculation↩
    of H
inpNewH = 'H_modified.inp'; % File that will be ↩
   created from inpH
inpCEA = 'CEA.inp'; % Name of prepared file for CEA
inpNewCEA = 'CEA_modified.inp'; % File that will be ↩
   created from inpCEA

% SELECT RANGE AROUND SQUEALING FREQUENCY

fs = 7400; % Squealing frequency
deltaF = 300;
resolution = 1;

f = linspace(fs-deltaF,fs+deltaF,2*deltaF/resolution↩
   +1);
s = i*2*pi*f;

% POSSIBLE POINTS FOR THE MODIFICATION

nodes = [1,2,3]; % position of the modification

points = 10; % number of points in parametric study
modes = 3;  % number of modes in range

% Initialisation.

re = zeros(modes,points,length(nodes));
frecuency = zeros(modes,points,length(nodes));
```

```
for n = nodes

    % COMPUTATION OF RECEPTANCE

    % *Step, name=H, nlgeom=NO, perturbation
    % *Steady State Dynamics, direct, frequency ↩
       scale=LINEAR, friction damping=YES
    % f1, f2, points,
    % **

    text = fileread(inpH);
    divisor1 = '*Steady State Dynamics, direct, ↩
       frequency scale=LINEAR, friction damping=YES'↩
       ;
    C = strsplit(text,divisor1);
    divisor2 = '** LOADS';
    C{2} = strsplit(C{2},divisor2);

    % Change frequency range

    C{2}{1} = ['\n' num2str(f-deltaF) ',' num2str(f+↩
       deltaF) ',' num2str(2*deltaF/resolution+1) '↩
       ,\n**\n'];

    fid = fopen(inpNewH,'w');
    fprintf(fid,'%s%s%s%s',C{1},divisor1,sprintf(C↩
       {2}{1}),divisor2,C{2}{2});
    fclose(fid);

    % Change node of load and displacement

    % *Nset, nset=<NAME>
    % node,

    text = fileread(inpNewH);
    divisor1 = '*Nset, nset=<NAME>';
    C = strsplit(text,divisor1);
    divisor2 = '*Elset, elset=<NAME>'; % take from ↩
       original h computation
    C{2} = strsplit(C{2},divisor2);

    C{2}{1} = ['\n' num2str(nodes) ',\n'];

    fid = fopen(inpNewH,'w');
    fprintf(fid,'%s%s%s%s',C{1},divisor1,sprintf(C↩
       {2}{1}),divisor2,C{2}{2});
```

```
fclose(fid);

% Compute H in frequency range

dos(['abaqus job=', inpNewH(1:end-4), ' ↩
    interactive']);

% Write h in dat file
% *NODE PRINT, NSET=<NAME>
% U2

text = fileread([inpNewH(1:(end-3)) 'dat']);

data = regexp(text,[nodo '\s+(?<re>[0-9.E-]+)'],↩
    'names');
re = str2num(data.re);

data = regexp(text,'SSD\s+(?<im>[0-9.E-]+)','↩
    names');
im = str2num(data.im);

h = complex(re,im);

% Modification

deltaM = -ones(length(h),1)./(s.^2.*h);
deltaM = deltaM > 0;

% For the mass modification

for m = linspace(min(deltaM),max(deltaM),points)

    text = fileread(inpCEA);
    divisor1 = '** MATERIALS';
    C = strsplit(text,divisor1);

    % Only real part

    mass = ['*Element, type=MASS, elset=<NAME>,'↩
         nodes '\n*Mass, elset=<NAME>\n' num2str↩
       (real(deltaM)) ', \n**\n']; % take from ↩
       prepared CEA

    fid = fopen(inpNewCEA,'w');
    fprintf(fid,'%s%s%s',C{1},sprintf(mass),↩
       divisor1,C{2});
```

```
        fclose(fid);

        dos(['abaqus job=', inpNewCEA(1:end-4), ' ↩
            interactive']);

        % Read results with regexp

        [re(:,m,n), frecuency(:,m,n)] = extractReF([↩
            inpNewCEA(1:end-4), '.dat']);

    end

end
```

Listing C.5: Sample code for automatic point mass modification

References

[1] P. Wickramarachi, R. Singh, G. Bailey, Analysis of friction-induced vibration leading to“ EEK” noise in a dry friction clutch, Internoise. (2005).

[2] Real Decreto 286/2006, de 10 de marzo, sobre la protección de la salud y la seguridad de los trabajadores contra los riesgos relacionados con la exposición al ruido., Spain, 2006.

[3] C. Cantoni, R. Cesarini, G. Mastinu, G. Rocca, R. Sicigliano, Brake comfort–a review, Vehicle System Dynamics. 47 (2009) 901–947. http://www.tandfonline.com/doi/abs/10.1080/00423110903100432.

[4] G. Sheng, Friction-induced vibrations and sound: principles and applications, CRC Press, 2008.

[5] F. Gautier, F. Gautier, C. Pezerat, J.-M. Duffal, How can automotive friction-induced noises be related to physical mechanisms?, Applied Acoustics. 76 (2014) 391–401.

[6] A.R. AbuBakar, H. Ouyang, Complex eigenvalue analysis and dynamic transient analysis in predicting disc brake squeal, International Journal of Vehicle Noise and Vibration. 2 (2006) 143–155. http://inderscience.metapress.com/index/E0X6654A34WLEB55.pdf.

[7] A. Tuchinda, Development of validated models for brake squeal predictions, PhD Thesis, Imperial College London (University of London), 2003.

[8] D. Crolla, A. Lang, Paper VII (i) Brake Noise and Vibration-The State of the Art, Tribology Series. 18 (1991) 165–174. http://www.sciencedirect.com/science/article/pii/S0167892208701329.

[9] F. Chen, C. Tan, R. Quaglia, M. AEC, Disc brake squeal, SAE International, 2006.

[10] F. Bergman, M. Eriksson, S. Jacobson, Influence of disc topography on generation of brake squeal, Wear. 225 (1999) 621–628. http://www.sciencedirect.com/science/article/pii/S0043164899000642.

[11] A.R.A. Bakar, Modelling and Simulation of Disc Brake Contact Analysis

and Squeal, PhD Thesis, University of Liverpool, 2005.

[12] N. Kinkaid, O. O'Reilly, P. Papadopoulos, Automotive disc brake squeal, Journal of Sound and Vibration. 267 (2003) 105–166. http://www.sciencedirect.com/science/article/pii/S0022460X02015730.

[13] A. McMillan, A non-linear friction model for self-excited vibrations, Journal of Sound and Vibration. 205 (1997) 323–335. http://www.sciencedirect.com/science/article/pii/S0022460X97910531.

[14] P. Duffour, Noise generation in vehicle brakes, PhD Thesis, University of Cambridge, 2002.

[15] J. Flint, J. Hultén, Lining-deformation-induced modal coupling as squeal generator in a distributed parameter disc brake model, Journal of Sound and Vibration. 254 (2002) 1–21. http://www.sciencedirect.com/science/article/pii/S0022460X01940520.

[16] M. North, Disc brake squeal: a theoretical model, Hillington Press, 1972.

[17] A. Akay, O. Giannini, F. Massi, A. Sestieri, Disc brake squeal characterization through simplified test rigs, Mechanical Systems and Signal Processing. 23 (2009) 2590–2607. http://www.sciencedirect.com/science/article/pii/S088832700900082X.

[18] N. Hoffmann, M. Fischer, R. Allgaier, L. Gaul, A minimal model for studying properties of the mode-coupling type instability in friction induced oscillations, Mechanics Research Communications. 29 (2002) 197–205. http://www.sciencedirect.com/science/article/pii/S0093641302002549.

[19] A. Akay, Acoustics of friction, The Journal of the Acoustical Society of America. 111 (2002) 1525. http://link.aip.org/link/jasman/v111/i4/p1525/s1.

[20] M. Bengisu, A. Akay, Stability of friction-induced vibrations in multi-degree-of-freedom systems, Journal of Sound and Vibration. 171 (1994) 557–570. http://www.sciencedirect.com/science/article/pii/S0022460X84711400.

[21] D. Beloiu, R. Ibrahim, Analytical and experimental investigations of disc brake noise using the frequency-time domain, Structural Control and Health Monitoring. 13 (2006) 277–300. http://onlinelibrary.wiley.com/doi/10.1002/stc.137/abstract.

[22] J.D. Fieldhouse, T. Newcomb, Double pulsed holography used to investigate noisy brakes, Optics and Lasers in Engineering. 25 (1996) 455–494. http://www.sciencedirect.com/science/article/pii/0143816695000941.

[23] O. Giannini, A. Akay, F. Massi, Experimental analysis of brake squeal noise on a laboratory brake setup, Journal of Sound and Vibration. 292 (2006) 1–20. http://www.sciencedirect.com/science/article/pii/S0022460X05006978.

[24] S. Rhee, P. Tsang, Y. Wang, Friction-induced noise and vibration of disc brakes, Wear. 133 (1989) 39–45. http://www.sciencedirect.com/science/article/

pii/0043164889901117.

[25] J. Mottershead, H. Ouyang, M. Cartmell, M. Friswell, Parametric resonances in an annular disc, with a rotating system of distributed mass and elasticity; and the effects of friction and damping, Proceedings of the Royal Society of London. Series A: Mathematical, Physical and Engineering Sciences. 453 (1997) 1–19. http://rspa.royalsocietypublishing.org/content/453/1956/1.short.

[26] H. Ouyang, Q. Cao, J. Mottershead, T. Treyde, Predicting disc brake squeal frequencies using two distinct approaches, in: Proceedings of the 22nd Int. Modal Analysis Conference, 2004.

[27] L. Afferrant, M. Ciavarella, TEDI (ThermoElasto-Dynamic Instability): a new mechanism for squeal & TEI, in: P. Wriggers, U. Nackenhorst (Eds.), Analysis and Simulation of Contact Problems, Springer Berlin Heidelberg, 2006: pp. 231–241. doi:10.1007/3-540-31761-9_26.

[28] L. Afferrante, M. Ciavarella, A note on thermoelastodynamic instability (TEDI) for a 1D elastic layer: Force control, International Journal of Solids and Structures. 44 (2007) 1380–1390. http://www.sciencedirect.com/science/article/pii/S0020768306002319.

[29] L. Afferrante, M. Ciavarella, J. Barber, Sliding thermoelastodynamic instability, Proceedings of the Royal Society A: Mathematical, Physical and Engineering Science. 462 (2006) 2161–2176. http://rspa.royalsocietypublishing.org/content/462/2071/2161.short.

[30] G. Adams, M. Nosonovsky, Elastic waves induced by the frictional sliding of two elastic half-spaces, Tribology Series. 39 (2001) 47–54. http://www.sciencedirect.com/science/article/pii/S0167892201800912.

[31] S. Oberst, J. Lai, Chaos in brake squeal noise, Journal of Sound and Vibration. 330 (2011) 955–975. http://www.sciencedirect.com/science/article/pii/S0022460X10005948.

[32] K. Shin, M. Brennan, J.-E. Oh, C. Harris, Analysis of disc brake noise using a two-degree-of-freedom model, Journal of Sound and Vibration. 254 (2002) 837–848. http://www.sciencedirect.com/science/article/pii/S0022460X01941276.

[33] B. Hervé, J.-J. Sinou, H. Mahé, L. Jezequel, Extension of the destabilization paradox to limit cycle amplitudes for a nonlinear self-excited system subject to gyroscopic and circulatory actions, Journal of Sound and Vibration. 323 (2009) 944–973. http://www.sciencedirect.com/science/article/pii/S0022460X09000352.

[34] E. Berger, C. Krousgrill, F. Sadeghi, Friction-induced sliding instability in a multi-degree-of-freedom system with oscillatory normal forces, Journal of Sound and Vibration. 266 (2003) 369–387. http://www.sciencedirect.com/science/article/pii/S0022460X03006096.

[35] N. Coudeyras, J.-J. Sinou, S. Nacivet, A new treatment for predicting the self-excited vibrations of nonlinear systems with frictional interfaces: The Constrained

Harmonic Balance Method, with application to disc brake squeal, Journal of Sound and Vibration. 319 (2009) 1175–1199. http://www.sciencedirect.com/science/article/pii/S0022460X08006111.

[36] N. Coudeyras, S. Nacivet, J.-J. Sinou, Periodic and quasi-periodic solutions for multi-instabilities involved in brake squeal, Journal of Sound and Vibration. 328 (2009) 520–540. http://www.sciencedirect.com/science/article/pii/S0022460X09006609.

[37] Q. Cao, M.I. Friswell, H.J. Ouyang, J.E. Mottershead, S. James, Car disc brake squeal: Theoretical and experimental study, in: Materials Science Forum, Trans Tech Publ, 2003: pp. 269–277.

[38] O. Giannini, Unstable transient response of gyroscopic systems with stable eigenvalues, Mechanical Systems and Signal Processing. (2016) –. doi:http://dx.doi.org/10.1016/j.ymssp.2016.01.008.

[39] F. Massi, O. Giannini, L. Baillet, Brake squeal as dynamic instability: an experimental investigation, The Journal of the Acoustical Society of America. 120 (2006) 1388. http://link.aip.org/link/%3FJASMAN/120/1388/1.

[40] D. Guan, Brake Vibration and Noise-A Review and Discussion, Proceedings of 20th International Congress on Acoustics, ICA. 2 (2010) 5.

[41] F. Cantone, F. Massi, A numerical investigation into the squeal instability: Effect of damping, Mechanical Systems and Signal Processing. 25 (2011) 1727–1737. http://www.sciencedirect.com/science/article/pii/S0888327010004292.

[42] G. Fritz, J.-J. Sinou, J.-M. Duffal, L. Jezequel, Effects of damping on brake squeal coalescence patterns–application on a finite element model, Mechanics Research Communications. 34 (2007) 181–190. http://www.sciencedirect.com/science/article/pii/S0093641306000929.

[43] A. Bajer, V. Belsky, S.-W. Kung, The influence of friction-induced damping and nonlinear effects on brake squeal analysis, SAE Technical Paper, 2004.

[44] J. Kang, Squeal analysis of gyroscopic disc brake system based on finite element method, International Journal of Mechanical Sciences. 51 (2009) 284–294. http://www.sciencedirect.com/science/article/pii/S0020740309000344.

[45] B. Hervé, J.-J. Sinou, H. Mahé, L. Jezequel, Analysis of squeal noise and mode coupling instabilities including damping and gyroscopic effects, European Journal of Mechanics-A/Solids. 27 (2008) 141–160. http://www.sciencedirect.com/science/article/pii/S0997753807000447.

[46] M. Eriksson, Friction and contact phenomena of disc brakes related to squeal, PhD Thesis, Uppsala Universitet; Acta Universitatis Upsaliensis, 2000.

[47] M. Eriksson, F. Bergman, S. Jacobson, Surface characterisation of brake pads after running under silent and squealing conditions, Wear. 232 (1999) 163–167. http://www.sciencedirect.com/science/article/pii/S0043164899001416.

[48] M. Eriksson, F. Bergman, S. Jacobson, On the nature of tribological contact

in automotive brakes, Wear. 252 (2002) 26–36. http://www.sciencedirect.com/science/article/pii/S0043164801008493.

[49] H. Sherif, Investigation on effect of surface topography of pad/disc assembly on squeal generation, Wear. 257 (2004) 687–695. http://www.sciencedirect.com/science/article/pii/S0043164804000717.

[50] F. Massi, Y. Berthier, L. Baillet, Contact surface topography and system dynamics of brake squeal, Wear. 265 (2008) 1784–1792. http://www.sciencedirect.com/science/article/pii/S004316480800238X.

[51] J.G. McDaniel, J. Moore, S.-E. Chen, C.L. Clarke, Acoustic radiation models of brake systems from stationary LDV measurements, Proceedings of IMEC. 99 (1999) 14–19.

[52] H. Lee, Modal acoustic radiation characteristics of a thick annular disk, PhD Thesis, The Ohio State University, 2003.

[53] S. Oberst, J. Lai, Numerical prediction of brake squeal propensity using acoustic power calculation, Proceedings of ACOUSTICS 2009. (2009).

[54] S. Oberst, J. Lai, Acoustic Radiation of Friction-induced Pad-mode Instability in Disc Brake Squeal, in: 20th International Congress on Acoustics (ICA 2010), 2010: pp. 23–27.

[55] S. Oberst, J. Lai, Numerical methods for simulating brake squeal noise, in: Proceedings of 20th International Congress on Acoustics, ICA, 2010: pp. 1505–1516.

[56] S. Oberst, Analysis of Brake Squeal Noise, PhD Thesis, UNSW, 2011.

[57] Y.-B. Yi, Finite element analysis of thermoelastodynamic instability involving frictional heating, Transactions American Society of Mechanical Engineers Journal of Tribology. 128 (2006) 718.

[58] A. AbuBakar, M. AbdulHamid, M. Mohamad, A. Dzakaria, B. AbdGhani, Numerical analysis of disc brake squeal considering temperature dependent friction coefficient, Conference on Natural Resources Engineering and Technology INRET2006. (2006). http://eprints.utm.my/3366/.

[59] H. Ouyang, W. Nack, Y. Yuan, F. Chen, Numerical analysis of automotive disc brake squeal: a review, International Journal of Vehicle Noise and Vibration. 1 (2005) 207–231. http://inderscience.metapress.com/index/DPF5TGFB4JFP5XR3.pdf.

[60] M. Rusli, M. Okuma, Effect of surface topography on mode-coupling model of dry contact sliding systems, Journal of Sound and Vibration. 308 (2007) 721–734. http://www.sciencedirect.com/science/article/pii/S0022460X07002489.

[61] M. Nishiwaki, Generalized theory of brake noise, Proceedings of the Institution of Mechanical Engineers, Part D: Journal of Automobile Engineering. 207

(1993) 195–202. http://pid.sagepub.com/content/207/3/195.short.

[62] R. Ibrahim, Friction-Induced Vibration, Chatter, Squeal, and Chaos—Part II: Dynamics and Modeling, Applied Mechanics Reviews. 47 (1994) 227.

[63] U. von Wagner, D. Hochlenert, P. Hagedorn, Active Control of Disk Brake Squeal, in: Proceedings of ICTAM, 2004.

[64] Y. Denou, M. Nishiwaki, First order analysis of low frequency disk brake squeal, SAE Technical Paper. 01 (2001) 3136. http://papers.sae.org/2001-01-3136.

[65] U. von Wagner, D. Hochlenert, P. Hagedorn, Minimal models for disk brake squeal, Journal of Sound and Vibration. 302 (2007) 527–539. http://www.sciencedirect.com/science/article/pii/S0022460X06008868.

[66] A. Fidlin, O. Drozdetskaya, B. Waltersberger, On the minimal model for the low frequency wobbling instability of friction discs, European Journal of Mechanics-A/Solids. 30 (2011) 665–672.

[67] C. Duan, R. Singh, Stick–slip behavior in torque converter clutch, in: SAE Noise and Vibration Conference, 2005: p. 2005.

[68] Y. Aktir, J.-F. Brunel, P. Dufrenoy, H. Mahé, Three-dimensional finite element model of an automotive clutch for analysis of axial vibrations, Proceedings of the Institution of Mechanical Engineers, Part D: Journal of Automobile Engineering. (2015). doi:10.1177/0954407015607377.

[69] P. Zagrodzki, Thermoelastic instability in friction clutches and brakes–transient modal analysis revealing mechanisms of excitation of unstable modes, International Journal of Solids and Structures. 46 (2009) 2463–2476.

[70] L. Afferrante, M. Ciavarella, Thermo-Elastic Dynamic Instability (TEDI)—a review of recent results, Journal of Engineering Mathematics. 61 (2008) 285–300. doi:10.1007/s10665-007-9184-0.

[71] P. Wickramarachi, R. Singh, G. Bailey, Analysis of friction-induced vibration leading to Eek noise, Noise Control Engineering Journal. 53 (2005) 138–144.

[72] B. Hervé, J. Sinou, H. Mahé, L. Jézéquel, Analysis of friction-induced self-generated vibrations originated from mode-coupling in clutches, International Journal of Pure and Applied Mathematics. 42 (2008) 369.

[73] M.H. Trinh, S. Berger, E. Aubry, Stability analysis of a clutch system with multi-element generalized polynomial chaos, Mechanics & Industry. 17 (2016) 205. doi:10.1051/meca/2015061.

[74] T. Butlin, J. Woodhouse, Friction-induced vibration: Should low-order models be believed?, Journal of Sound and Vibration. 328 (2009) 92–108.

[75] A. Papinniemi, Vibro-acoustic Studies of Brake Squeal Noise, PhD Thesis, University of New South Wales, Australian Defence Force Academy, School of

Aerospace, Civil; Mechanical Engineering, 2008.

[76] F. Massi, L. Baillet, others, Numerical analysis of squeal instability, in: Proceedings of NOVEM 2005: Noise and Vibration: Emerging Methods International Congress, 2005. http://hal.archives-ouvertes.fr/insu-00355496/.

[77] D. Guan, J. Huang, The method of feed-in energy on disc brake squeal, Journal of Sound and Vibration. 261 (2003) 297–307. http://www.sciencedirect.com/science/article/pii/S0022460X0201074X.

[78] A.T. Papinniemi, J.C. Lai, Comparison of Energy Based Methods for Assessing Brake Squeal Propensity, in: 18th International Congress on Acoustics, 2004.

[79] J.-J. Sinou, Transient non-linear dynamic analysis of automotive disc brake squeal–On the need to consider both stability and non-linear analysis, Mechanics Research Communications. 37 (2010) 96–105. http://www.sciencedirect.com/science/article/pii/S0093641309001293.

[80] F. Chevillot, J.-J. Sinou, N. Hardouin, Nonlinear transient vibrations and coexistences of multi-instabilities induced by friction in an aircraft braking system, Journal of Sound and Vibration. 328 (2009) 555–574. http://www.sciencedirect.com/science/article/pii/S0022460X09006865.

[81] R. Allgaier, L. Gaul, W. Keiper, K. Willner, N. Hoffmann, A study on brake squeal using a beam-on-disc model, Proceedings IMAC XX. 1 (2002) 528–534.

[82] A. Heussaff, L. Dubar, T. Tison, M. Watremez, R. Nunes, A methodology for the modelling of the variability of brake lining surfaces, Wear. 289 (2012) 145–159. http://www.sciencedirect.com/science/article/pii/S0043164812000981.

[83] P.D. Vincent Magnier Jean-Baptiste Colliat, Multi-Scale Modeling of Friction Materials Taking into Account the Porosity: Consequence on the Squeal, Eurobrake. (2013).

[84] A. Renault, F. Massa, B. Lallemand, T. Tison, Experimental investigations for uncertainty quantification in brake squeal analysis, Journal of Sound and Vibration. (2016) –. doi:http://dx.doi.org/10.1016/j.jsv.2015.12.049.

[85] T. Tison, A. Heussaff, F. Massa, I. Turpin, R. Nunes, Improvement in the predictivity of squeal simulations: Uncertainty and robustness, Journal of Sound and Vibration. 333 (2014) 3394–3412. doi:http://dx.doi.org/10.1016/j.jsv.2014.03.011.

[86] O. Fazio, S. Nacivet, others, Reduction strategy for a brake system with local frictional non-linearities–Application for the prediction of unstable vibration modes, Applied Acoustics. 91 (2015) 12–24.

[87] G.V. Des Roches, Frequency and time simulation of squeal instabilities. Application to the design of industrial automotive brakes., PhD Thesis, Ecole Centrale Paris, 2011. http://tel.archives-ouvertes.fr/tel-00594224/.

[88] R.F. Nunes, J. Will, V. Bayer, K. Chittepu, Robustness Evaluation of brake

systems con-cerned to squeal noise problem, 6th Weimar Optimization and Stochastic Days. (2009).

[89] J. Abdo, G. Meinhardt, Vibration response of a disc brake: evaluation and design, Applied Mechanics and Engineering. 11 (2006) 467.

[90] W.W. Tworzydlo, O.N. Hamzeh, W. Zaton, T.J. Judek, Friction-induced oscillations of a pin-on-disk slider: analytical and experimental studies, Wear. 236 (1999) 9–23. http://www.sciencedirect.com/science/article/pii/S0043164899002513.

[91] R. Schroth, N. Hoffmann, R. Swift, Mechanism of Brake Squeal–from Theory to Experimentally Measured Mode Coupling, XXII IMAC. (2004).

[92] J. Elguezabal, Stiffness, damping and working conditions influence on squeal behaviour of a brake system representative simplified test set up, Tesis doctoral, Mondragon Unibertsitatea, 2016.

[93] F. Massi, L. Baillet, A. Culla, Structural modifications for squeal noise reduction: numerical and experimental validation, International Journal of Vehicle Design. 51 (2009) 168–189. doi:http://dx.doi.org/10.1504/IJVD.2009.02712.

[94] S. James, H.J. Ouyang, D. Brookfield, J.E. Mottershead, Disc brake squeal–an experimental approach, in: Materials Science Forum, Trans Tech Publ, 2003: pp. 237–244.

[95] O. Zarraga, J.M. Abete, U. Galfarsoro, M. Mondragon, O. Uzkudun, I. Ulacia, Analysis of the Vibration Phenomena in Brake-Clutches. Experimental Measurement of Squeal, Eurobrake. (2013).

[96] A. Papinniemi, D. Stanef, S. Moore, S. Hamdi, Brake noise in practice, ICSV14. (2007).

[97] M. Tan, K. Stepper, K. Abdelhamid, A.-H. Afaneh, P. Blaschke, An integrated process for design against brake squeal, in: International Modal Analysis Conference (IMAC XXI), 2003.

[98] O. Giannini, A. Sestieri, A. Akay, Prediction of squeal in a laboratory disk brake, in: IMAC-XXI: A Conference & Exposition on Structural Dynamics, 2003.

[99] R. Krupka, Application of ESPI techniques for the study of dynamic vibrations, in: Proceedings of SPIE, 2004: pp. 79–84.

[100] T. Walz, A. Ettemeyer, others, Fast and full-field measurement of brake squeal using pulsed ESPI technique, Optical Engineering. 42 (2003) 1354–1358.

[101] F. Chen, G.M. Brown, M. Marchi, M. Dale, Recent advances in brake noise and vibration engineering using laser metrology, Optical Engineering. 42 (2003) 1359–1369.

[102] S. Yang, R. Gibson, Brake Vibration and Noise: Reviews, Comments, and Proposed Considerations, in: Proceedings SPIE the International Society

for Optical Engineering, SPIE INTERNATIONAL SOCIETY FOR OPTICAL, 1996: pp. 1342–1349.

[103] G. Spelsberg-Korspeter, Breaking of symmetries for stabilization of rotating continua in frictional contact, Journal of Sound and Vibration. 322 (2009) 798–807. http://www.sciencedirect.com/science/article/pii/S0022460X08009425.

[104] A.R. Abu-Bakar, M.R. Buang, M.Z.A. Rashid, R.A. Rahman, Suppression of drum brake squeal through structural modifications using finite element method, International Journal of Vehicle Design. 51 (2009) 3–20. doi:http://dx.doi.org/10.1504/IJVD.2009.027113.

[105] K. Shintani, H. Azegami, Shape optimization for suppressing brake squeal, Structural and Multidisciplinary Optimization. (2014) 1–9.

[106] L. Hammerström, S. Jacobson, Surface modification of brake discs to reduce squeal problems, Wear. 261 (2006) 53–57. http://www.sciencedirect.com/science/article/pii/S0043164805004758.

[107] S. Oberst, J. Lai, Statistical analysis of brake squeal noise, Journal of Sound and Vibration. 330 (2011) 2978–2994. http://www.sciencedirect.com/science/article/pii/S0022460X10008357.

[108] C. Kim, K. Zhou, Analysis of automotive disc brake squeal considering damping and design modifications for pads and a disc, International Journal of Automotive Technology. 17 (2016) 213–223. doi:10.1007/s12239-016-0021-1.

[109] A. Kyprianou, J.E. Mottershead, H. Ouyang, Structural modification. Part 2: assignment of natural frequencies and antiresonances by an added beam, Journal of Sound and Vibration. 284 (2005) 267–281.

[110] J.E. Mottershead, C. Mares, M. Friswell, An inverse method for the assignment of vibration nodes, Mechanical Systems and Signal Processing. 15 (2001) 87–100.

[111] J. He, Structural modification, Philosophical Transactions of the Royal Society of London A: Mathematical, Physical and Engineering Sciences. 359 (2001) 187–204.

[112] H. Ouyang, Prediction and assignment of latent roots of damped asymmetric systems by structural modifications, Mechanical Systems and Signal Processing. 23 (2009) 1920–1930. doi:http://dx.doi.org/10.1016/j.ymssp.2008.08.001.

[113] P. Liu, H. Zheng, C. Cai, Y. Wang, C. Lu, K. Ang, et al., Analysis of disc brake squeal using the complex eigenvalue method, Applied Acoustics. 68 (2007) 603–615. http://www.sciencedirect.com/science/article/pii/S0003682X06000739.

[114] K.P. Sang Chan Park WonTae Jeong, Improvement of Brake Squeal using Shape Optimization based on Frequency Separation, Eurobrake 2012. (2012).

[115] K. Shintani, H. Azegami, Shape Optimization for Brake Squeal, 10th World

Congress on Structural and Multidisciplinary Optimization. (2013).

[116] G. Spelsberg-Korspeter, Structural optimization for the avoidance of self-excited vibrations based on analytical models, Journal of Sound and Vibration. 329 (2010) 4829–4840. http://www.sciencedirect.com/science/article/pii/S0022460X10002427.

[117] G. Spelsberg-Korspeter, Eigenvalue optimization against brake squeal: Symmetry, mathematical background and experiments, Journal of Sound and Vibration. 331 (2012) 4259–4268. http://www.sciencedirect.com/science/article/pii/S0022460X12003422.

[118] S. Lakkam, S. Koetniyom, Optimization of constrained layer damping for strain energy minimization of vibrating pads, Songklanakarin Journal of Science and Technology. 34 (2012) 179–187.

[119] H. Ouyang, D. Richiedei, A. Trevisani, G. Zanardo, Eigenstructure assignment in undamped vibrating systems: A convex-constrained modification method based on receptances, Mechanical Systems and Signal Processing. 27 (2012) 397–409.

[120] F. Hugo, C. Gaël, R. Franck, D. Jean-Luc, L. Remy, Effectiveness of multilayer viscoelastic insulators to prevent occurrences of brake squeal: A numerical study, Applied Acoustics. 73 (2012) 1121–1128. http://www.sciencedirect.com/science/article/pii/S0003682X12001247.

[121] J. Kang, Finite element modelling for the investigation of in-plane modes and damping shims in disc brake squeal, Journal of Sound and Vibration. 331 (2012) 2190–2202. http://www.sciencedirect.com/science/article/pii/S0022460X11009801.

[122] M. Triches Jr, S. Gerges, R. Jordan, Reduction of squeal noise from disc brake systems using constrained layer damping, Journal of the Brazilian Society of Mechanical Sciences and Engineering. 26 (2004) 340–348.

[123] K. Cunefare, A. Graf, Experimental active control of automotive disc brake rotor squeal using dither, Journal of Sound and Vibration. 250 (2002) 579–590. http://www.sciencedirect.com/science/article/pii/S0022460X01939094.

[124] J.J. Thomsen, Using fast vibrations to quench friction-induced oscillations, Journal of Sound and Vibration. 228 (1999) 1079–1102. http://www.sciencedirect.com/science/article/pii/S0022460X99924604.

[125] M. Neubauer, R. Oleskiewicz, Suppression of brake squeal using shunted piezoceramics, Journal of Vibration and Acoustics. 130 (2008) 021005. http://cat.inist.fr/?aModele=afficheN&cpsidt=20295326.

[126] P. Pandey, Vibration control implementation in a braking system, PhD Thesis, Thapar University, 2011. http://dspace.thapar.edu:8080/dspace/handle/10266/1423.

[127] A.-B. Hashemi-Dehkordi S.M., Reducing friction-induced vibration using

intelligent active force control (AFC) with piezoelectric actuators, Sadhana. 37 (2012) 637–655.

[128] S. Oberst, J. Lai, S. Marburg, Guidelines for numerical vibration and acoustic analysis of disc brake squeal using simple models of brake systems, Journal of Sound and Vibration. 332 (2013) 2284–2299. doi:http://dx.doi.org/10.1016/j.jsv.2012.11.034.

[129] ABAQUS Documentation, Dassault Systèmes, 2014.

[130] A. Bajer, V. Belsky, L. Zeng, Combining a nonlinear static analysis and complex eigenvalue extraction in brake squeal simulation, SAE Paper. 01 (2003) 3349. http://papers.sae.org/2003-01-3349.

[131] O. Giannini, F. Massi, Characterization of the high-frequency squeal on a laboratory brake setup, Journal of Sound and Vibration. 310 (2008) 394–408. http://www.sciencedirect.com/science/article/pii/S0022460X07006402.

[132] P. Grange, D. Clair, M. Fogli, Caractérisation spectrale du crissement de freins à disques, 18ème Congrès Français de Mécanique (Grenoble 2007). (2007).

[133] D.E. Yuhas, J. Ding, S. Venkatesan, Non-linear aspects of friction material elastic constants, SAE Technical Paper, 2006.

[134] SAEJ3013: Friction Material Elastic Constants Determination through FRF Measurements and Optimization, SAE International; Brake NVH Standards Commitee, n.d.

[135] D. Yuhas, M. Yuhas, Friction Material Elastic Constant Measurements, Disc Brake Squeal-Mechanism, Analysis, Evaluation, and Reduction, Eds. RL Quaglia, CA Tan and F. Chen, SAE December. (2005).

[136] O. Giannini, A. Sestieri, Predictive model of squeal noise occurring on a laboratory brake, Journal of Sound and Vibration. 296 (2006) 583–601. http://www.sciencedirect.com/science/article/pii/S0022460X06002082.

[137] A. Nobari, H. Ouyang, P. Bannister, Uncertainty quantification of squeal instability via surrogate modelling, Mechanical Systems and Signal Processing. 60–61 (2015) 887–908. doi:http://dx.doi.org/10.1016/j.ymssp.2015.01.022.